UNIVERSIDADE FEDERAL DO PARANÁ

MAILSON DE MATOS

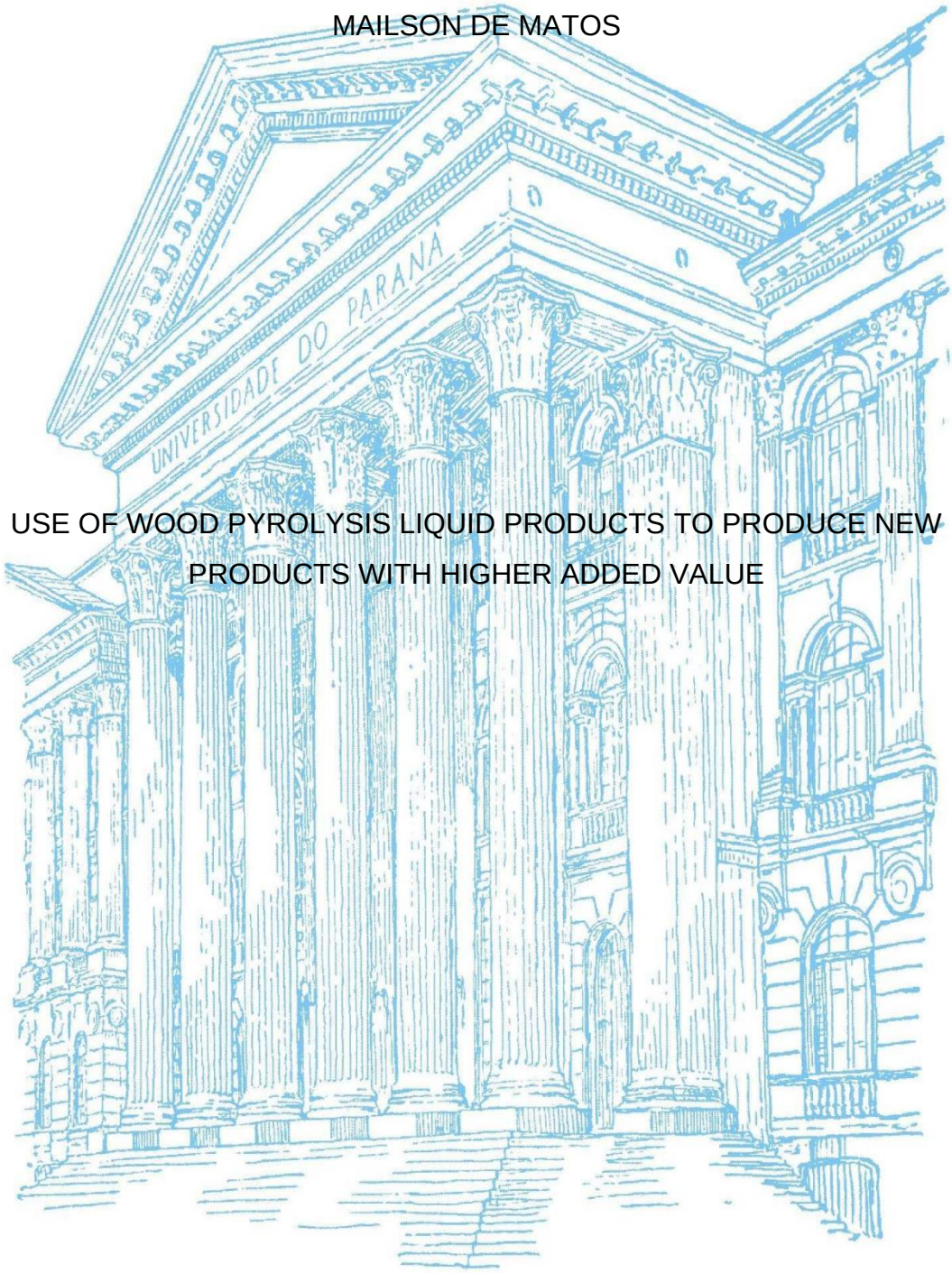

USE OF WOOD PYROLYSIS LIQUID PRODUCTS TO PRODUCE NEW PRODUCTS WITH HIGHER ADDED VALUE

CURITIBA

2021

MAILSON DE MATOS

USE OF WOOD PYROLYSIS LIQUID PRODUCTS TO PRODUCE NEW PRODUCTS WITH HIGHER ADDED VALUE

Versão final da tese apresentada ao Programa de Pós-Graduação em Engenharia e Ciência dos Materiais (PIPE) do Setor de Tecnologia da Universidade Federal do Paraná (UFPR), como requisito para a obtenção do título de doutor em Engenharia e Ciência dos Materiais.

Orientador: Prof. Dr. Washington Luiz Esteves Magalhães

Co-orientador: Prof. Dr. Diego Lomonaco

CURITIBA

2021

Catalogação na Fonte: Sistema de Bibliotecas, UFPR
Biblioteca de Ciência e Tecnologia

M433u Matos, Mailson de
Use of wood pyrolysis liquid products to produce new products with higher added value [recurso eletrônico] / Mailson de Matos – Curitiba, 2021.

Tese - Universidade Federal do Paraná, Setor de Ciências Exatas, Programa de Pós-Graduação em Engenharia e Ciência dos Materiais (PIPE).
Orientador: Prof. Dr. Washington Luiz Esteves Magalhães
Co-orientador: Prof. Dr. Diego Lomonaco

1. Pirolise. 2. Biomassa. 3. Catálise. 4 Antioxidantes I. Universidade Federal do Paraná. II. Magalhães, Washington Luiz Esteves. III. Lomonaco, Diego. IV. Título.

CDD: 543.57

Bibliotecária: Roseny Rivelini Morciani CRB-9/1585

MINISTÉRIO DA EDUCAÇÃO
SETOR DE CIENCIAS EXATAS
UNIVERSIDADE FEDERAL DO PARANÁ
PRÓ-REITORIA DE PESQUISA E PÓS-GRADUAÇÃO
PROGRAMA DE PÓS-GRADUAÇÃO ENGENHARIA E CIÊNCIA DOS MATERIAIS - 40001016033P9

TERMO DE APROVAÇÃO

Os membros da Banca Examinadora designada pelo Colegiado do Programa de Pós-Graduação em ENGENHARIA E CIÊNCIA DOS MATERIAIS da Universidade Federal do Paraná foram convocados para realizar a arguição da tese de Doutorado de **MAILSON DE MATOS** intitulada: **Use of wood pyrolysis liquid products to produce new products with higher added value**, sob orientação do Prof. Dr. WASHINGTON LUIZ ESTEVES MAGALHÃES, que após terem inquirido o aluno e realizada a avaliação do trabalho, são de parecer pela sua aprovação no rito de defesa.

A outorga do título de doutor está sujeita à homologação pelo colegiado, ao atendimento de todas as indicações e correções solicitadas pela banca e ao pleno atendimento das demandas regimentais do Programa de Pós-Graduação.

CURITIBA, 25 de Agosto de 2021.

WASHINGTON LUIZ ESTEVES MAGALHÃES
Presidente da Banca Examinadora

MARCO AURÉLIO DA SILVA CARVALHO FILHO
Avaliador Externo (UNIVERSIDADE POSITIVO)

ANDRÉ LUIZ MISSIO
Avaliador Externo (UNIVERSIDADE FEDERAL DE PELOTAS)

PEDRO HENRIQUE GONZALEZ DE CADEMARTORI
Avaliador Interno (UNIVERSIDADE FEDERAL DO PARANÁ)

CAMILLA KARLA BRITES QUEIROZ MARTINS DE OLIVEIRA
Avaliador Interno (UNIVERSIDADE FEDERAL DO PARANÁ)

ACKNOWLEDGEMENTS

I would like to thank the agencies and institutions that contributed to the financing of this work:

To CAPES (Coordenação de Aperfeiçoamento de Pessoal de Nível Superior) for supporting this work through the provision of a scholarship.

To EMBRAPA (Empresa Brasileira de Pesquisa Agropecuária) for providing me with free access to the laboratories and for providing me with all the material necessary to carry out my work.

To the Graduate Program in Materials Science and Engineering of Federal University of Paraná (UFPR, where I had the opportunity to do my doctorate.

To Federal University of Ceará (UFC) and Federal University of Technology - Paraná (UTFPR).

In addition, I would like to thank all the professors people who have walked beside me during the past four years:

Dr. Washington L. E. Magalhães for all the support for my doctoral study. For your criticisms. For encouraging me to get out of my comfort zone and instigating me to understand "why things are".

I thank all my labmates and friends from EMBRAPA, specially Tiélidy A. de Lima, Francine C. Claro, Soraia Zaioncz, Aline Krolow, Caroline Jordão, Mirela Artner, Fabricio A. Hansel, Edson A. Lima, Cristiane Helm, Simone Sopchaki, Patrícia Zanoni and Dayanne Mendes for their continuous support and friendship.

I would like to thank my family. Specially my boyfriend Anderson Skorobohaty, that helped me a lot in the elaboration of the illustrations.

RESUMO

A conversão da biomassa por rota termoquímica é uma das alternativas disponíveis para otimizar recursos, minimizando a destinação de resíduos e agregando valor. Entre estes, a pirólise rápida emprega temperaturas moderadas e tempos de residência curtos para maximizar o alcance da fração líquida, que é chamada de bio-óleo. Essa fração possui alta densidade energética (quando comparada à madeira), com grande potencial para a produção de combustíveis renováveis. No entanto, possui algumas propriedades que dificultam seu uso direto como combustível, necessitando de um aprimoramento, visando a obtenção de produtos que possam ser utilizados diretamente como combustível e ou compostos de interesse da indústria química. O presente estudo tem como objetivo principal desenvolver aplicações para o líquido obtido através da pirólise rápida de biomassa florestal. Com base em uma estratégia de bioeconomia circular, finos de madeira de eucalipto rejeitados de uma linha de celulose Kraft foram usados como matéria-prima em um processo de pirólise rápida em escala piloto. O bio-óleo e seus coprodutos foram caracterizados quanto aos aspectos físicos, químicos e térmicos. Suas propriedades foram colocadas em perspectiva para apresentar considerações para aplicações em biocombustíveis, materiais e precursores. Os rendimentos do processo de pirólise rápida em escala piloto alcançaram valores interessantes, mesmo se comparados com as condições de laboratório otimizadas. Os resultados indicaram maiores valores de aquecimento (22-27 MJ kg-1) para bio-óleo, carvão e material da crosta. O maior teor de água do extrato aquoso teve efeito negativo para sua aplicação como combustível. A relação lignina/carboidrato para o bio-óleo (2,82) e extrato aquoso (0,53) identificou uma maior concentração de compostos derivados da lignina nas primeiras unidades, principalmente siringil. O bio-óleo e o extrato aquoso apresentaram compostos químicos com diversas funcionalidades, como o siringaldeído e o levoglucosan, ampliando seu potencial de aplicação para produtos de maior valor agregado além da energia. Uma das estratégias para agregar valor ao bioóleo é o fracionamento da mistura. Nesse contexto, a lignina pirolítica é obtida a partir do bio-óleo, que é a fração insolúvel em água do bio-óleo de pirólise rápida. A separação da lignina pirolítica pode melhorar a extração de monofenóis. Estudos revelam a eficácia dos compostos fenólicos aromáticos derivados da lignina como antioxidantes e antimicrobianos. Neste estudo, foram utilizadas soluções aquosas de acetona, para melhorar o fracionamento da lignina pirolítica de eucalipto. A fração mais solúvel resultou em uma fração mais homogênea, concentrando compostos fenólicos, carboxílicos e de menor peso molecular. A atividade antioxidante foi atribuída principalmente a compostos fenólicos com substituintes metoxil. Frações de lignina pirolítica também apresentaram ação antimicrobiana contra Staphylococcus aureus e Escherichia coli. Outra estratégia para a utilização do bio-óleo é o aprimoramento, com foco na sua conversão em compostos químicos finos. Esses compostos podem ser usados como blocos de construção na síntese de outros compostos químicos e/ou polímeros. Como os compostos fenólicos são componentes importantes do bio-óleo. Portanto, entender seu comportamento de reação durante a hidrogenação ajuda a esclarecer a rede de reação durante a melhoria do bio-óleo.

PALAVRAS-CHAVE: Bio-óleo. Pirólise. Madeira. Biomassa. Catálise. Antioxidante. Lignina Pirolítica.

ABSTRACT

The use of biomass by thermochemical route is one of the available alternatives for optimizing resources, minimizing waste disposal and adding value. Among these, fast pyrolysis employs moderate temperatures and short residence times to maximize the achievement of the liquid fraction, which is called bio-oil. This fraction has a high energy density (when compared to wood), with great potential for the production of renewable fuels. However, it has some properties that hinder its direct use as a fuel, requiring an improvement, aiming to obtain products that can be used directly as fuel and or compounds of interest to the chemical industry. The present study has as main objective to develop applications for the liquid obtained through the fast pyrolysis of forest biomass. Based on a circular bioeconomy strategy, eucalypt wood fines rejected from a Kraft pulp line were used as starting material in a pilot-scaled fast pyrolysis process. The bio-oil and its coproducts were characterized regarding their physical, chemical and thermal aspects. Its properties were put into perspective to present considerations for applications in biofuels, materials and precursors. The yields of pilot-scaled fast pyrolysis process reached interesting values even if compared with optimized laboratory conditions. The results indicated highest heating values (22-27 MJ kg^{-1}) for bio-oil, char and crust material. The higher water content of aqueous extract had negative effect for its application as fuel. The lignin/carbohydrate ratio for the bio-oil (2.82) and aqueous extract (0.53) identified a higher concentration of lignin-derived compounds in the first, mainly syringyl units. Bio-oil and aqueous extract presented chemical compounds with many functionalities, such as syringaldehyde and levoglucosan, expanding their potential application for higher value-added products besides energy. One of the strategies to add value to bio-oil is the fractionation of the mixture. In this context, pyrolytic lignin is obtained from bio-oil, which is the water-insoluble fraction of the fast pyrolysis bio-oil. The separation of pyrolytic lignin can improve the extraction of monophenols. Studies reveal the effectiveness of aromatic phenolic compounds derived from lignin as antioxidants and antimicrobials. In this study, aqueous acetone solutions were used to improve the fractionation of eucalypt pyrolytic lignin. The more soluble fraction resulted in a more homogeneous fraction, concentrating phenolic, carboxylic and lower molecular weight compounds. The antioxidant activity was mainly attributed to phenolic compounds with methoxy substituents. Pyrolytic lignin fractions also showed antimicrobial action against *Staphylococcus aureus* and *Escherichia coli*. Another strategy for the use of bio-oil is the improvement focused on converting it into fine chemical compounds. These compounds could be used as building blocks in the synthesis of other chemical compounds and or polymers. Therefore, understanding their reaction behavior during hydrogenation helps to clarify the reaction network during bio-oil improvement.

KEYWORDS: Bio-oil. Pyrolysis. Wood. Biomass. Catalysis. Antioxidant. Pyrolytic Lignin.

LIST OF FIGURES

CHAPTER I

CHAPTER II

CHAPTER III

CHAPTER IV

SUPPLEMENTARY MATERIAL

LIST OF TABLES

CHAPTHER II

CHAPTER III

CHAPTER III

SUPPLEMENTARY MATERIAL

TABLE OF CONTENTS

CHAPTER IV - ELUCIDATION OF THE BEHAVIOR OF MODEL COMPOUNDS OF BIO-OIL IN HYDROGENATION ON Ag/SiO_2 AND Pd/SiO_2 CATALYSTS

CHAPTER I

GENERAL ASPECTS

I.1 GENERAL INTRODUCTION

The increase in world demand for energy, which in 2050 is likely to be double the energy used in the year 2000 (BULUSHEV; ROSS, 2011), together with the decrease in resources from non-renewable sources lead to the search for alternative technologies, materials and more strategies to produce energy, fuels and chemicals. Under this new energy scenario, the development of new processes and the use of renewable materials to achieve energy production and environmentally sustainable chemicals, are of paramount importance to satisfy the energy consumption requirements required by humanity. In this context, the use of biomass as a renewable raw material to deal with energy issues in the current market is gaining more and more attention (REMÓN et al., 2016). Among the different biomass recovery processes, pyrolysis is the most mature and industrially used technology. This thermochemical conversion technology produces solid (charcoal), liquid (bio-oil) and gaseous products, which can be converted into biochemicals and liquid intermediates (JACOBSON; MAHERIA; DALAI, 2013; PARK et al., 2013). The reuse of these products is part of the concepts proposed in the biorefinery, especially the total use of the biomass source with minimal loss of energy and mass (KAMM et al., 2005).

Lignocellulosic bio-oils contain biomass degradation products from cellulose, hemicellulose and lignin (CHATTANATHAN; ADHIKARI; ABDOULMOUMINE, 2012); its composition depends a lot on the process, separation and condensation efficiency, as well as on the type of material used to obtain this oil (TRANE et al., 2012). This being a complex mixture of oxygenated compounds such as alcohols, organic acids, ketones, esters and with the possible presence of small particles of coal; bio-oil can be considered a micro emulsion: in which the continuous phase is an aqueous solution of the products of cellulose and hemicellulose fragmentation, which stabilizes the discontinuous phase, which are the pyrolytic lignin macromolecules (BRIDGWATER, 2012).

These bio-oils are a promising source of liquid biofuels, having the potential to replace conventional fossil liquid fuels (HU; GHOLIZADEH, 2020; JACOBSON;

MAHERIA; DALAI, 2013; LV et al., 2007; PARK et al., 2013). However, this product has some undesirable properties, such as low calorific value, high moisture content, instability, corrosivity, high viscosity and high Oxygen/Carbon ratio (LU; LI; ZHU, 2009; OASMAA; MEIER, 2005). Preliminary research on the use of bio-oil has focused on obtaining separated fractions in a relatively simple way, with the use of conventional technologies, such as liquid chromatography, extraction, centrifugation and distillation (CZERNIK; BRIDGWATER, 2004). For the use of bio-oil as a substitute for liquid fossil fuels, upgrading processes are necessary, these processes can be: physical, through the addition of solvents to reduce viscosity, emulsification in diesel oil; or chemicals, which are based on hydrodeoxygenation, catalytic cracking using zeolites and steam reforming. The chemical and catalytic routes are of greatest interest due to the possibility of obtaining chemicals with high added value and biofuels with properties similar to conventional ones (VENDERBOSCH; PRINS, 2010). In general, the main difficulty in the improvement processes of bio-oil is the formation of carbonaceous deposits in the catalytic bed, originated from heavy compounds derived from lignin (WANG; RINALDI, 2013, 2016).

In this context, the development of applications for products obtained through fast pyrolysis from forest biomass has great relevance to overcome the difficulties associated with the efficient use of biomass. The information obtained and evaluated in this work can contribute to improve the use of forest biomass and for a more sustainable agro-industrial sector. This thesis was developed in chapters to promote a pleasant reading and facilitate a satisfactory understanding of all the concepts covered. **CHAPTER I** provides a review of the concepts inherent in the pyrolysis process of lignocellulosic materials, as well as the possibilities and challenges to be overcome for the efficient use of bio-oil. **CHAPTER II** presents the physical-chemical characterization of bio-oil and co-products, produced by fast pyrolysis, on a pilot scale, of fine eucalypt wood. In addition, considerations are presented for applications in biofuels, materials, and precursors, based on the properties of properties of each product. **CHAPTER IV** presents an evaluation of the products formed in the hydrogenation of model compounds of bio-oil and lignin, as well as a brief discussion of the mechanisms involved in the conversions.

I.2 HYPOTHESIS AND OBJECTIVES

I.2.1 HYPOTHESIS

"Pyrolytic liquids could be used to obtain higher value-added products and chemicals."

I.2.2 MAIN OBJECTIVE

This work aimed to investigate and develop products and processes for the optimal use of liquid products from forest biomass pyrolysis.

I.2.3 SPECIFIC OBJECTIVES

- Characterize and propose applications for fast pyrolysis bio-oil produced in a pilot plant.
- Evaluate the potential of the water-insoluble fraction of the bio-oil to produce antioxidant and antibacterial agents.
- Develop a metal catalyst anchored in silica, for the catalytic hydrogenation of bio-oil model compounds.

I.3 LITERATURE REVIEW

I.3.1 WOOD CHEMISTRY

Wood is a natural biocomposite, whose complex composition and organization is due to the different cell types that act synergistically in order to supply the main needs of a plant (ROWELL, 2012). Wood is the secondary xylem of vascular plants, being the result of the differentiation of cells in the exchange meristem for horizontal and vertical transport of water, nutrients and extracts (SJÖSTRÖM, 1993). In addition, it has the function of providing mechanical support to the plant structure, as well as performing synthesis and storage of biomolecules (ROWELL, 2012). Its structure is formed by an interconnected network of cellulose (30-55 wt%), hemicelluloses (13-35 wt%) and lignin (14-36 wt%) (ROWELL, 2012). The proportion of these constituents varies with each tree species. However, a greater amount of polymeric carbohydrates is generally found than lignin (SJÖSTRÖM, 1993). In addition to the macromolecular components responsible for the composition of the cell wall, there is the presence of low molecular weight compounds, the extractives (tannins, fatty acids, resins) and inorganic salts (GOODWIN; MERCER, 1983).

I.3.1.1 Cellulose

Cellulose is the most abundant biopolymer in nature. It is an anhydroglucose homopolymer of molecular formula $(C_6H_{10}O_5)_n$, composed of the union of β-D-glucopyranose molecules through the β-1,4-glycosidic bonds (HOENICH, 2006), with the repetition unit being the cellobiose (**Erro! Fonte de referência não encontrada.**). The degree of polymerization of native celluloses depends on the source, ranging from 6,000 to 8,000 for wood (SEVERIAN, 2008). At the ends of the cellulosic chain, two distinct groups are observed, being a non-reducing group, represented by the cyclic structure, and another reducing one, with an aliphatic structure with a carbonyl (SHAFIZADEH, 1982).

Cellulose molecules form inter and intramolecular hydrogen bonds. Aggregating in the form of microfibrils, which have unordered (amorphous) regions that alternate,

periodically or randomly, with ordered (crystalline) regions (IWAMOTO; NAKAGAITO; YANO, 2007), forming a highly inert structure and inaccessible to chemical reagents, being very difficult to break under mild conditions (FRASSOLDATI; RANZI, 2019). The amorphous zone is more reactive than the crystalline one, this generates complexities in the thermal decomposition of cellulose (SEVERIAN, 2008).

I.3.1.2 Hemicelluloses

Hemicelluloses are the branched-chain and low molecular weight polysaccharides (**Erro! Fonte de referência não encontrada.**). It is a heteropolymer formed by pentoses (xylose and arabinose), hexoses (glucose, mannose and galactose), uronic acids and acetyl groups (FENGEL; WEGENER, 1989). Main chain carbohydrates in hemicelluloses are usually connected by β-1-4 glycosidic bonds. The classes of hemicelluloses are named according to their main carbohydrate, which are xylans, mannans and xyloglucans. Different classes of hemicelluloses are found in different parts of the plant, in addition to being variable according to the species in which it is found. In the case of hardwoods, hemicellulose is basically formed by heteroxylans (FRASSOLDATI; RANZI, 2019).

Hemicelluloses act as a binding agent between cellulose, this set forming the solid structure that makes up the primary plant cell wall (HAYASHI; MARSDEN; DELMER, 1987). In addition, it is an amorphous polymer, this is due to the random distribution of its carbohydrates, without ordered repetition units of β-1-4 bonds. This makes it much more susceptible to hydrolysis and thermal extractions (PETERSON et al., 2008).

FIGURE I.1 - DIAGRAM OF THE MAIN MACROMOLECULES PRESENT IN LIGNOCELLULOSIC MATERIALS

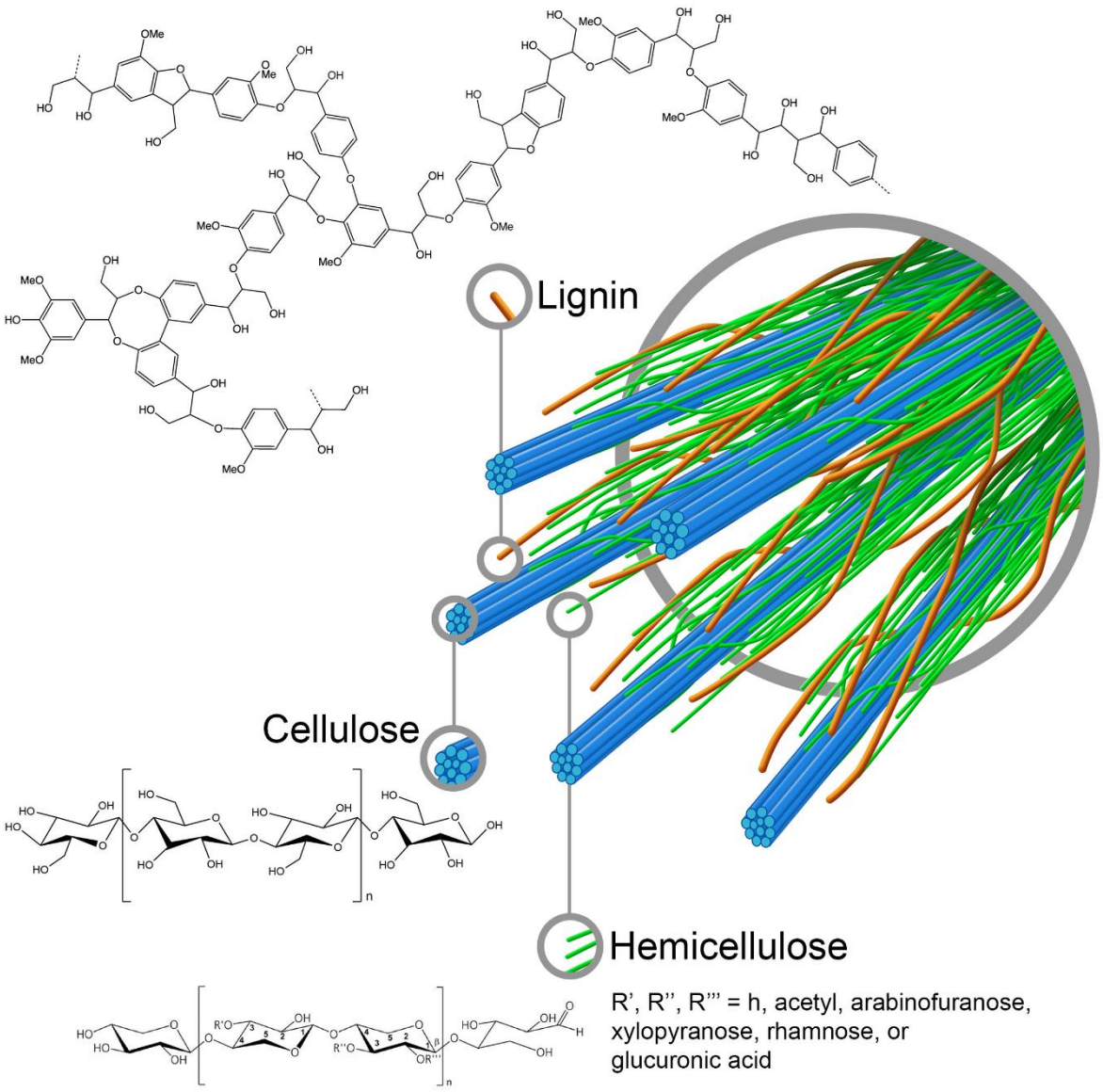

I.3.1.3 Lignin

Lignin is the second most abundant organic polymer in nature, after cellulose, being the most abundant aromatic renewable material (HATAKKA, 2001). In the plant, this macromolecule acts by providing rigidity to the plant tissue. In addition, lignin protects the plant against biochemical stress by inhibiting the enzymatic degradation of other components (GRABBER, 2005).

Lignin consists of methoxylated phenylpropane units. Its structure is formed from three precursor monolignols. These monolignols have different levels of methoxylation: The *p*-coumaryl alcohol of origin to the non-methoxylated aromatic group, *p*-hydroxyphenyl; Guaiacyl, with a methoxyl, originated from coniferyl alcohol; The syringyl aromatic group, from synaphyl alcohol, bimethoxylated (FIGURE I.2). The quantity, chemical composition and characteristics of lignin are influenced by the species, growing conditions and stage of development of the plant. In hardwoods, such as eucalypt, syringyl (50-75%) and guaiacil (25-50%) units are present (GELLERSTEDT, G. HENRIKSSON, 2008).

As a result of the links between the monomeric units a complex, three-dimensional and amorphous molecule is formed. Among the bonds distributed by the lignin polymer, approximately two thirds are ether bonds and one third are condensed, carbon-carbon bonds. (HENRIKSSON, 2010). During the formation of the lignin polymer, the type of bond is driven by the monolignol composition. The phenylpropane units have a series of characteristic bonds with each other and the most abundant is of the β-O-4 type. In hardwood lignins, there is a greater occurrence of β-O-4 type bonds, due to the predominance of syringyl units, which do not have the C5 reactive carbon available (GELLERSTEDT, G. HENRIKSSON, 2008). However, C5 available in guaiac units, allows reactions with other aromatic phenylpropane structures. Therefore, forming bonds that are more difficult to be cleaved, leading to greater thermal stability than lignin S (DEL RÍO et al., 2005).

FIGURE I.2 - BASIC UNITS OF LIGNIN AND THEIR RESPECTIVE PRECURSOR MONOLIGNOLS

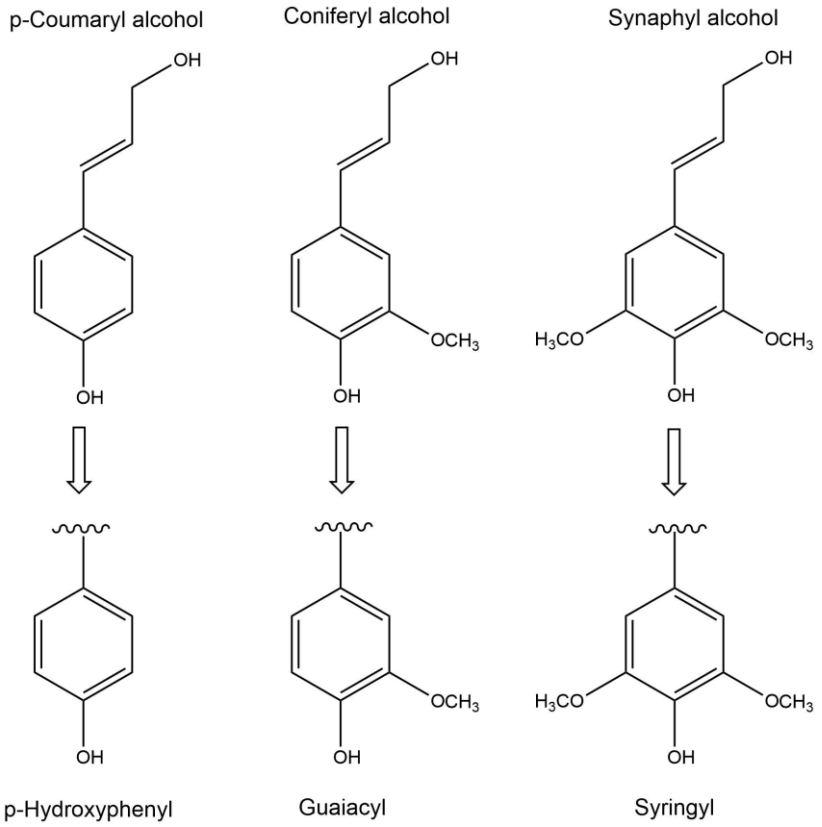

The complexity of the lignin structure is increased by the presence of several functional groups. The most common are the methoxy groups, hydroxyl groups, benzyl alcohol and a few terminal aldehyde groups. In addition, the aromatic rings and hydroxyl groups of lignin allow the formation of bonds with hemicellulose and pectins, forming the well-known Lignin Carbohydrate Complex (HENRIKSSON, 2010).

I.3.2 THERMOCHEMICAL CONVERSION PROCESSES

The concern with environmental conservation has increased the interest in the use of biomass resources. Biomass can be converted into more valuable forms of energy and products through a number of processes, including chemical, thermal, biological and physical processes. Among the thermochemical processes, pyrolysis, gasification and combustion stand out (BRIDGWATER, 2012). Gasification, whose main product is fuel gas, this process has been used for several years in pre-commercial activities, however, there are still few successful operational units

(HOFBAUER, 2009). Combustion is a well-established commercial technology with applications in most countries, heat is the main product and can be used to produce steam and generate electricity. Pyrolysis has been applied for thousands of years to the production of coal. However, in the last few years pyrolysis processes at moderate temperatures and short reaction times have become one of the promising pathways for converting biomass (BRIDGWATER, 2012). This is because the process provides a higher yield of liquid products. They can be used in a variety of applications (CZERNIK; BRIDGWATER, 2004), thus playing an important role in the production of biofuels and chemicals from clean and renewable sources (YANG et al., 2007).

I.3.2.1 Pyrolysis

Pyrolysis is the thermal decomposition process that occurs in the absence of oxygen. It is important to note that pyrolysis is the first stage of combustion and gasification (BASU, 2010; JAHIRUL et al., 2012). During the pyrolytic process, long chains of carbon, hydrogen and oxygen present in complex biomass macromolecules are broken down into smaller and simpler molecules, providing the three main products: gas, liquids (tar or oil) and charcoal (BASU, 2010). These three products are always produced, but the proportions can vary over a wide range, depending on the pyrolysis process, the operating conditions and the biomass used. In addition, pyrolysis is a more efficient conversion method compared to other thermochemical technologies and allows for raw material flexibility (BRIDGWATER, 2012; JAHIRUL et al., 2012).

The wood pyrolysis process is very complex, involving several simultaneous and successive reactions that occur when the organic raw material is heated. The pyrolysis processes have different reaction pathways, due to the variability of biomass composition. Carbohydrates and lignin, which make up most of the wood, decompose by different mechanisms, at different rates of degradation and different temperature ranges (BASU, 2010; KAN; STREZOV; EVANS, 2016). During the thermal decomposition of wood, hemicelluloses are the first to decompose, between 250-350 °C, followed by cellulose at 300-400 °C. Levoglucosan is the main pyrolysis product (KAN; STREZOV; EVANS, 2016). The degradation of lignin occurs over a wide

temperature range (250-500 °C). However, the interaction between these components during pyrolysis can change the behavior of biomass during pyrolysis (KAN; STREZOV; EVANS, 2016; STEFANIDIS et al., 2014).

During the pyrolysis of the wood different stages are observed. Initially, drying occurs at around 100 °C, when free moisture and a little loosely bound water is released (BASU, 2010; VENDERBOSCH; PRINS, 2011). Second, in the range of 100-300 °C, exothermic dehydration occurs causing the release of water and gases of low molar mass, such as CO and CO_2. Then, at temperatures above 200 °C, the composition of the polymers that make up the biomass starts due to the primary pyrolysis reactions, producing primary charcoal, condensable gases (precursors of bio-oil) and non-condensable gases. Finally, during the last stage (~ 300-900 °C), condensable gases can break even further by secondary cracking reactions, forming secondary charcoal and non-condensing gases, such as CO, CO_2, H_2 and CH_4. Therefore, if the product of interest is bio-oil, the condensable gases must be removed quickly from the reaction zone in order to condense them. In general, the general decomposition occurs partially in homogeneous gas phase reactions and partially through heterogeneous thermal gas-solid reactions, catalyzed by charcoal (STEFANIDIS et al., 2014).

The thermochemical conversion of wood during pyrolysis is influenced by several factors, which affect the conversion time, the distribution and the quality of the products. The most important parameters to be considered are the composition of the raw material and its physical and chemical characteristics, the type of pyrolytic unit, as well as operational parameters such as heating rate, temperature, pressure and residence time of steam or solid in the reaction (JAHIRUL et al., 2012; KAN; STREZOV; EVANS, 2016; SHARMA; PAREEK; ZHANG, 2015).

The composition of biomass influences the pyrolysis process, as each component has unique pyrolysis reaction pathways, thus giving rise to different products. In general, volatiles are mainly derived from cellulose and hemicelluloses, while lignin predominantly originates from coal residues. In addition, the pyrolysis process can be influenced by the physical and chemical properties of biomass, such

as specific heat, thermal conductivity and emissivity, density, and moisture content. The particle size has a significant effect on the mass and heat transfer phenomena. Larger particles imply larger thermal gradients, longer residence time and the possibility of secondary cracking, which ultimately reduces the liquid yield (SHARMA; PAREEK; ZHANG, 2015).

Lower process temperatures and longer steam residence times favor charcoal production. High temperatures and longer residence times increase the conversion of biomass to gas, and moderate temperatures and short residence times are ideal for the production of liquids. The rate of heating also influences the yield of the products to a great extent. Fast heating rate causes fast biomass fragmentation, therefore it generates more gas and less coal. Bio-oil production can be increased and secondary reactions minimized, with fast heating and cooling. Slow heating rates lead to higher charcoal production (SHARMA; PAREEK; ZHANG, 2015; STEFANIDIS et al., 2014).

Considering the different operational parameters and, in particular, the residence time and the heating rate, the pyrolysis processes can be divided into three main categories: slow (or conventional), fast and flash pyrolysis (FIGURE I.3). In slow pyrolysis and carbonation, carbonization is the primary process, which maximizes charcoal production, while in fast pyrolysis, bio-oil is the main product of interest (VENDERBOSCH et al., 2010). Bio-oil is a liquid mixture of organic compounds of various types, such as sugar monomers and oligomers derived from cellulose and hemicellulose, sugar derivatives, such as carboxylic acids, alcohols, aldehydes, ketones, esters, in addition to phenolic derivatives of lignin, lignin pyrolytic and a high water content (HU et al., 2013; MOHAN; PITTMAN; STEELE, 2006).

The FIGURE I.3 indicates the distribution of product yields obtained from different pyrolysis modes, showing the flexibility that can be obtained by simply changing the process conditions. In summary, fast pyrolysis is carried out at approximately 500 °C, a short residence time for hot vapor, around 1 second. Flash pyrolysis can achieve up to 75% bio-oil yield, applying an even higher temperature and shorter residence time than fast pyrolysis. The intermediate pyrolysis also takes place at around 500 °C, the residence time of hot vapor varies from 10 to 30 seconds, and

the liquid product obtained has two phases. Carbonization (slow pyrolysis) is carried out between 300 and 500 °C, long residence time of the vapor (JAHIRUL et al., 2012; KAN; STREZOV; EVANS, 2016; PAPARI; HAWBOLDT, 2015)

FIGURE I.3 – MAIN PYROLYSIS METHODS, IMPORTANT PARAMETERS (A) AND PRODUCT YIELDS (B)

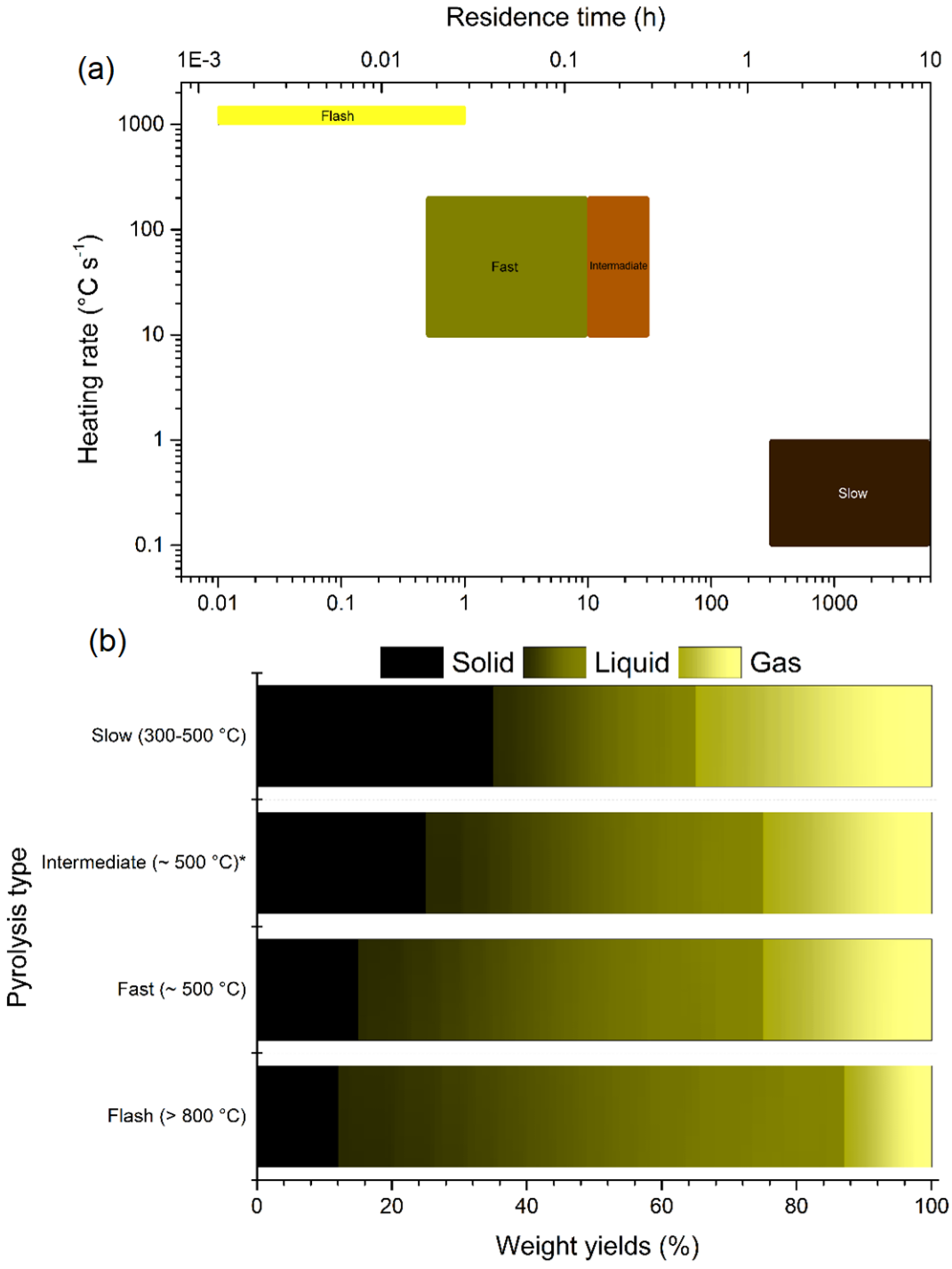

* Two phases are formed in the liquid product.

I.3.3 BIO-OIL APPLICATIONS

Among pyrolytic products, the production of liquid oils from biomass has been the focus of interest for several reasons. Among them: pyrolysis oils have a higher energy density, which can cause transportation and handling costs; can be used as conventional fuel in boilers and turbines (JAHIRUL et al., 2012; MOHAN; PITTMAN; STEELE, 2006). In addition, they represent a wide possibility of acting as precursors of high value-added chemical products, which may replace petrochemical products (VENDERBOSCH; PRINS, 2011). However, the main disadvantage is its complex chemical and physical characteristics: its instability; corrosivity, due to the presence of carboxylic acids, such as acetic acid; high water content, usually ranging from 20% to 30% by weight; high content of oxygenated compounds, which makes these organics susceptible to polymerization (HU; GHOLIZADEH, 2019; JACOBSON; MAHERIA; DALAI, 2013).

All this complexity of the bio-oil is due to the combined result of the biomass properties, the pyrolysis operation parameters, the oil recovery and the storage conditions. Although pyrolytic oil added-value chemicals are interesting possibilities, the low concentration in the oil and the recovery costs make this approach economically unfeasible (LU et al., 2011). Even with improvements in technologies and production on a larger scale (HU; GHOLIZADEH, 2019), products from pyrolysis still do not compete with petrochemicals. To become attractive, pyrolysis products must have low cost and perform as well as those of fossil origin (TUCK et al., 2012).

Currently, the development processes of uses for bio-oil are focused on the recovery of phenolic compounds from the lignin fraction (WANG et al., 2016), resins, sugars and polyols (LI et al., 2017), carboxylic acids, furfural derivatives and levulinates (HU et al., 2012, 2017).

I.3.3.1 Bio-oil as fuel

Bio-oil can be used directly or co-fed with fossil fuels such as fuels for boilers and ovens. It has some advantages in terms of use, as boiler fuel, compared to heavy fossil fuels. For example, combustion of bio-oil emits less CO_2, NO_x and SO_x than fossil fuels, this can contribute to the reduction of air pollution (HOU et al., 2016). However, bio-oil is an inefficient fuel when compared to fossils. The most evident difference is the water content, which does not reach 0.5% in the case of fossils, but can reach up to 30% in the case of bio-oil, all of this humidity reduces the calorific value. In addition, the lower pour point and flash point, and the high viscosity of bio-oil, in relation to conventional fuels, indicate that the pumping and burning systems must be modified, so that the use of bio-oil in boilers for example. In addition, the amount of solid particulate material in the bio-oil must be reduced, in order to avoid blocking the burner nozzles and sprayers (HU; GHOLIZADEH, 2020).

Even with its undesirable properties, the direct use of bio-oil as a fuel has been explored. Studies in European countries have shown that burning bio-oil could cost up to 50% less to generate the same amount of heat generated by burning fossil fuel. This is due to the cost of labor, price of biomass, among other factors (BRAMMER; LAUER; BRIDGWATER, 2006). Some companies have shown that bio-oil can replace fossil fuels in large-scale boilers, with admissible combustion performance. With considerable reduction in NOx emissions (LEHTO et al., 2014). Nevertheless, However, different bio-oils showed different levels of emissions. In addition, inhomogeneity and high water content in bio-oil generate more emissions (CHIARAMONTI et al., 2014; LEHTO et al., 2014).

Co-feeding bio-oil with fossil fuels is an strategy to reduce the need for adaptations to the burner system, and also to avoid possible blockages in the injection systems. Some studies (BARI, 2014; GE et al., 2015; HOU et al., 2016) show that bio-oil can be co-burned, with different fossil fuels, in concentrations of up to 5%, without noticeable damage to the oven. However, amounts greater than 5% of co-fed bio-oil, require modifications to the flaring system.

A promising strategy to overcome the problems inherent in bio-oil is improvement through hydrodeoxygenation (HDO) (HAN et al., 2019; MANTE et al., 2015). HDO is a catalytic process, usually carried out under high pressure and high temperature, to reduce the oxygen content of the bio-oil (BARI, 2014; CHIARAMONTI et al., 2014; GE et al., 2015; HAN et al., 2019; LEHTO et al., 2014; VAN DE BELD; HOLLE; FLORIJN, 2013). After the upgrade, the bio-oil, converted into biofuel, can reach parameters similar to fossil fuel oil, reaching practically identical calorific value. This occurs due to the drastic reduction in the water content and the significant decrease in the amount of oxygen (ZACHER et al., 2014). However, this improvement process is limited by the fast deactivation of the catalysts, due to the extensive formation of coke. Aromatic compounds and sugars present in bio-oil are identified as the main responsible for the formation of coke (HAN et al., 2019). In addition, the biggest difficulty with this approach is the cost of upgrading bio-oil to biofuels. The cost is increased mainly by loss of material, in the conversion of bio-oil organics into biofuels, by the formation of coke (GHOLIZADEH et al., 2016).

Different types of catalysts have already been used to update the bio-oil. Initially, catalysts already used in oil refineries, in hydrodesulfurization and hydrodenitrogenation, such as NiMo/Al_2O_3 and CoMo/Al_2O_3, were evaluated. In a few hours of operation, these catalysts were severely deactivated, due to the high water content, acidity and the formation of coke, which makes it difficult to apply these types of catalysts (ELLIOTT; BAKER, 1986; HAN et al., 2019). Carbon-anchored noble metal catalysts have also been tested (HAN et al., 2019). A longer service life of the catalyst has been achieved. However, the high cost of these catalysts and the difficulty in regenerating a carbon-based catalyst, makes it difficult to apply on a large scale. The literature points out that catalysts based on the HZSM-5 zeolite can provide greater yield in the production of hydrocarbons, providing high yields in liquid products and selectivity for the production of propylene (ADJAYE; BAKHSHI, 1995; BRIDGWATER, 2012), and catalysts based on silica , have greater selectivity for the production of aliphatic compounds (BRIDGWATER, 2012). Most studies with the HZSM-5 zeolite are focused on comparing yields between processes with or without the use of the catalyst (AHO et al., 2008; CAMPANELA; HAROLD, 2012; WANG et al., 2012), with the little

explored catalyst activity investigation. Some studies show efficiency in the use of Pd/C catalyst (palladium anchored on activated carbon) in depolymerization and hydrogenation of alkaline lignins, producing monomeric phenolic compounds (CHEN et al., 2018; JIE-WANG; GUI-ZHEN; CHUN-DE, 2012; SHU et al., 2015, 2018).

Noble metal catalysts supported on ceramics are considered the most suitable catalysts for HDO in bio-oil due to their dual properties: metals and acidic sites (Jafarian et al., 2019). The HDO process is still in the early stages of development. Further studies are needed to identify the reasons for the deactivation. In addition, type of reactor, type of catalyst and process conditions, should also be studied in more detail, in order to arrive at an economically viable process (HU; GHOLIZADEH, 2020).

I.3.3.2 Chemicals from the bio-oil

Great of the chemicals used by humanity are of fossil origin. However, due to price instability and environmental concerns about the use of non-renewable resources, they have stimulated research in the production and separation of chemicals from alternative sources, such as bio-oil (HU et al., 2020). Different solvents have already been used to separate the chemical compounds present in the bio-oil such as water, alkaline solutions, ketones, ethers, supercritical CO_2, ethyl acetate, n-hexane and others (GARCIA-PEREZ et al., 2007; SHAH et al., 2017; WANG et al., 2010).

Water, sodium hydroxide, dichloromethane and hydrogen chloride to extract the phenolic compounds from the bio-oil (WANG et al., 2014b). The phenols can be extracted from the bio-oil by adding ethyl ether and NaOH (10 wt%) to the bio-oil. Thus, phenol is extracted in the form of sodium phenoxide. Then, the phenol salt is converted to phenol by the addition of a strong acid (SHAH et al., 2017).

Water can be used to separate sugars and polar compounds, such as furfurals and furfuryl alcohol. These compounds of the phenolic compounds, can be converted into levulinic acid by acid catalysis. This chemical is a precursor in the manufacture of other value-added chemicals (HU et al., 2012). When water is added to the bio-oil,

precipitation of pyrolytic lignin occurs (MULLEN; BOATENG, 2011). Pyrolytic lignin are fragments of lignin, mostly phenolic compounds. This fraction of the water-insoluble bio-oil can be transformed into liquid fuels through upgrading processes (RINALDI et al., 2016). Phenolic compounds also have antioxidant properties, being the focus of current research. Antioxidant compounds in different composite materials, as well as medicines, dietary products and biofuels susceptible to oxidative processes (GOSSELINK et al., 2004; POUTEAU et al., 2005). In addition, phenolic compounds have antibacterial activity (DONG et al., 2011; YANG et al., 2016).

CHAPTER II

PILOT-SCALED FAST PYROLYSIS CONVERSION OF EUCALYPTUS WOOD FINES INTO PRODUCTS: DISCUSSION TOWARD POSSIBLE APPLICATIONS IN BIOFUELS, MATERIALS AND PRECURSORS

BioEnergy Research. p.1 - 12, 2020.
DOI: 10.1007/s12155-020-10094-y

II.1 INTRODUCTION

Petroleum is the main feedstock for fuels, and its derivatives are also the basis for most engineering materials and fine chemicals. These applications are considered one of the main causes of global warming. Moreover, there are other concerns with peak oil, security supply, price instability and global equity. Thus, putting the human kind, especially the scientific community, on a trajectory toward fast mentality change. In order to change this panorama, innumerous research groups (ISIKGOR; BECER, 2015) have engaged in biomass-to-fuel/chemical projects to supplement the petroleum production chain. Pyrolysis is one of the most interesting and discussed process to convert biomass into fuels or fine chemicals (MALINS, 2017; SINGH et al., 2016). It is defined as a thermal decomposition process of biomasses at inert atmospheres resulting in char, bio-oil and non-condensable gases which yields differently according to the processes parameters (PIDTASANG; SUKKASI; PATTIYA, 2016; ROUX et al., 2015).

Fast pyrolysis is a thermal route-based biorefinery especially designed to improve the yields of liquid products by controlling the reaction temperature near to 500 °C, and increasing significantly the heating and heat transfer rates usually via fluidized bed. The dark brown organic liquid, referred to as bio-oil, is the main product obtained in this process and it shows potential as fuel and as a precursor for obtaining hydrocarbons. In fact, as deeply discussed by Isikgor and Becer (ISIKGOR; BECER, 2015), the chemical compounds usually found in fast-pyrolysis bio-oils could be used as precursors of a wide range of synthetic polymers such as poly(styrene), poly acrylates, poly(ethylene), and poly(acrylonitrile). The higher oxygen content of bio-oil compared to petroleum derivatives is still a barrier to overcome before turning it into a competitive fuel. However, some strategies to improve the fraction of hydrocarbons in bio-oils have been discussed in the last years (KARNJANAKOM et al., 2016; ZHANG et al., 2016b). Besides the bio-oil, the fast pyrolysis conversion of biomass results in charcoal as an important coproduct. Charcoal is commonly used as source to attend the heat requirements of the fast pyrolysis process (BRIDGWATER, 2012), but its use as char has potential for higher value-added purposes. For example: the char can be

chemically modified and used as an adsorbent to remove chemicals from aqueous solutions (LIU et al., 2012).

Considering the great potential of obtaining fuels and fine chemicals from both fast pyrolysis bio-oil and char, some research groups have investigated the techno-economic assessment of their production costs (MIRKOUEI et al., 2017; ROGERS; BRAMMER, 2012). As the bio-oil and the char costs are strongly associated to biomass transportation, it is interesting that the fast pyrolysis plants were integrated or near to well-consolidated biomass-based industries, such as a pulp and paper plant. For instance, the wood materials rejected from a pulp process can achieve up to 200 kg ton^{-1} paper in a Kraft mill (BAJPAI, 2015), and they are usually destined for low-value applications. In Brazil, the Kraft pulp lines are mostly fed by fast-growing eucalypt wood species, which had drawn especial attention over the last few years due their high productivity (EUFRADE JUNIOR et al., 2016). The wood from these species is composed by *ca.* 2-6% of extractives, 20-30% of lignin, and 55-70% of holocellulose (NEIVA et al., 2015). These characteristics placed it as the main raw material for the Kraft mills in Brazil; besides, it has showed interesting responses for bio-oil production (WANG et al., 2013).

This is a timely topic, given the growing socio-environmental-economical concerns that have motivated the petroleum replacement. In this sense, several scientific works have discussed the bio-oil production at lab-scale conditions; however, that studies on the up-scaling of this process is paramount in the development of a sustainable bioeconomy. Thus, this study aimed at the pilot-scaled fast pyrolysis conversion of wasted eucalypt fines into several products. A thoroughly physical, chemical and thermal characterization of the obtained products is presented, putting in perspective their unique characteristics in order to bring forward necessary considerations for upcoming applications on biofuels, materials and precursors.

II.2 MATERIAL AND METHODS

II.2.1 PILOT-SCALED FAST PYROLYSIS PROCESS AND RAW MATERIAL CHARACTERIZATION

Eucalypt wood fines (~ 1 mm, with 10% humidity) from a Kraft pulp line, without pretreatment, were used as start material for the coproduction of char (1), bio-oil (2), aqueous extract (3), and gas (not evaluated in this study - however, the gas is mainly composed of nitrogen (N_2), hydrogen (H_2), carbon monoxide (CO), carbon dioxide (CO_2) and methane (CH_4)). In addition, a brittle carbonaceous solid material, called crust material (4), was encrusted inside the reactor after the fast pyrolysis (FIGURE II.1). The pilot-scale fast pyrolysis reactor was set to operate in fluidized bed mode with nominal biomass supply of 20 kg/h^{-1}, with a poor oxygen atmosphere, reaction temperature at 500 °C for 5 seconds, and 100 mmH_2O of static pressure. The pyrolysis temperature was achieved by partial combustion of the biomass, with preheated atmospheric air at a flow rate of 7 $Nm^3\ h^{-1}$. Then, the reactor was fed with hot non-condensable gases. If the temperature difference between the bottom and top of the reactor was greater than 20 °C, automatic injection of atmospheric air would occur. In order to keep the temperature constant throughout the reaction bed. The fluidization gas flow was maintained at 15 $Nm^3\ h^{-1}$ during the reaction. The optimization of the process conditions, in order to obtain a higher yield of bio-oil, was performed by the equipment manufacturer according to the biomass to be used. The yield of the selected products was informed based on the total biomass fed to the reactor.

The eucalypt wood fines were characterized according to their ethanol:toluene extractives, acid insoluble lignin and ash content using the procedures developed by the National Renewable Energy Laboratory (NREL) (SLUITER et al., 2004, 2005, 2010). Their holocellulose content was quantified by using the procedure from WISE, MAXINE and D'ADDIECO (1946)

FIGURE II.1 - SIMPLIFIED REPRESENTATION OF THE PILOT-SCALED FAST PYROLYSIS CONVERSION OF EUCALYPT WOOD FINES REJECTED IN A KRAFT PULP LINE INTO SEVERAL PRODUCTS

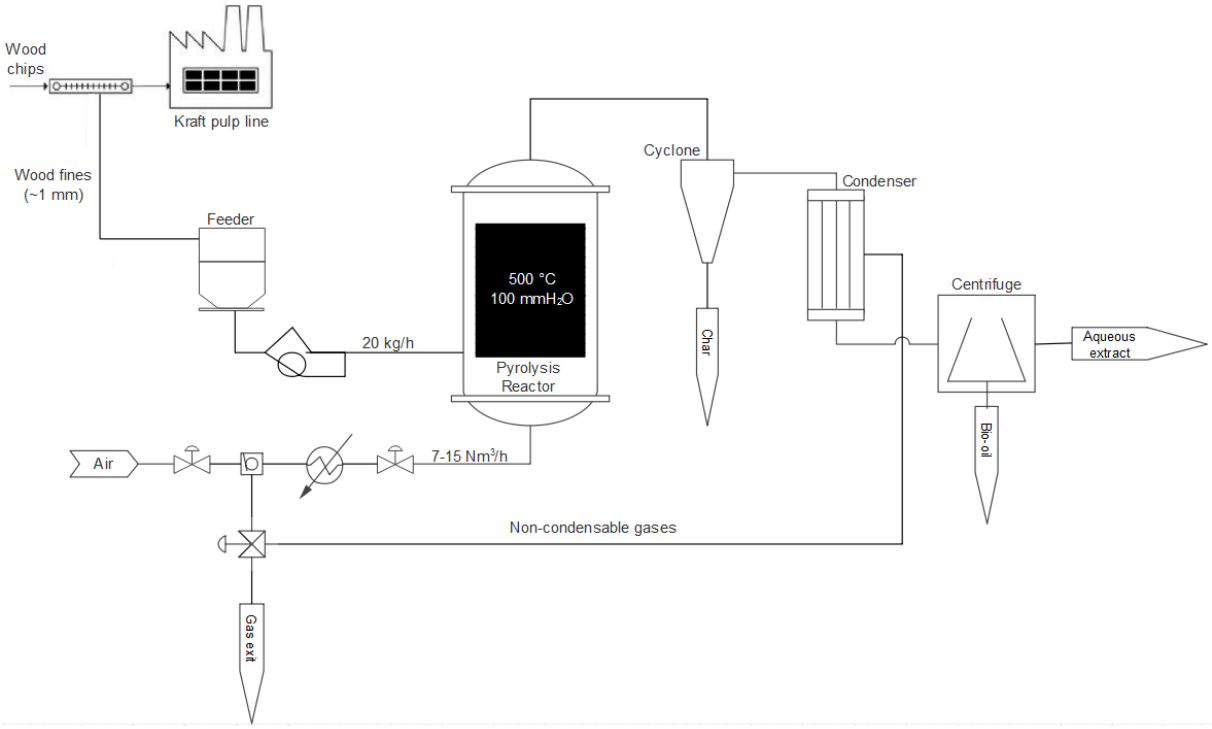

II.2.2 PHYSICOCHEMICAL AND ELEMENTAL COMPOSITION MEASUREMENTS

The bio-oil and aqueous extract were characterized as liquid biofuels according to the standardized specification for pyrolysis liquids (ASTM D7544 – 12). The physicochemical properties of the pyrolysis liquids for biofuels were evaluated by quantifying their total sulfur content (ASTM D4294-10), density at 20 °C (ASTM D4052-11), pour point (ASTM D97-15), kinematic viscosity at 40 °C (ASTM D445-15) and ash content (ASTM D482-13). The volumetric Karl Fischer (Quimis, model Q349) titration method was applied to determine the water content in the samples, and the pH of the liquids was measured in a benchtop pH meter (HANNA, model HI 2214).

The higher heating value of the start material and both solids and liquids coproducts was measured in an adiabatic calorimeter (IKA®,model C5000), and the elemental analysis was performed in a CHNS analyzer (Elementar Vario Macro Cube). Solid materials were also characterized for ash content.

II.2.3 FULL EVAPORATION - HEADSPACE - GAS CHROMATOGRAPHY (FE/HS – GC)

The FE/HS – GC (GC-2010 Shimadzu) was used for quantification of volatile organic compounds (VOCs) in the bio-oil and aqueous extract, following Lima *et al*. (2018). VOCs were introduced via a split/splitless injector (0.5 mL, 200 °C, split 1:25) and, the compounds were separated using a DB624 UI column (30 m, 0.25 mm diameter 1.40 µm thick film). Headspace equilibration temperature and time were 90 °C and 7 min respectively. The sample preparation and measurement procedures were as follow: injection of 4 µL of sample into a closed 20 mL vial using a microsyringe and immediate closure. The volatiles were converted to compound mass using a 5 points external calibration curve using a flame ionization detector (300 °C). GC oven was programmed from 40 °C (held 7 min) to 70 °C at 10 °C min^{-1} (held 6 min), then to 110 °C at 10 °C min^{-1} (held 5 min), and to 120 °C at 20 °C min^{-1} (held 5 min). Helium at a constant flux of 2.0 mL min^{-1} was used as carrier gas.

II.2.4 THERMAL STABILITY

The thermal stability and degradation behavior of the raw material, solids and liquids derived from the fast pyrolysis were investigated in a DTG-60 Shimadzu equipment. The experiments were carried out using *ca.* 10 mg in alumina pans under N_2 atmosphere with gas flow of 50 mL min^{-1}, temperature range from 25 to 900 ºC, and heating rate of 10ºC min^{-1}.

II.2.5 GC - MASS SPECTROMETRY (GC-MS) AND ANALYTICAL PYROLYSIS (PY) GC-MS

The GC-MS analysis was applied to investigate the potential of the liquid products as fine chemical precursors, following Lyu *et al*. (2015). For this, 2 mL of acetone and 20 µL of internal standard 5-iodovanillin (10 mg/ml) were added to the bio-oil or aqueous extract (100 µL). The mixture was vortexed and centrifuged (5 min, 3000 rpm), then *ca.* 1 g of anhydrous sodium sulfate was added to dehydrate, and the sample was centrifuged once again (5 min, 3000 rpm). The supernatant was collected

and analyzed by GC-MS. The extract was injected (1 µL, split 1:100 at 230 °C) into gas chromatography tandem to an ion trap mass spectrometer (Thermo, Focus GC, PolarisQ), equipped with a capillary column Thermo DB-5ms (30 m x 0.25mm, 25µm film thickness). The GC oven was set at 40 °C and held for 6 min, then to 280 °C at 7°C min^{-1} and held at 280 °C for 30 min. Helium, with gas flow of 1.0 mL min^{-1}, was the carrier gas. The GC-MS interface and ion source temperatures were 250 and 200 °C, respectively. The ion trap mass spectrometer operated in the positive impact electronic mode at 70 eV, scanning *m/z* range from 40 to 650 in a 0.59 of total scan time and emission current 250 mA.

Pyrolysis (CDS 5000 pyropobe) was carried out at 700 ºC during 10 s for the solid samples (i.e. raw material and char). The pyroprobe extra conditions were: temperature interface program from 110 to 290 ºC at 100 ºC min^{-1} held for 120 s, oven at 240 ºC, transfer line at 240 ºC, coil heater at 10 ºC s^{-1}. GC oven was programmed from 40 °C (held for 8 min) to 280°C at 7°C min^{-1} then held for 15 min. The GC-MS conditions were the same adopted in the section 2.6. This analysis was based on Kaal and Rumpel (KAAL; RUMPEL, 2009).

II.2.6 ION CHROMATOGRAPHY (IC)

To quantify the amount of carbohydrates contained in the liquid products, the samples were subjected to total acid hydrolysis with sulfuric acid 12 mol L^{-1} for 1 h at 37 ºC, followed by dilution from the reaction medium to 1 mol L^{-1} keeping for 2 h at 100 ºC in a heating block. The hydrolysate was analyzed by ion chromatography to quantify the monomeric sugars. The separation was performed on a CarboPac PA 20 column (4 mm x 250 mm, 5 µL looping, flow rate 0.5 mL min^{-1} at 30 °C).

II.3 RESULTS AND DISCUSSION

II.3.1 RESULTS

The eucalypt wood fines used as raw material in the fast pyrolysis presented 1.5 ± 0.2% of ethanol/toluene extractives, 24 ± 1% of acid insoluble lignin and 71 ± 2% of holocellulose. The fast pyrolysis of this precursor at the configured pilot-scale procedure yielded 14 ± 1% of char and 53 ± 1% bio-oil. After centrifugation, the crude bio-oil was separated in a heavy fraction (bio-oil, 30 ± 1%), and in a light fraction (aqueous extract, 22± 1%). Approximately 4% of crust material has formed. TABLE II.1 shows the product yields (liquid and charcoal) obtained from fast pilot scale pyrolysis of some lignocellulosic materials. Considering all reactor types the yield ranges from 40% to 60% for liquids and from 10% to 30% for charcoal. These values are similar to the expected yield for biomass pyrolysis (BRIDGWATER, 2006, 2003) and the values found in this study.

The char and crust material presented higher carbon content compared to the start material and liquid products (*i.e.* bio-oil and aqueous extract) – TABLE II.2. The lowest carbon content was observed for the aqueous extract. The higher heating values of the obtained coproducts increased as their carbon content increased. The ash content of the liquid products was lower compared to the solid products – char presented the highest ash content. The relative amount of nitrogen was under 0.5% for all samples, and it was concentrated mostly in solid samples. The H/C atomic ratio was notably higher for the aqueous extract compared to the other products.

The H/C ratio of the liquid coproducts had direct relationship with their water content, and the pH was acid for both liquid products (TABLE II.2 and TABLE II.3). Remarkable differences were found for water content and kinematic viscosity, meanwhile density was only 10% lower for aqueous extract (TABLE II.3). Total sulfur content measured for both liquids could be considered equal, and they are within the limit specified by the ASTM D6751 (which is 500 mg kg^{-1}) for S500 biodiesel grade. The total sulfur of these products does not attend the EU normative (EN 590:2004 and

14214:2012), which allowed values only below 50 mg kg^{-1}. Pour point was probably affected by water content, in which aqueous extract occurred at earlier temperature.

TABLE II.1 - CHAR AND LIQUID PRODUCT YIELDS FROM DIFFERENT PILOT-SCALE PYROLYSIS PROCESSES OF SOME TYPES OF BIOMASS

Biomass	Reactor type	Liquids yield (%)	Char yield (%)	Reference
Empty fruit bunch	Fluidized bed reactor	50	20	Park *et al*. (2019)
Sawdust	Fluidized bed reactor	60	15	Park *et al*. (2019)
Giant *Miscanthus*	Fluidized bed reactor	50	20	Park *et al*. (2019)
Stem wood from spruce and pine	Cyclone reactor	57	16	Johansson *et al*. (2018)
Stem wood from spruce and pine	Cyclone reactor	56	16	Sandström *et al*. (2016)
Willow	Cyclone reactor	52	20	Sandström *et al*. (2016)
Reed canery grass	Cyclone reactor	51	11	Sandström *et al*. (2016)
Brown forest residue	Cyclone reactor	50	14	Sandström *et al*. (2016)
Bark	Cyclone reactor	41	17	Sandström *et al*. (2016)
Palm shell residue	Fluidized bed reactor	60	19	Ghorbannezhad *et al*. (2020)
Pinus pinaster	Continuous fixed bed reactor	50 to 60	20 to 30	Milhé *et al*. (2013)
Switch grass	Fluidized bed reactor	55	20	Greenhalf *et al*. (2013)
Willow	Fluidized bed reactor	50	20	Greenhalf *et al*. (2013)
Giant *Miscanthus*	Fluidized bed reactor	45	30	Greenhalf *et al*. (2013)
Beech wood	Fluidized bed reactor	60	15	Greenhalf *et al*. (2013)

Bio-oil and aqueous extract presented higher mass losses at lower temperatures (FIGURE II.2a). Most of the mass loss of bio-oil sample occurred from 50 to 250 °C in three overlapped events, while the mass loss of the aqueous extract took place below 100 °C in a well-defined event (FIGURE II.2b). The solid materials had a small event bellow 100 °C. A discrete event at 650 °C was observed in the bio-oil and char. The thermal degradation of the eucalypt wood fines took place at 280 and 360 °C, and a similar event at 360 °C was detected in the char (FIGURE II.2b). The crust material had thermal decomposition behaving intermediary to the bio-oil and char, with a long event starting at 200 °C and finishing at 650 °C.

TABLE II.2 - ULTIMATE ANALYSIS, HIGHER HEATING VALUE AND ASH CONTENT OF THE OBTAINED COPRODUCTS FROM THE PILOT SCALE FAST PYROLYSIS PLANT.

Product	Relative% of total mass			Ash content	HHV[b]	H/C
	Nitrogen	Carbon	Hydrogen	(%)	(MJ kg^{-1})	atomic
Raw material	0.16 ± 0.06	43.90 ± 0.10	6.88 ± 0.20	1.12 ± 0.11	18.82 ± 0.10	1.84
Char	0.38 ± 0.09	67.18 ± 1.82	3.86 ± 0.06	12.25 ± 1.46	26.38 ± 0.91	0.68
Crust material	0.28 ± 0.04	62.24 ± 0.16	5.56 ± 0.06	2.31 ± 0.41	23.27 ± 0.99	1.06
Bio-oil	0.17 ± 0.01	53.63 ± 0.27	7.37 ± 0.22	1.27 ± 0.41	22.39 ± 0.40	1.63
Aqueous extract[a]	0.04 ± 0.02	13.18 ± 0.58	5.25 ± 1.64	0.68 ± 0.04	a	4.74

[a]Aqueous extract sample did not present ignition in the higher heating value test.

[b]Higher heating value was corrected by the ash content.

TABLE II.3 - PHYSICOCHEMICAL PROPERTIES OF THE OBTAINED BIO-OIL AND AQUEOUS EXTRACT

Property	Bio-oil	Aqueous extract
Total sulfur (mg kg^{-1})	85 ± 9.2	76 ± 9.2
Density at 20 °C (kg m^{-3})	1 225.6 ± 0.1	1 101.6 ± 0.1
pH	3.3 ± 0.1	3.3 ± 0.1
Pour point (°C)	-24 ± 0.7	-16 ± 0.7
Water content (%)	14.2 ± 0.55	65.8 ± 0.01
Kinematic viscosity at 40 °C (mm² s^{-1})	436.13 ± 9.81	1.16 ± 0.01

TABLE II.4 - PERCENTAGE OF VOLATILE ORGANIC COMPOUNDS (VOCS) IN THE BIO-OIL AND AQUEOUS EXTRACT

Organic compound	Bio-oil	Aqueous extract
	(wt.%)	
Methanol	0.40 ± 0.04	0.72 ± 0.01
Ethanol	0.27 ± 0.02	0.08 ± 0.00
Acetone	0.04 ± 0.00	0.05 ± 0.00
Acetic acid	11.22 ± 1.49	8.73 ± 1.50
Furfural	0.01 ± 0.00	0.03 ± 0.00

Bio-oil and aqueous extract were composed by 12 and 10% of volatile organic compounds, respectively, and the major identified compounds were acetic acid, methanol and ethanol (TABLE II.4).

FIGURE II.2 - THERMOGRAVIMETRIC CURVES (A) AND THEIR RESPECTIVE DERIVATIVES (B) OF THE RAW MATERIAL AND THE PRODUCTS OBTAINED FROM THE FAST PYROLYSIS PROCEDURE.

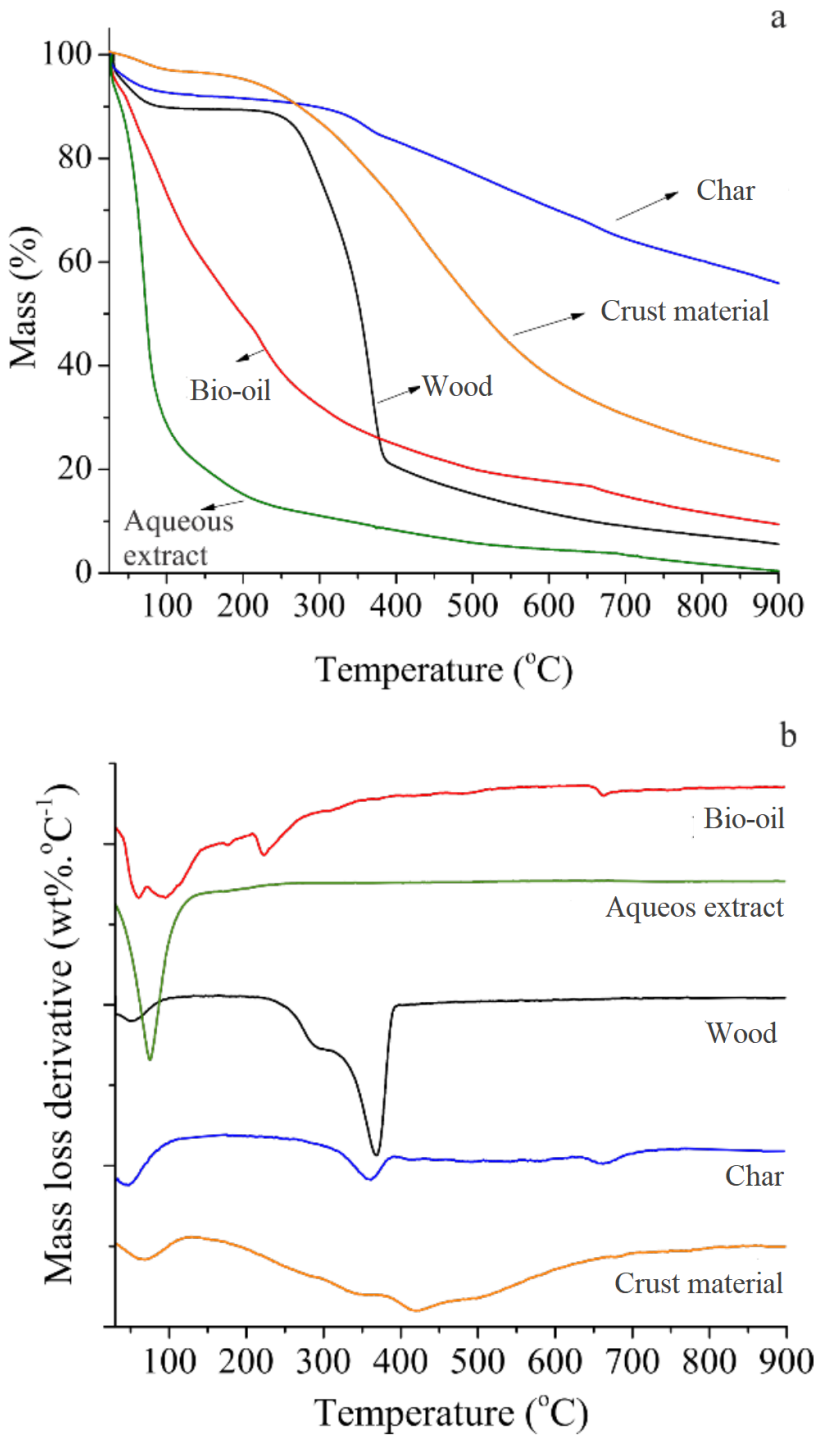

TABLE II.5 - IDENTIFICATION AND QUANTIFICATION OF BIO-OIL AND AQUEOUS EXTRACT COMPOUNDS BY GC-MS ANALYSIS

Compounds[a]	**m/z**[b]	**BA**[c]	**Bio-oil (g L^{-1})**	**Aqueous extract (g L^{-1})**
C2 - furan	**95**, 81, 67	Carbohydrates	2.6	4.2
4-hydroxy-4-methyl-2-pentanone	**43**	Carbohydrates	2.4	-
Furanone	**55,** 84	Carbohydrates	2.8	2.9
Phenol	**94,** 66	CH/Lignin	1.4	1.7
C1 - pyranone	**112**, 84, 55	Carbohydrates	3.8	1.7
C1-Phenol	**108**, 77, 51	CH/Lignin	-	0.8
C1 - phenol	**107**, 77, 51	CH/Lignin	2.0	1.7
C1 - furan	**81**, 53, 51	Carbohydrates	1.8	-
Guaiacol	**124**, 81, 109	Lignin	4.7	3.1
Catechol	**110**, 63, 81	CH/Lignin	8.1	4.6
C1 - guiacol	**138**, 123, 95	Lignin	4.3	3.4
1,4:3,6-dianhydro-α-d-glucopyranose	**69**, 57, 41	Carbohydrates	2.9	1.4
C1 - catechol	**124**, 78, 106	CH/Lignin	1.4	-
Hydroquinone	**110**, 81, 53	CH/Lignin	1.7	1.2
Hydroxy-guaiacol	**140**, 97, 125	Lignin	2.3	-
C1 - catechol	**124**, 78, 106	CH/Lignin	2.8	-
C2 - guaiacol	**137**, 152, 122	Lignin	4.9	1.0
Syringol	**154**, 139, 93	Lignin	16.7	6.7
Eugenol	**164**, 149, 131	Lignin	1.7	-
Vanillin	**151**, 81, 109	Lignin	8.9	1.0
C1 - syringol	**168**, 153, 125	Lignin	13.3	3.4
Levoglucosan	**60**, 42, 73, 97	Carbohydrates	5.0	23.9
Acetoguiacone	**151**, 166, 123	Lignin	3.4	1.4
C2 - syringol	**167**, 182, 107	Lignin	10.0	1.6
Guacylcetone	**137**, 137, 180	Lignin	4.0	0.8
4-allyl-syringol	**194**, 91, 133	Lignin	5.7	0.7
C3 - syringol	**167**, 196	Lignin	2.3	-
Dihydroconyferyl alcohol[d]	**194**, 137, 182	Lignin	2.1	-
Syringaaldehyde	**182**, 65, 139	Lignin	15.0	4.3
4-propenyl-syringol (trans)	**194**, 91, 119	Lignin	1.7	-
Homosyringaldehyde	**167**, 196, 123	Lignin	2.7	-
Acetosyringone	**181**, 196, 153	Lignin	9.2	2.3
Conyferyl aldehyde (trans)	**178**, 147, 135	Lignin	2.1	-
Syringyl acetone	**167**, 210, 123	Lignin	12.2	2.5
Synapyl alcohol (allyl)	**167**, 182, 210	Lignin	1.9	-
Propyosiringone	**181**, 210, 153	Lignin	2.8	-
Homosyringic acid/Dihydrosynapyl alcohol[d]	**168**, 212, 153	Lignin	2.0	-
Synapylaldehyde (trans)	**208**, 165, 137	Lignin	2.6	-
Total			175.2	76.3
Lignin/Carbohydrate ratio			2.82	0.53
S/G ratio			3.66	2.22

[a] Isomer abbreviations, C1 - methyl, C2 - dimethyl or ethyl, C3 - trimethyl, methyl – ethyl or propyl; [b] mass-to-charge ratio, bold values are the main mass fragment; [c] biological assignment

TABLE II.6 - IDENTIFICATION AND RELATIVE QUANTIFICATION (% TOTAL) OF WOOD AND CHAR COMPOUNDS BY PY/GC-MS ANALYSIS.

Compounds[a]	m/z[b]	BA[c]	% total	
			Wood	Char
Benzene	**78**, 63, 50	Charcoal	-	12.2
Furan	68	Carbohydrates	-	1.2
Cyclopentadiene	65	alkane	-	1.0
Cyclohexadiene	**77**, 51	alkane	-	5.6
Toluene	**91**, 65	Charcoal	-	10.5
Furanone	**55,** 84	Carbohydrates	0.2	-
Furfural	**95**, 67	Carbohydrates	0.4	0.6
furfuyl alcohol	**84**, 55, 42	Carbohydrates	0.4	-
C2 – benzene	**106**, 91, 65	Charcoal	-	0.8
C3 – benzene	**120**, 105, 91	Charcoal	-	0.1
Styrene	**104**, 78, 51	Charcoal	-	0.5
dihydro - methyl - furanone	**98**, 70, 41	Carbohydrates	1.7	0.4
C1 – cyclopentenone	**96**, 81, 67	Carbohydrates	-	0.1
Phenol	**94,** 66	CH/Lignin	-	9.9
C1 – styrene	**117**, 103, 77	Charcoal	-	0.3
2-hydroxy-5,6-dihydropyran-4-one	**114**,85,58	Carbohydrates	8.9	-
hydroxy - methyl - cyclopentenone	**112**, 84, 55	Carbohydrates	0.5	-
Indene	**115**, 89, 43	Charcoal	-	0.4
C1 – phenol	**107**, 77, 51	CH/Lignin	-	7.5
C1 – furan	**81**, 53, 51	Carbohydrates	-	0.2
Guaiacol	**124**, 81, 109	Lignin	4.0	3.5
C2 – phenol	**122**, 107, 77	CH/Lignin	-	1.0
dihydroxy – benzene	**110**, 63, 81	CH/Lignin	1.1	2.9
C1 – guaiacol	**138**, 123, 95	Lignin	4.2	2.0
Naphthalene	**128**, 102	Charcoal	-	3.9
hydroxy - methyl - furaldehyde	**126**, 97, 69	Carbohydrates	0.1	-
C1 - dihydroxy - benzene	**124**, 78, 106	CH/Lignin	0.0	0.3
Hydroxy-guaiacol	**140**, 97, 125	Lignin	2.2	1.6
C2 – guaiacol	**137**, 152, 122	Lignin	0.7	0.4
4 - vinyl guaiacol	**150**, 135, 107	Lignin	7.6	1.1
Syringol	**154**, 139, 93	Lignin	19.0	9.5
Eugenol	**164**, 149, 131	Lignin	1.0	0.1
Unidentified	**182**, 167, 139	Lignin	-	0.2
Vanillin	**151**, 81, 109	Lignin	2.7	1.7
C1 – syringol	**168**, 153, 125	Lignin	14.5	7.0
isoeugenol (trans)	**164**, 149, 131	Lignin	4.6	0.5
Homovanillin	**166**, 137, 122	Lignin	0.3	-
Levoglucosan	**60**, 42, 73, 97	Carbohydrates	0.1	-
Acetoguiacone	**151**, 166, 123	Lignin	0.2	0.4
C2 – syringol	**167**, 182, 107	Lignin	0.6	1.3
4 - vinyl – syringol	**180**, 165, 137	Lignin	14.2	4.1
4-allyl-syringol	**194**, 91, 133	Lignin	2.1	0.4
C3 – syringol	**167**, 196	Lignin	-	0.2
4-propenyl-syringol (cis)	**194**, 91, 119	Lignin	0.6	-
Syringaaldehyde	**182**, 65, 139	Lignin	1.5	4.1
4-propenyl-syringol (trans)	**194**, 91, 119	Lignin	5.4	2.3
Homosyringaldehyde	**167**, 196, 123	Lignin	0.1	-
Acetosyringone	**181**, 196, 153	Lignin	0.3	-

Syringyl acetone	**167**, 210, 123	Lignin	0.1	0.3
Synapyl alcohol (trans)	**167**, 182, 210	Lignin	0.3	-
S/G ratio			2.37	3.07

[a] Isomer abbreviations, C1 - methyl, C2 - dimethyl or ethyl, C3 - trimethyl, methyl – ethyl or propyl; [b] mass-to-charge ratio, bold values are the main mass fragment; [c] biological assignment

The bio-oil and aqueous extract composition was studied using GC-MS. The syringyl and guaiacyl-derived compounds totalized 59 and 30% of all identified molecules in the bio-oil and aqueous extract, respectively. On contrary, the carbohydrate-derived compounds were responsible for 21 and 57% of the compounds in the bio-oil and aqueous extract, respectively. The lignin/carbohydrate ratio of the bio-oil was 2.82 and it has decreased to 0.53 for the aqueous extract, stating a concentration of lignin-derived compounds in the oil (TABLE II.5).

The major compounds identified in the bio-oil were derived from the syringyl units of lignin. In fact, syringaldehyde, syringyl acetone and syringol represented more than 25% of all identified compounds in the bio-oil. Other less representative compounds, but also with higher concentration, were vanillin, catechol and acetosyringone. On the other hand, the aqueous extract had levoglucosan as the only one remarkable compound, which represents over 30% of the total (

TABLE II.5). Phenolic compounds (excluding syringyl and guaiacyl components) totalized 10.3 and 11.3% of the bio-oil and aqueous extract composition, respectively.

Py-GC-MS gives an insight of the chemical structures of the solid materials (TABLE II.6). The lignin derived compounds totalized over 83 and 38% of the identified molecules after the pyrolysis of the raw material and char, respectively. It is important to emphasize that analytical pyrolysis does not represent a sensible tool for the evaluation of carbohydrates. It was easily confirmed after comparing the 12% of carbohydrates quantified via analytical pyrolysis for the raw material, against the 70% quantified by wet chemistry. By doing relative comparisons, it was possible to observe that the carbohydrate compounds slightly decreased in the solid products (1.3 times lower).

Syringyl derived compounds were predominant in the solid samples. The S/G ratio among the products confirm such predominance: bio-oil (3.66) > char (3.07) > raw material (2.37) > aqueous extract (2.22). The phenolic compounds (excluding syringyl and guaiacyl components) resulted from the pyrolysis of the char (21%) were higher than those identified in the pyrolytic products of the raw material (1.1%). Aromatics were not identified in the raw material pyrolytic products; but it corresponded to 28% of the compounds identified in char, resulting in an aromatic/alkyl aromatic ratio of 1.45 (TABLE II.6).

TABLE II.7 - QUANTIFICATION OF CARBOHYDRATE PERCENTAGE PRESENT IN LIQUID PRODUCTS BY ION CHROMATOGRAPHY

Sugar	**wt.%**	
	Bio-oil	**Aqueous extract**
Arabinose	0.30 ± 0.04	0.07 ± 0.01
Galactose	0.11 ± 0.01	0.03 ± 0.01
Glucose	6.60 ± 0.90	2.34 ± 0.23
Xylose	0.60 ± 0.07	0.12 ± 0.06
Mannose	0	0
Cellobiose	0.06 ± 0.01	0

Considering the fact that analytical pyrolysis is not the ideal tool for carbohydrate assessment, amount of carbohydrates present in liquid products was evaluated (TABLE II.7). Bio-oil and aqueous extract presented 7.7 and 2.6% of sugars, respectively, with glucose found in major amount. It is worth mentioning that ion chromatography of liquid products was also performed, without the hydrolysis reaction, and no free sugars were found.

II.3.2 PERFORMANCE OF THE PILOT-SCALE REACTOR FOR FAST PYROLYSIS OF EUCALYPT WOOD FINES

The yield of bio-oil obtained in the pilot plant was similar to those found in the recent published works carried out at laboratory scale (ASADULLAH et al., 2013; WIGLEY; YIP; PANG, 2017), which was *ca.* 50%. At laboratory conditions the reaction parameters are usually very well controlled, which may not be the case of larger scales. The centrifugation step at the final of the fast pyrolysis plant stands as a tool to

concentrate pyrolysis products coming from carbohydrates in an aqueous extract (light fraction), and lignin-derived compounds in a bio-oil (heavy fraction).

The char is indeed a high-thermally stable carbon-rich material (TABLE II.2) in the pyrolysis plant, but it does not is as aromatized (H/C ratio) as the traditional charcoal prepared under slow-pyrolysis (XIAO; CHEN; CHEN, 2016). The high ash content of the obtained char is a result of a not entirely efficient fluidized bed, but it is usually observed for this type of fast pyrolysis coproducts (BOATENG; LANE; PENNSYL, 2007).

The crust material formation inside the tubes between the reactor and condensation system is a negative point of this kind of larger scale procedure (FIGURE II.1). As showed by Wang *et al*. (2013) it occurs due the continuous heating of the bio-oil, leading to the repolymerization of the lignin or carbohydrates monomeric compounds. The crust material formation reduces the bio-oil recovery and increases maintenance costs. Thus, by effectively controlling the reaction and vapor transporting temperatures it is possible to improve the efficiency of the pilot-plant bio-oil production.

This pilot-scale plant for bio-oil production is interesting as it operates using rejected material from a Kraft pulp line, to which it was integrated. In this case, the costs related to transportation of feedstock can be reduced to near zero. By doing so, the profitability of the bio-oil production can be improved (ROGERS; BRAMMER, 2012) and the smart use of biomass wastes can contribute to apply the concepts of bioeconomy, especially for sustainable solutions in the replacement of fossil fuels and energy self-sufficiency.

II.3.3 CHARACTERIZATION OF THE PRECURSOR WOOD MATERIAL AND THE COPRODUCTS

The first significant mass loss, event in the thermogram of the raw material (FIGURE II.2b) is related to the thermal decomposition of hemicelluloses and amorphous cellulose, while the second mass loss corresponds to the degradation of crystalline cellulose (POLETTO et al., 2012). Thermal events related to the lignin

degradation were not observed as a single peak due its degradation in a broad temperature range. The main events are related to degradation of lignin-carbohydrate complexes at 235 ºC, aliphatic side chains starting at 300 ºC up to cleavage of more stable carbon-carbon bonds at 370-400 ºC (NASSAR; MACKAY, 1984).

The thermal behavior of all obtained coproducts is explained by their chemical composition. The chemical composition of bio-oil and aqueous extract was similar; however, different concentrations of some specific compounds were observed. As a result, their thermogravimetric curves had similar pattern of mass loss. Nevertheless, the higher water content of the aqueous extract sample promoted a very intense mass loss at temperatures below 100 ˚C, which was not observed in the bio-oil curve. Besides water, the presence of VOCs in these liquid samples was also responsible for their lower thermal stability when compared with the solid products and raw material.

The char was the most thermally stable coproduct among the solids (lower H/C, TABLE II.2); its mass loss occurred from 350 to 900 ˚C in a slower rate compared with the raw material and crust material. The residual mass after 900 ˚C was higher than 60%, which was also a result of its high ash content (TABLE II.2). The char would be even more thermal stable if all carbohydrates had been pyrolyzed during the fast pyrolysis procedure, which was not the case since a peak at around 360 ˚C was observed in the DrTG curve of this sample (FIGURE II.2), and carbohydrate pyrolysis products were detected (TABLE II.6). The higher carbon content, lower H/C ratio and lower amount of non-alkylated aromatic compounds (TABLE II.6) indicates its recalcitrant character (KAAL; RUMPEL, 2009).

The DrTG of the crust material showed a series of overlapped mass loss events occurring from 150 to 700 ˚C. Crust material can be formed by heating both carbohydrate and lignin-derived compounds (*i.e.* both pyrolytic water soluble and insoluble compounds) in a wide range of temperatures, but especially between 250-400 ˚C (WANG et al., 2013). Considering this, it is possible to infer that the observed overlapped peaks correspond to the thermal decomposition of oligomerized carbohydrate and lignin monomeric units, which is different from the thermal decomposition of the original macromolecules.

II.3.4 COPRODUCTS FROM FAST PYROLYSIS TOWARD BIOFUEL APPLICATION

The elevated water content of the aqueous extract affected its pour point, density and kinematic viscosity as well, making it not suitable as a potential biofuel. In fact, no ignition was observed for this sample in the HHV measurement. Another aspect was its high H/C molar ratio when compared to the other samples, which means a very non aromatized structure (XIAO; CHEN; CHEN, 2016).

The fast pyrolysis bio-oil obtained under pilot scale conditions is composed by a wide range of organic compounds, but most of them are phenolic and its derivatives which are oxygenated compounds. Although the bio-oil has over 20 MJ kg^{-1} of heating value, its high oxygen content limits their directly application as biofuel (ASADULLAH et al., 2013) and contributes to the chemical instability of the product. In such cases, catalytic hydrogenation strategies (KABIR; HAMEED, 2017) and esterification (SUNDQVIST; OASMAA; KOSKINEN, 2015) have been discussed. Besides, hydrogen-lacking characteristic of the fast pyrolysis bio-oil is the main responsible for crust material formation inside the reactor (ZHANG et al., 2016b). Another problem to overcome is still the high corrosiveness of the bio-oil, which is related to its acidity (low pH), mainly due to the presence of carboxylic acids such as acetic acid. The acetic acid present is mainly formed by the thermal degradation of hemicellulose (DONG et al., 2012), in this process the uronic acid ring ruptures and the acetyl group bound to xylose is eliminated (LV; WU; LOU, 2010). Lignin also contributes to the formation of acetic acid by breaking the lignin side-chain (BERTERO et al., 2014). Cellulose, when subjected to pyrolysis, depolymerizes, producing levoglucosan, then the breakdown of levoglugosan produces acetic acid (SHEN; GU, 2009).

The energy recovery (calculated using the HHV of the starting material and bio-oil, and the yield of the conversion of the first into the second) for the bio-oil production was *ca.* 40%, which is below of the numbers obtained in the lab-scale catalytic bio-oil production (MALINS, 2017). However, the value obtained here is in agreement with the energy recovery of bio-oil production at lab-scale non catalytic process (MALINS, 2017). Besides, the low density of the wood decreases the energy produced by

volume, which stands as one of the main drawbacks of this biofuel. In addition, wood stabilizes its moisture content according to the surroundings, usually equilibrating at 15-20%. Thus, higher energy is lost to dry this biofuel or to evaporate this moisture during the heat production. On the other hand, the higher density of the bio-oil promotes higher heat capacity by volume, making transportation and storage easier.

The crust material and char presented the highest HHV (23 and 26 MJ kg^{-1}, respectively) and the lowest H/C (0.68 and 1.06, respectively), stating their highly aromatized structures. These results are in agreement with the observed in the thermogravimetric curves for these two solid samples. Moreover, the HHV of the char would be even higher if no carbohydrate-derivatives had remained in this sample, which was observed in its TGA curve. Even though, the char presented the most favorable characteristics to be used as a solid biofuel, *i.e.*, higher HHV and aromatized structure. In parallel there is an option to compact these char fines in order to increase the specific energy production (BAZARGAN; ROUGH; MCKAY, 2014). Nevertheless, the influence of its higher ash content should be examined toward the performance and operation in the combustion stage.

II.3.5 COPRODUCTS FROM FAST PYROLYSIS AS PRECURSOR FOR CHEMICALS AND MATERIALS

Both bio-oil and aqueous extract showed chemical compounds with many functionalities (C-H, C=O, C=C, C-C, O-H), opening a wide road of possibilities to be effectively exploited for the production of fine chemicals (SINGH et al., 2016). The obtained bio-oil presented significant concentration of interesting compounds such as syringaldehyde, which can be further converted in BTX chemicals by catalytic dehydroxylation of phenolics compounds (WANG; RINALDI, 2013), methanol and naphthalene (ISIKGOR; BECER, 2015). From BTX chemicals a wide range of phenolic resins and unsaturated polyester could be synthetized (CHERUBINI; STRØMMAN, 2011; ISIKGOR; BECER, 2015). On the other hand, the levoglucosan-rich aqueous extract can serve as a precursor material for furan compounds, cyclopentenones and other aliphatic oxygenates by dehydration of levoglucosan (ZHANG et al., 2013).

Further interesting applications of levoglucosan-rich aqueous extract is the conversion of these pyrolytic sugars into ethanol by fermentation or lipids (LIAN; GARCIA-PEREZ; CHEN, 2013) as well as to manufacture surfactants, food additives, biodegradable polymers and pharmaceuticals (NEGAHDAR et al., 2016). The sugars present in the bio-oil are probably derived from higher molecular weight holocellulose fragments, which remained attached to the lignin chain after pyrolysis (FORTIN et al., 2015). They may be used for the production of ethanol as well as anydrosugars (BENNETT; HELLE; DUFF, 2009; SUKHBAATAR et al., 2014).

The higher content of phenolic compounds in the bio-oil can be useful as antifungal agent for wood preservation (LOURENÇON et al., 2016), as these compounds tend to have primary responsibility for any antimicrobial activity, mainly against brown-rot fungus (MOHAN et al., 2008). The amphoteric properties of the bio-oil are interesting to increase both the dimensional stability and water repellency of wood through the blocking of its capillary microstructures.

The char from pyrolyzing biomass is recognized as a potential sorbent for aromatic contaminants. For example: char of orange peels - with similar elementary composition of char from wood - could be used as a good alternative for the sorption of naphthalene and 1-naphthol (CHEN; CHEN, 2009); char from pine wood gasification seemed to be more attractive than activated carbon to remove toluene from water (SILVANI et al., 2017).

II.4 CONCLUSIONS

The yield of bio-oil obtained in a pilot plant was similar to laboratory conditions described in the literature. Bio-oil, char and crust material presented higher HHV than the raw material. The higher water content of aqueous extract and the oxygen-rich composition of the bio-oil denote the limitations for their use as fuel. The GC-MS showed a higher concentration of lignin compounds in the bio-oil, mainly syringyl monomers, whereas the aqueous extract presented higher concentration of carbohydrate-derived compounds, especially levoglucosan. Valuable phenolic compounds were identified in the bio-oil and its coproducts, highlighting their potential as antifungal agent and to produce fine chemicals. These chemical characteristics confirm the valuable application of both materials in a biorefinery system. Wood fines can be used to produce energy for industry's self-sufficiency replacing fossil fuels, generating interesting coproducts containing high added-value extractable materials.

CHAPTER III

ACETONE:WATER FRACTIONATION OF PYROLYTIC LIGNIN IMPROVES ITS ANTIOXIDANT AND ANTIBACTERIAL ACTIVITY

Journal of analytical and applied pyrolysis. v.156, p.105175 - , 2021.
DOI: 10.1016/j.jaap.2021.105175

III.1 INTRODUCTION

Non-agricultural biomass is an abundant source with great potential for producing carbon-neutral fuels and chemicals. A biomass-based refinery will require efficient methods to produce commodity chemical feedstocks from plants (ZAKZESKI et al., 2010). Lignocellulosic biomass pyrolysis is a well-established thermochemical process that can convert 40 to 60% of biomass into crude bio-oil (GREENHALF et al., 2013; MATOS et al., 2020; PARK et al., 2019). Initially, the use of biomass pyrolytic oil was concentrated on the application as a fuel. However, crude bio-oil has a high oxygen content, complex composition, and low calorific value (LEHTO et al., 2014), which limits its use as a fuel. Currently, attention has been focused on developing non-combustible and higher-value applications.

During the thermal decomposition of the biomass, lignin is cleaved into smaller fragments, and these remain in the bio-oil. In addition, the formation of these lignin oligomers may be based on pyrolysis mechanisms involving depolymerization and recombination of lignin fragments (BAYERBACH; MEIER, 2009). The presence of these lignin oligomers is one of the factors that lead to the instability of the bio-oil. These oligomers usually have relatively high molecular weight, are non-volatile, are viscous and highly reactive, making them difficult to process into valuable products (BAYERBACH; MEIER, 2009; MULLEN; BOATENG, 2011). On the other hand, in a biorefinery strategy, the content and structural characteristics of oligomers must also be considered. Therefore, there is an urgent need to develop techniques to extract these oligomers from bio-oil to facilitate the valorization and use of high-value bio-oil (ZHANG et al., 2019b).

These fragments can be separated from the bio-oil by adding water, because most of the bio-oil is soluble in water, while these fragments, a part which can be called pyrolytic lignin (PL) are not (SCHOLZE; MEIER, 2001). Pyrolytic lignin is an important component of bio-oil and can occur in the content of up to 30% by weight (OASMAA; MEIER, 2005). The separation and characterization of pyrolytic lignin can improve the extraction of monophenols and assist in understanding the structural variation of lignin

after pyrolysis (WANG et al., 2015). PL has a high carbon content and natural aromatic structures, therefore, it is a renewable resource with the potential for the production of high-value chemicals (FAN et al., 2017).

Phenolic compounds of natural origin have been the focus of research. Such studies reveal the efficacy of phenolic aromatic compounds derived from lignin as antioxidants in various types of materials, and as antimicrobials (DONG et al., 2011; SADEGHIFAR et al., 2017; ZHAO et al., 2018a). As antioxidants, phenolic compounds act in the elimination of free radicals, by the donation of protons or electrons, and thus prevent the spread of chain reactions (SALEM; ABDEL-MEGEED; ALI, 2014). As also occurs with lignins obtained by other processes, PL has a complex structure, increased reactivity, mainly due to the presence of phenolic hydroxyls. Depending on the process of obtaining, lignins are generally heterogeneous, polydispersed, and have a variable and complex distribution of functional groups (ROPPONEN et al., 2011). Solvent fractionation methods appear like a viable solution to solve the problems related to the heterogeneity of lignins. These methods result in relatively homogeneous lignin fractions, thus facilitating the understanding of their structure, composition, and possible applications (DOMÍNGUEZ-ROBLES et al., 2018; SADEGHIFAR et al., 2017; ZHANG et al., 2019a, 2019b). It is worth noting that, in recent years, many studies have reported several fractionation techniques for lignin oligomers, such as membrane separation (MONIZ et al., 2018), solvent extraction (DOMÍNGUEZ-ROBLES et al., 2018; SADEGHIFAR et al., 2017), and column chromatography (ZHAO et al., 2018b). Among these methods, solvent extraction is more economical than other fractionation methods because solvents can be recovered and reused (DODGE et al., 2019).

In this study, was used a simple and environmentally-safe solvent (KOKOSA, 2019) fractionation protocol (DOMÍNGUEZ-ROBLES et al., 2018), for the fractionation of *Eucalyptu*s spp. pyrolytic lignin. The fractionation was carried out to examine the effects of the method on its functional groups, molecular weight distribution, monolignol and interunit linkage composition, physicochemical, antioxidant, and antimicrobial properties.

III.2 MATERIAL AND METHODS

The heavy bio-oil from *Eucalyptus* spp., produced in a pyrolysis reactor as described in chapter II, has the following physicochemical composition: Insoluble lignin (32%); Soluble lignin (28%); Carbohydrates (11%); Volatile compounds (9%); Ashes (1%); Moisture (19%).

III.2.1 PYROLYTIC LIGNIN PRODUCTION

Experiments to obtain the pyrolytic lignins were carried out based on a central composite factorial design. The agitation speed (4,000 to 11,000 rpm) and the amount of bio-oil added in 1 L of DI water at 5 ± 1 °C (5 to 40 g) were defined as independent variables. The percentage of precipitated material in the water was defined as response variable. For the performance of the experiments the bio-oil was added dropwise into the water under ultra-turrax stirring, after addition of the bio oil the stirring was continued for 10 min. Subsequently, the pyrolytic lignin was vacuum filtered through Büchner funnel and dried under vacuum at 40 °C. Additionally, the effect of droplet size and mild agitation speed for the experiment with the lowest amount of insoluble material was evaluated. The quantification of lignin present in the samples was performed by the Klason hydrolysis extraction method (TAPPI T222 om-88). The carbohydrate content in the samples were quantified by ion exchange chromatography (IC) ((SCHROEDER et al., 2017). The separation was done on CarboPac PA 20 column (4 mm x 250 mm, 5 µL looping, flow rate 0.5 $mL.min^{-1}$ and temperature 30 °C).

FIGURE III.1 - SCHEMATIC ILLUSTRATION OF THE PYROLYTIC LIGNIN FRACTIONATION PROTOCOL IN AQUEOUS ACETONE SOLUTIONS

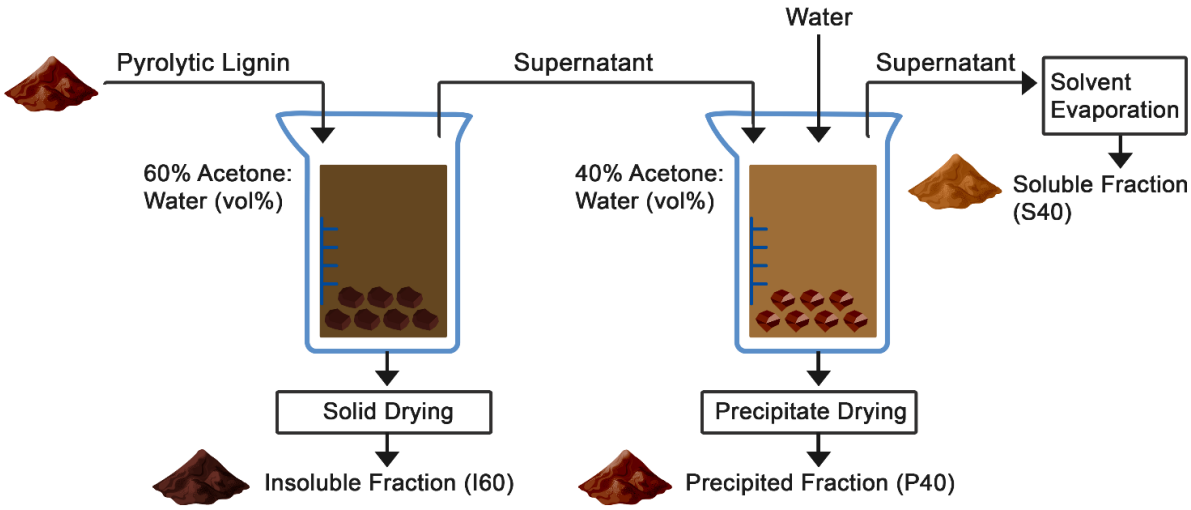

III.2.2 PYROLYTIC LIGNIN FRACTIONATION

Pyrolytic lignin fractionation was performed in aqueous acetone solutions, based on the protocol proposed by DOMÍNGUEZ-ROBLES et al. (2018). Briefly, 10 g of lignin was dispersed in 100 mL of aqueous acetone solution 60% (vol%). The dispersion was made under magnetic stirring for 60 min. The solution was centrifuged for 30 min at 5k rpm, and the supernatant was recovered. The insoluble lignin fraction (I60) was dried in a vacuum oven at 40 °C and weighed. Water was then added to the supernatant to reduce the acetone concentration from 60% to 40%. This solution was mixed for 60 min to allow lignin to precipitate followed by centrifugation at 5k rpm for 30 min and the insoluble fraction in 40% acetone (P40) was separated from the soluble one. Once again, the precipitate was dried in a vacuum oven at 40 °C. The final remaining soluble lignin fraction (S40) in 40% acetone solution was separated by evaporating the solvent and dried under vacuum at 40 °C (FIGURE III.1). Ten repetitions were performed.

III.2.3 GEL-PERMEATION CHROMATOGRAPHY

Gel permeation chromatography (GPC) analyses were carried out in a Shimadzu LC-20AD (Kyoto, Japan) at 40 °C using a setup comprising two analytical GPC columns in series (Phenogel 5 µm 50 Å and Phenogel 5 µm $10E^3$ Å columns, 300 mm x 4.6 mm, Phenomenex), at flow rate of 0.35 mL min^{-1}. HPLC-grade THF was used

as eluent. A UV-Vis detector (Shimadzu SPD-M20A) was used for monitoring the samples at 280 nm. Lignin solutions (1 mg mL^{-1}) were filtered using 0.22 µm PTFE filter and they were injected (20 µL) into the GPC system. Standard calibration was performed with polystyrene standards PSS (PSS KYTH, Allcrom, São Paulo, Brazil, M*w* range 162 – 1.30 x 105 g mol^{-1}).

III.2.4 ^{1}H-^{13}C HSQC NMR ANALYSES

The heteronuclear single quantum coherence (HSQC) experiments were performed in a Bruker Avance DPX 300 spectrometer (300 and 75 MHz for ^{1}H and ^{13}C nuclei), respectively. Lignin (30 mg) was dissolved in 500 µL of DMSO-d_6, and the residual solvent peak (DMSO δ_H/δ_C 2.49/39.5) was used for calibrating peak.

III.2.5 DETERMINATION OF FUNCTIONAL GROUPS

Determination of carbonyl groups was performed by oximation. Total acidic groups determination carried out according to Zakis (1994). Carboxyl groups and aliphatic hydroxyls were also determined according to Zakis. The phenolic hydroxyl content was determined by a spectrophotometric method, proposed by Wexler (1964).

III.2.6 FOURIER TRANSFORM INFRARED SPECTROSCOPY (FT-IR) ANALYSES

Fourier transform infrared spectroscopy (FT-IR) was performed in a Bruker Tensor 37 spectrometer, in the direct transmittance mode. FTIR spectra were recorded from KBr discs containing 1.0% wt. of lignin in the range of 4000-700 cm^{-1} with a 4 cm^{-1} resolution and 32 scans. Spectra were baseline corrected and normalized to the aromatic peak at 1515 cm^{-1} (BYKOV, 2008). Condensation index: calculated according to the method of Faix (1991a), based on the absorption minima and maxima of the baseline corrected and normalized FTIR spectra of non-acetylated PL. Hydroxyl groups: the ratio between phenolic and aliphatic hydroxyls was determined using the method of Faix et al. (1994) based on the absorption bands at 1765 and 1740 cm^{-1} for acetylated PL. From this data the total phenolic OH relative amount (FAIX; GRÜNWALD; BEINHOFF, 1992) and the aliphatic OH content were calculated.

III.2.7 GAS CHROMATOGRAPHY-MASS SPECTROMETRY (GC-MS)

The pyrolytic lignin fractions were dissolved in pyridine (10 mg mL^{-1}). Then, 50 µL of each solution was transferred to a 2 mL microcentrifuge tube, and 10 µL nonadecanoic acid was added as an internal standard (2 mg mL^{-1} in chloroform). After 50 µL of the BSTFA (N, O-Bis(trimethylsilyl)trifluoroacetamide) for the silylation was added and the solution was vortexed and incubated at 70 °C in a dry bath incubator for 60 min. Soon after the solution was transferred to a vial with an insert (100 µL) suitable for gas chromatography mass spectrometry analysis (GC- MS, Thermo, Focus-PolarisQ). One microliter of the sample was injected in a split/splitless injector at 230 °C with a split ratio of 1:25. Trimethylsilyl-derived compounds (TMS compound) were separated on a DB-5ms capillary column (30 m × 0.25 mm, 0.25 µm film thickness). GC oven program: 70 °C to 320 °C (8 °C min^{-1}, held for 15 min). Helium served as the carrier gas (1.0 mL min^{-1}). The GC-MS interface and ion source temperatures were 250 °C and 200 °C, respectively. The ion-trap mass spectrometer was operated in the positive impact electronic mode at 70 eV, and the total scan time was 0.58 s for the m/z 50–650 range; emission current: 250 mA. Mass spectral deconvolution and automated calculation of RI were performed by the automated mass spectral deconvolution and identification system (AMDIS, National Institute of Standards and Technology, Gaithersburg, MD, USA). Standard solutions of linear alkanes (C_7-C_{30}, Sigma-Aldrich 49451-U) were used for retention index (RI) calibration. Compound mass spectra were identified using a target mass spectra library confectioned in the AMDIS software from previous biomass analysis (MELO et al., 2018) and by comparison with published MS data (ŁUCEJKO et al., 2012; MATTONAI et al., 2016; TAMBURINI et al., 2017).

III.2.8 ANTIOXIDANT ASSAYS

The free radical scavenging through the DPPH assay was determined according to Brand-Williams et al. (1995), with minor modifications. Briefly, 0.1 mL of the PL solution in dioxane was added to 3.9 mL of 2,2-Diphenyl-1-picrylhydrazyl (DPPH) solution in methanol (0.06 mmol L^{-1}). The mixture was allowed to react in the dark until

the absorbance, at λ = 515 nm, was constant. The concentration that inhibits 50% of the DPPH present in the solution (IC50) was calculated graphically using a calibration curve in the linear range, plotting the concentration of the PL solution versus the corresponding elimination effect. The results are expressed in antioxidant activity index (AAI) (SCHERER; GODOY, 2009).

The free radical scavenging by radical monocation of 2,2′-azinobis-(3-ethylbenzothiazoline-6-sulfonic acid) (ABTS) was determined according to Re et al. (1999). A volume of 88 µL of potassium persulfate (140 mmol L^{-1}) was added to 5 mL of ABTS (7 mmol L^{-1}). The mixture was stored in the dark and at room temperature for 16 h. The ABTS solution absorbance was adjusted, with ethanol, to 0.70 ± 0.05 at λ = 734 nm. Then, 30 µL of the PL solution in dioxane were added to a 3 mL ABTS solution. The mixture remained in the dark for 2 h. Results are expressed in Trolox equivalent.

The ferric reducing antioxidant power assay (FRAP) was determined according to the methodology described by Benzie and Strain (BENZIE; STRAIN, 1996), with minor modifications. The FRAP reagent was prepared by a mixture of acetate buffer (300 mmol L^{-1}, pH 3.6), TPTZ (10 mmol L^{-1}) solubilized in HCl (40 mmol L^{-1}) and ferric chloride (20 mmol L^{-1}), in the volumetric ratio 10:1:1, respectively. Then, 3 mL of the FRAP reagent was added to 0.1 mL of PL solution in dioxane. The mixture was kept at room temperature in the dark. After 30 min, the absorbance was measured at λ = 595 nm. Results are expressed in ferrous sulfate equivalent.

III.2.9 ANTIBACTERIAL ACTIVITY ANALYSIS

The evaluation of the antibacterial activity of the PL fractions was performed using the broth microdilution method, described by Wiegand et al. (2008). In short, bacterial inocula for antimicrobial testing were prepared by picking colonies from 24 h-old cultures (colonies cultured onto nutrient agar at 37 °C) and suspending them in an appropriate saline solution (to achieve 10^8 CFU mL^{-1}). The suspensions were diluted in Müeller Hinton Broth to standardize inocula at 10^5 CFU mL^{-1}. For the broth microdilution test 50 µL of each bacterial suspension (*Staphylococcus aureus* ATCC

6538, *Escherichia coli* ATCC 25922 and *Salmonella enterica* serovar Enteritidis ATCC 13076) was added to the wells of a sterile 96-well microtitre plate already containing 50 µL of serially diluted pyrolytic lignin (5 mg mL^{-1}) in dimethyl sulfoxide (DMSO) at 25%. The final volume in each well was 100 µL. Control wells were prepared with culture medium and bacterial suspension only in amounts corresponding to the highest quantity present. For control 50 µL of the Bactrim® antibiotic (200 mg L^{-1}) was pipetted and a serial dilution was performed, reaching a concentration of 0.195 mg L^{-1} in a row of wells. The same was done in row for the DMSO solvent (250 mL L^{-1}). The minimal inhibitory concentration (MIC) was the lowest concentration where bacterial growth was not observed after incubation for 24 h. Cellular viability was confirmed by the presence of color in the wellsafter adding 10 µL/well of TTC (2,3,5- triphenyl tetrazoliumchloride) or resazurin (7-hydroxy-3H-phenoxazin-3-one-10-oxide sodium salt , Sigma), and incubation for 30 min in the dark at 37 °C. All measurements of MIC values were repeated in triplicate.

III.3 RESULTS AND DISCUSSION

III.3.1 PYROLYTIC LIGNIN PRODUCTION

The contour plot obtained from the factorial design (FIGURE III.S1) shows that under the conditions tested, the amount of bio-oil added to the water has a greater influence on the separation process ($p = 0.0022$) than the agitation speed ($p = 0.3768$). From the experiments tested was defined it as the ideal condition for the most efficient separation, 10 g per liter of water and 10k rpm (EXP10). However, although the concentration has a greater influence on separation, velocity has a considerable influence. It is noteworthy that there were no significant variations in the pH of the samples. Therefore, was also tested below the design speed (2k rpm), and as expected, the separation did not occur efficiently - 53% undissolved material - TABLE III.S1). Since agitation using ultra-turrax is a high shear agitation, an experiment (10 g L^{-1} and 2.0k rpm) with non-shear agitation was performed. It was observed that the lack of shear prevents separation (TABLE III.S1). This occurs because when the drop of bio-oil comes into contact with water, a film of water-insoluble material is formed that

prevents contact of water with the bio-oil. Therefore, it is necessary to break the drops for efficient separation. In this context, was evaluated the addition of all bio-oil in one go, in this experiment was obtained 65% of non-solubilized material. Under poorly separated conditions the material remains mainly in the container in a sticky form.

In evaluating the effect of temperature, on the condition on the best separation condition of the experimental design, was observed that no efficient separation occurred for the experiments performed at 20 and 50 °C (TABLE III.S1). However, the experiment performed at 90 °C showed the same amount of non-solubilized material as the ideal experiment performed at 5 °C. However, there was a great adhesion of the material to the recipient, thus hindering the removal.

The physicochemical analyzes (

TABLE III.S2) showed that the less efficient separation (EXP1 – 40 g L^{-1} and 7.5k rpm) produces samples with a lower content of acid-insoluble lignin fragments (~66%) and higher carbohydrate content (~5%). When compared to experiments with the most efficient separation (EXP10), which has ~90% acid-insoluble lignin and only ~1% carbohydrates. Glucose, cellobiose, and xylose are the most present sugars in the samples obtained. The sugars present in the bio-oil are probably derived from higher molecular weight holocellulose fragments, which remained attached to the lignin chain after pyrolysis (FORTIN et al., 2015). This lignin-carbohydrate combination may be the cause of the higher average molecular weight and higher polydispersity index, 773 g mol^{-1} and 1.8, respectively (TABLE III.S3), found for EXP1. Carbohydrate signals from xylans were observed at δ_C/δ_H 63.5/3.3 ppm (C_5–H_5 in β-D-xylopyranoside (WEN et al., 2012)), were detect in the aliphatic side-chain region of the EXP1 spectra (FIGURE III.S2). In the material obtained in EXP10, this signal is not observed. The following studies were conducted with the material obtained in EXP10, which presented a higher amount of lignin, which has an average molecular weight of 623 g mol^{-1} with a polydispersity index of 1.51 Hereafter, the material obtained in EXP10 will be called pyrolytic lignin (PL).

III.3.2 PYROLYTIC LIGNIN FRACTION AND CHARACTERIZATIONS

Acetone:water fractionation process yields 3 fractions with the following amounts of PL: 19% PL insoluble in 60% acetone (I60), 48% PL precipitated in 40% acetone (P40) and 33% PL soluble in 40% acetone (S40).

GC-MS analysis were used to characterize the monomers and dimers of PL (TABLE III.S4). Seventy-one main peaks were identified, being 63% of the compounds present in the S40 fraction detected by GC-MS, indicating that this fraction is composed mainly of lower molecular weight compounds than the P40 sample, in which only 17% of the compounds were detected. In fact, the fraction P40 presented as a major compound the dimer of H and S (1-Hydroxyphenyl-1'-syringyl-ethene, 25.83 mg g^{-1}), the high abundance of such lignin dimer when compare with lignin monomers, and the low fraction percentage detected in GC-MS may indicate a more polymerized material.

In the S40 fraction, 13% are derived from carbohydrates (8.4% of the total sample), 73% are derived from lignin (48.7% of the total). Also, S40 syringol present as the major compound (67.91 mg g^{-1}), with a similar amount of dimer 1-Hydroxyphenyl-1'-syringyl-ethene. Interestingly, levoglugosan, a common pyrolysis product of cellulose was also detected (FIGURE III.2). The majority of compounds (> 25 mg g^{-1}) in all fractions are mostly syringic derivatives, this behavior is because the eucalypt is a hardwood, phenols are also the predominant class reaching 30% of the S40 fraction. Phenol derivatives are mostly generated from the decomposition of lignin during pyrolysis (DENG et al., 2019; XIONG et al., 2020). The I60 fraction showed 41% of compounds analyzed by GC-MS, lignoceric acid is the most abundant compound. In fact, 24% of the identified compounds are lipids, such as sterols and fatty acids), and their corresponding to approximately 10% of the total sample. The source of lipids in samples may be associated with wood extractives (ARISANDI et al., 2020) and indicates that the extractives present in the wood resisted the pyrolysis process. Solvent fractionation may be an interesting approach to clean up such lipids.

The following techniques analyze the PL fractions as a whole, different that GC-MS analyses, in which only the volatiles and semi-volatile compounds are detected. In the FTIR the presence of carbonyl groups (0.9 - 1.1 mol kg^{-1}) was detected in all fractions obtained (FIGURE III.3d). The I60 fraction showed the highest content of these groups (3.1%). Albeit, carbonyl groups are formed during pyrolysis due to thermal cleavage, and due to the high reactivity, they are also bet as one of the responsible for the instability of bio-oils (SCHOLZE; HANSER; MEIER, 2001).

TABLE III.1 - HYDROXYL CONTENT IN PL FRACTIONS, DETERMINED BY WET CHEMISTRY AND SPECTROSCOPIC METHODS.

Relative content (wt%)	Fraction		
	S40	P40	I60
OH_{aliph} wet chemical	3.3 ± 0.1 b	3.5 ± 0.2 b	4.0 ± 0.1 a
OH_{phen} wet chemical	6.2 ± 0.3 c	5.2 ± 0.2 b	2.5 ± 0.2 a
Carboxyl wet chemical	3.5 ± 0.2 c	1.2 ± 0.4 b	0.7 ± 0.1 a
Total acidic groups	12.1 ± 0.3 b	10.8 ± 1.3 b	7.3 ± 0.3 a
OH_{aliph} FTIR	3.0 ± 0.1 b	3.0 ± 0.1 b	3.7 ± 0.1 a
OH_{phen} FTIR	6.3 ± 0.1 b	5.9 ± 0.1 b	3.9 ± 0.6 a

Averages followed by the same letters in the same row do not differ statistically by Tukey's test ($p<0.05$).

FIGURE III.2 - MAJOR COMPOUNDS IDENTIFIED BY GC-MS IN THE PYROLYTIC LIGNIN FRACTIONS, AND THEIR RESPECTIVE CHEMICAL CLASSES. BOLD VALUES IDENTIFY IN WHICH FRACTIONS THE COMPOUNDS ARE MAJOR (> 25 MG G^{-1}). (B) CHEMICAL CLASS CONTENT OF COMPOUNDS IDENTIFIED BY GC-MS.

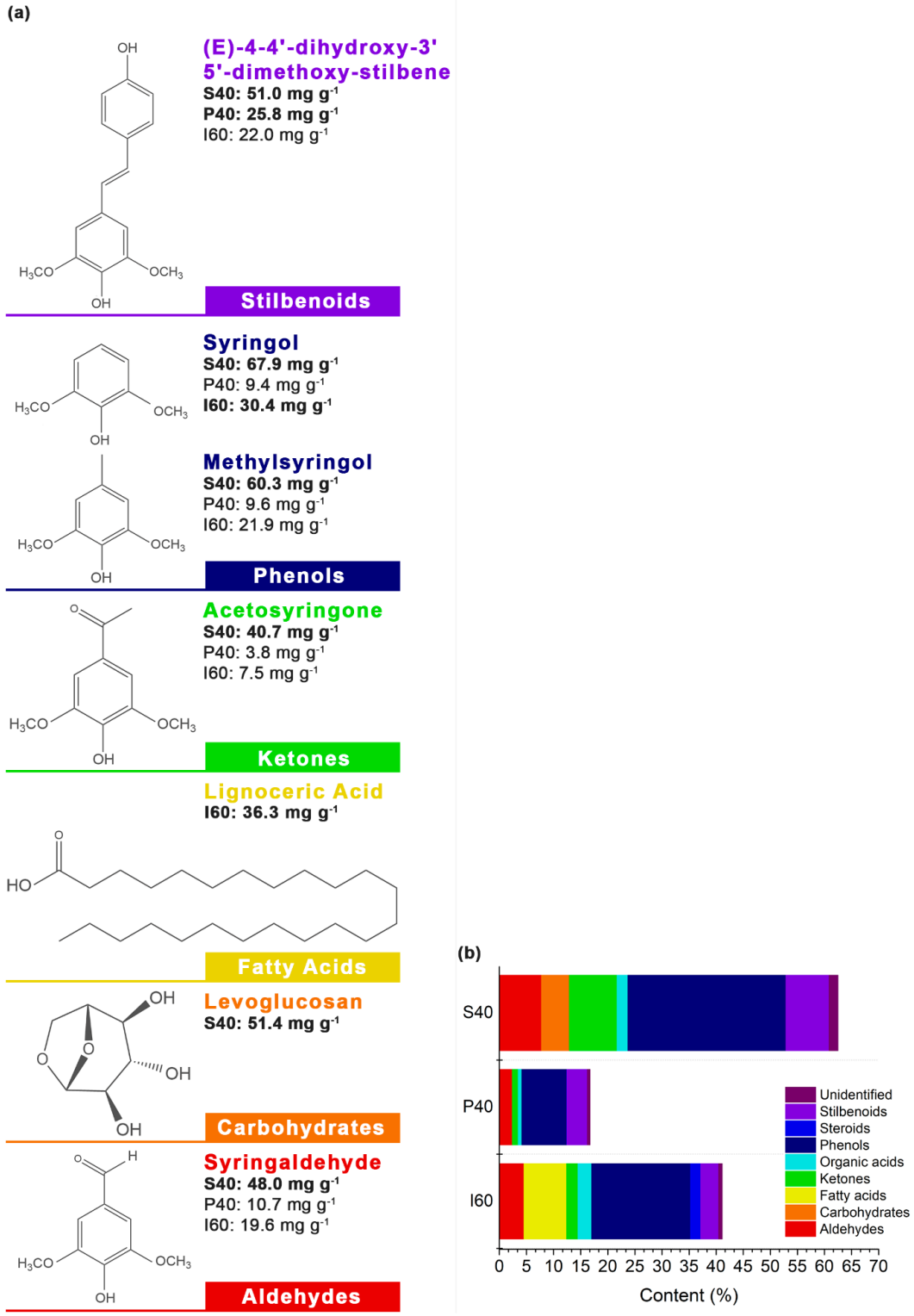

The results of the OH group via wet chemical analysis are listed in TABLE III.1. The values are between 3.3 and 4.0% for aliphatic hydroxyls and between 3.2 and 6.2% for phenolic hydroxyls. The range as determined with FTIR spectroscopy is in the same order of magnitude. With the fractionation of the PL, the S40 sample showed a higher content of hydroxyl groups (phenolic plus aliphatic) between the fractions, due to the greater interaction of these groups with the solvents used. Some of these hydroxyl groups may have been derived from breaking the β–O–4 ether bonds (JIANG; ELLIS; ZHONG, 2010). The I60 fraction has a higher aliphatic OH content, probably due to the presence of aliphatic alcohol in sterols. In FTIR spectra (FIGURE III.3a), the band at 3420 cm^{-1} is attributed to hydroxyl groups. In the region between 3000 and 2750 cm^{-1}, several peaks overlap. The shoulder at 2960 cm^{-1} indicates asymmetric vibration of –C–H of CH_3.The I60 fraction shows an intense peak in 2918 cm^{-1}, not evident in the other fractions, such peak is attributed to asymmetric vibration of –C–H of CH_2 (MOHARAM; ABBAS, 2010), which indicates the presence of fatty acids. The presence of such nonpolar compounds was confirmed by GC-MS (TABLE III.S4). This presence of lipids in the insoluble fraction is due to the low solubility of these compounds in the solution used, which is considerably polar. The peak at 2850 cm^{-1} represents symmetric vibration of –C–H of CH_2 and CH_3.

The band at 1710 cm^{-1} is attributed to the unconjugated C=O stretching vibrations (LENG et al., 2017), which refers to the unconjugated carbonyl of ketones and esters (WANG et al., 2015). It is observed that the relative intensity of these peaks is higher in sample I60 and lower in S40 (FIGURE III.3b). Confirming that reduction of these groups occurs when the concentration of acetone in the solutions decreases. Strong peaks at 1610 and 1515 cm^{-1} due to the aromatic skeletal vibrations are observed. The peak at 1430 cm^{-1} is due to the aromatic skeletal vibrations combined with C–H in-plane deformation. The peak at 1460 cm^{-1} is due to the C–H asymmetric deformations, in -CH_3 and –CH_2. The peaks at 1330 and 1275 cm^{-1} represent C–O in syringyl (S) and guaiacyl (G) units, respectively. The peak at 1154 cm^{-1} represents the aromatic C–H in-plane deformation in G units. Meanwhile, the peak at 1115 cm^{-1} is attributed to the deformation of C–H in S units (WANG et al., 2015). The presence of these peaks shows that there was a permanence of units S and G after pyrolysis. This

is probably due to the high thermal stability of methoxy groups when linked to aromatic rings. However, at 830 cm^{-1}, the presence of C–H vibrations out-of-plane in p-hydroxyphenyl (H) units is observed (FAIX, 1991a). It is known that *Eucalyptus* spp. is classified as a hardwood, for that reason, it produces lignins composed mainly by the guaiacyl and syringil units. Therefore, the presence of H units in PL suggests the cleavage of structures and bonds during pyrolysis, for example, the demethoxylation of G units (BEN; RAGAUSKAS, 2011). Corroborating with this, the GC-MS analysis (TABLE III.S4) showed the presence of compounds with H units, such as 4-ethenylphenol, 4-hydroxybenzaldehyde, 4-Hydroxycinnamic acid, and 1-Hydroxyphenyl-1'-syringyl-ethene. The presence of H units was also observed in the 2D HSQC NMR spectra (FIGURE III.5). It is also observed the abundant presence of side chains in the PL fractions, due to the presence of the peaks: 1366 cm^{-1} attributed to stretching of aliphatic CH (not in methoxyl groups); 1216 cm^{-1} attributed to stretching CC plus CO plus C=O stretch, also diphenyl ether structures (BAYERBACH; MEIER, 2009), and 1035 cm^{-1} attributed to C=O stretching (unconjugated) plus aromatic C–H in-plane deformation plus C–O deformation in primary alcohols. The relative absorption intensity at 1366 cm^{-1} suggests that there is a greater amount of methoxy groups in the I60 fraction, insoluble in 60% acetone, probably from the lipid aliphatic chain present in this fraction (FIGURE III.2b). The presence of side chain peaks suggests the presence of carbonyls, hydroxyls, unsaturated double bonds, aliphatic side chains, among others, making this lignin more reactive which could facilitate their subsequent utilization (WANG et al., 2015). The peak at 910 cm^{-1} attributed to out-of-plane vibrations in aromatic rings.

FIGURE III.3 - (A) FTIR SPECTRA OF THE PYROLYTIC LIGNIN FRACTIONS (B) RELATIVE INTENSITY OF EACH FUNCTIONAL GROUP. CALCULATED BY THE RATIO BETWEEN THE INTENSITY OF VIBRATION (IN A GIVEN WAVENUMBER) AND THE INTENSITY OF ABSORPTION OF THE AROMATIC SKELETAL VIBRATION IN 1515 CM^{-1}. (C) CONDENSATION INDEX OF THE PYROLYTIC LIGNIN FRACTIONS, CALCULATED FROM THE FTIR SPECTRA OF THE NON-ACETYLATED FRACTIONS. (D) CONTENT OF CARBONYL GROUPS IN THE LIGNIN FRACTIONS, DETERMINED BY OXIMATION

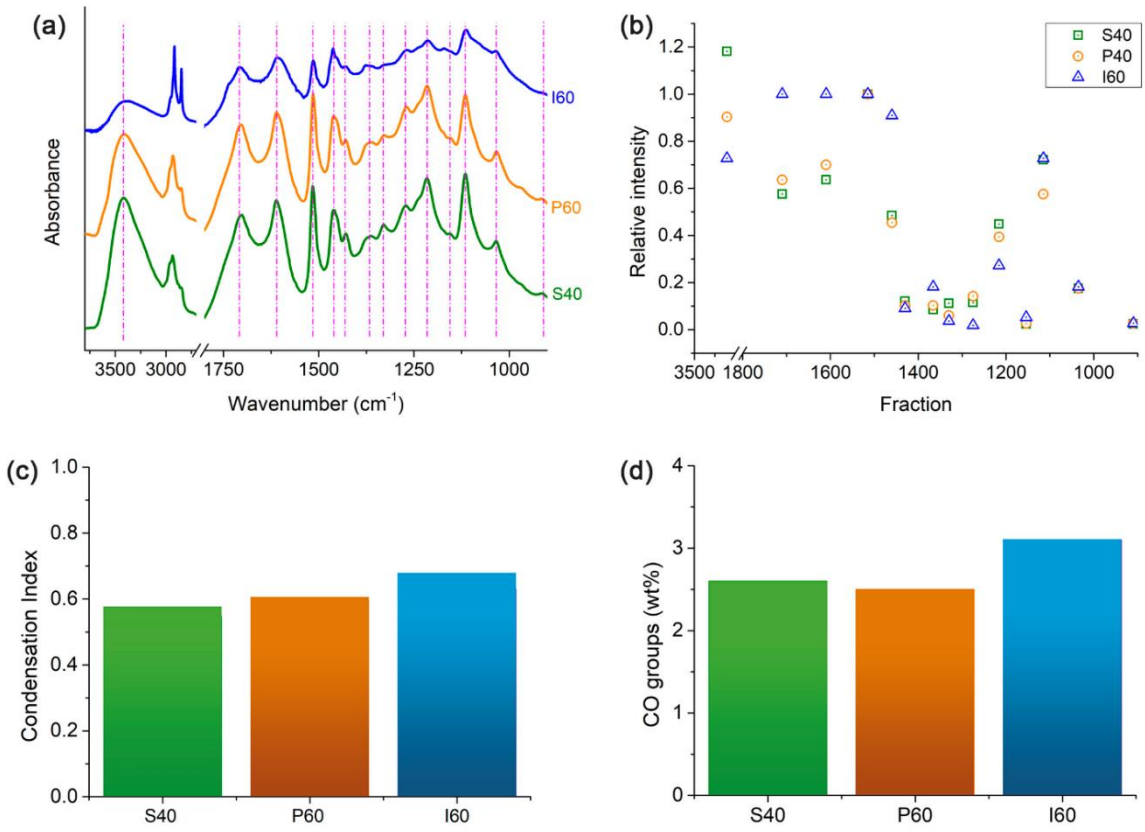

TABLE III.2 - WEIGHT-AVERAGE (M_w), NUMBER-AVERAGE (M_n) MOLECULAR WEIGHTS DATA AND POLYDISPERSITY INDEX (PDI) OF THE PL FRACTIONS.

Fraction	M_w (g mol^{-1})	M_n (g mol^{-1})	PDI (M_w/M_n)
I60	1435	596	2.4
P40	1527	625	2.4
S40	841	448	1.9

The average (M_w) and the number average (M_n) molecular weights of I60, P40 and S40 are presented in TABLE III.2. It is known that PL consists of oligomers with different degrees of polymerization (WANG et al., 2014a). The S40 fraction is mostly formed by monomers, dimers, and trimers, which was suggested by GC-MS analysis (TABLE III.S4). P40 and I60 are probably composed of PL with higher molecular

weights such as trimers, tetramers. Oligomers derived from lignin tend to form large molecular weight compounds (DENG et al., 2019). S40 is less polydispersed when compared to P40 and I60. The molecular weight distribution of PL can be influenced by the raw material, the degree of pyrolysis, and the method of extraction (WANG et al., 2015). For example, they obtained less polydispersed pyrolytic lignin fractions using sequential fractionation using different organic solvents (ZHANG et al., 2019b). However, the study cited uses solvents such as dichloromethane, which together with other chlorinated solvents, are dangerous for the environment or toxic. While, acetone is placed in fifth place in the ranking of safe solvents, being referred to as a green alternative (TOBISZEWSKI; NAMIEŚNIK; PENA-PEREIRA, 2017). The occurrence of reactions between active functional groups, present in PL, with unsaturated bonds of aldehydes and ketones in the bio-oil, which increases the molecular mass of PL over time, may also affect the molecular mass distribution (BAYERBACH; MEIER, 2009). The average molecular weight of the I60 fraction may also have been affected by the presence of lipids, these compounds contribute to the increase in molecular weight (XIONG et al., 2020).

2D HSQC NMR was used to elucidate the structural characteristics of the PL fractions. The side chain (δ_C/δ_H 50-90/2.5-5.0 ppm) and aromatic (δ_C/δ_H 100-150/5.5-8.0 ppm) regions of the HSQC spectra, and their main identified structures are shown in FIGURE III.4 e FIGURE III.5. The cross-peaks assignments (BEN; RAGAUSKAS, 2011; LANCEFIELD et al., 2018; LI et al., 2020; PEREIRA et al., 2017; WANG et al., 2015; ZHOU et al., 2016) are summarized in TABLE III.1. The side chain region shows the presence of several interunit bonds in the pyrolytic lignins. The presence of a pronounced signal corresponding to the methoxyl groups in the three fractions is observed. Signs of $C_2 – H_2$, $C_3 – H_3$, $C_4 – H_4$ and $C_6 – H_6$ in levoglucosan are observed in the S40 fraction, corroborating with the results of GC-MS that the show the presence of this substance only in S40 (FIGURE III.2). The presence of this pyrolytic sugar may be due to the enrichment of sugars in the heavy fraction of bio-oil. Therefore, when carrying out the PL precipitation, the dragging of levoglucosan and other water-soluble compounds occurs. In addition, the presence of levoglucosan only in the S40 fraction may be related to the polarity of the solution used for fractionation, which is relatively

polar, facilitating the solubilization of this compound. As well as sugar fragments linked to lignin. The C_β and C_γ signals from resinol structures (C) are present in I60 and S40 fractions, respectively. This suggests the presence of β-β' bonds. The relative proportion of β-aryl-ether structures is higher in the S40 fraction (FIGURE III.4b), possibly due to the interaction of OH present in the structure with the solvent, which facilitates solubilization. The β-aryl-ether structures (A) tend to be cleaved during pyrolysis. However, some of them may remain due to their high activation energies (LENG et al., 2017). In addition to the carbon-carbon bonds present in native lignin. The formation of new C-C bonds can occur due to repolymerization caused by reactive intermediates formed during the depolymerization process. Leading to the condensation of the lignin structure (SCHUTYSER et al., 2018).

FIGURE III.4 - 2D HSQC NMR SPECTRA OF PYROLYTIC LIGNIN FRACTIONS AND THEIR MAIN STRUCTURES. (A) OXYGENATED ALIPHATIC SIDE CHAIN (δC/δH 50-90/2.5-5.0 ppm) REGIONS OF PL FRACTIONS; (b) RELATIVE PROPORTION OF INTERUNIT LINKAGES; (c) THE MAIN LIGNIN SIDE CHAIN IDENTIFIED STRUCTUREs: (A) β-ARYL-ETHER STRUCTURES, (C) RESINOL STRUCTURES, (LG) LEVOGLUCOSAN, ORANGE PEAKS CORRESPOND TO METHOXYL GROUPS.

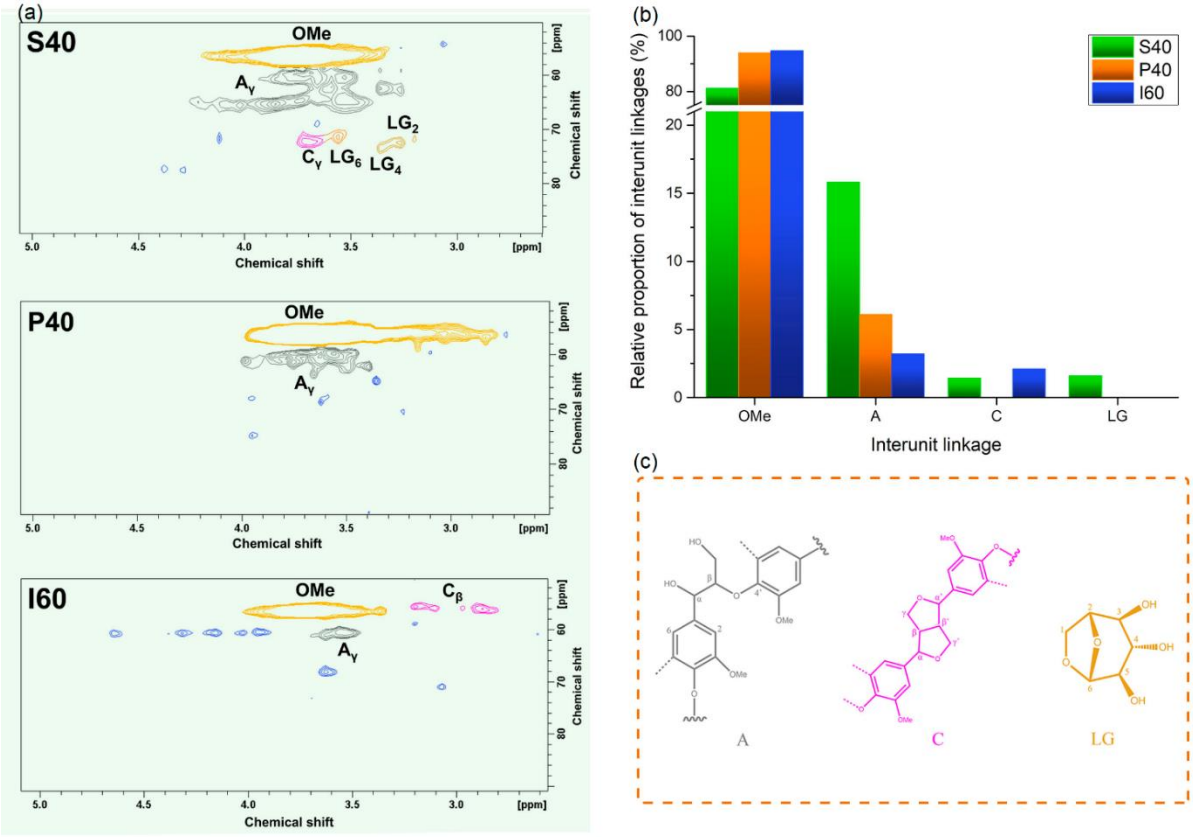

Corroborating with the results obtained by GC-MS, syringyl (S), guaiacyl (G) and *p*-hydroxyphenyl (H) units were found in the main cross-peaks in the aromatic region of the HSQC spectra. In the S40 fraction, the presence of a cross-peak (δ_C/δ_H 108/7.2 ppm) attributed to stilbene substructures (SB5) is observed. Nevertheless, according to GC-MS, the presence of stilbene was detected in all fractions, this probably occurred due to signal overload and the low concentration of these compounds. The cross-peak (δ_C/δ_H 108/7.2 ppm) can also be attributed to the oxidized syringyl units (S'), the presence of this type of structure is confirmed by the presence of compounds such as acetosyringone (FIGURE III.2a). At 115 ppm, the cross-peaks corresponding to C_5–H_5 are observed in etherified and non-etherified guaiacyl substructures. Non-etherified structures are mainly derived from the cleavage of interunit bonds during pyrolysis (WANG et al., 2015).

FIGURE III.5 - 2D HSQC NMR SPECTRA OF PYROLYTIC LIGNIN FRACTIONS AND MAIN STRUCTURES. (a) AROMATIC (δC/δH 100-150/5.5-8.0 ppm) REGIONS; (b) RELATIVE PROPORTION OF LIGNIN UNITS OF PL FRACTIONS; (c) THE MAIN LIGNIN AROMATIC STRUCTURES IDENTIFIED: (S) SYRINGYL UNITS, (S') OXIDIZED SYRINGYL UNITS (G) GUAIACYL UNITS, (H) *p*-HYDROXYPHENYL UNITS, (SB5) STILBENE STRUCTURES.

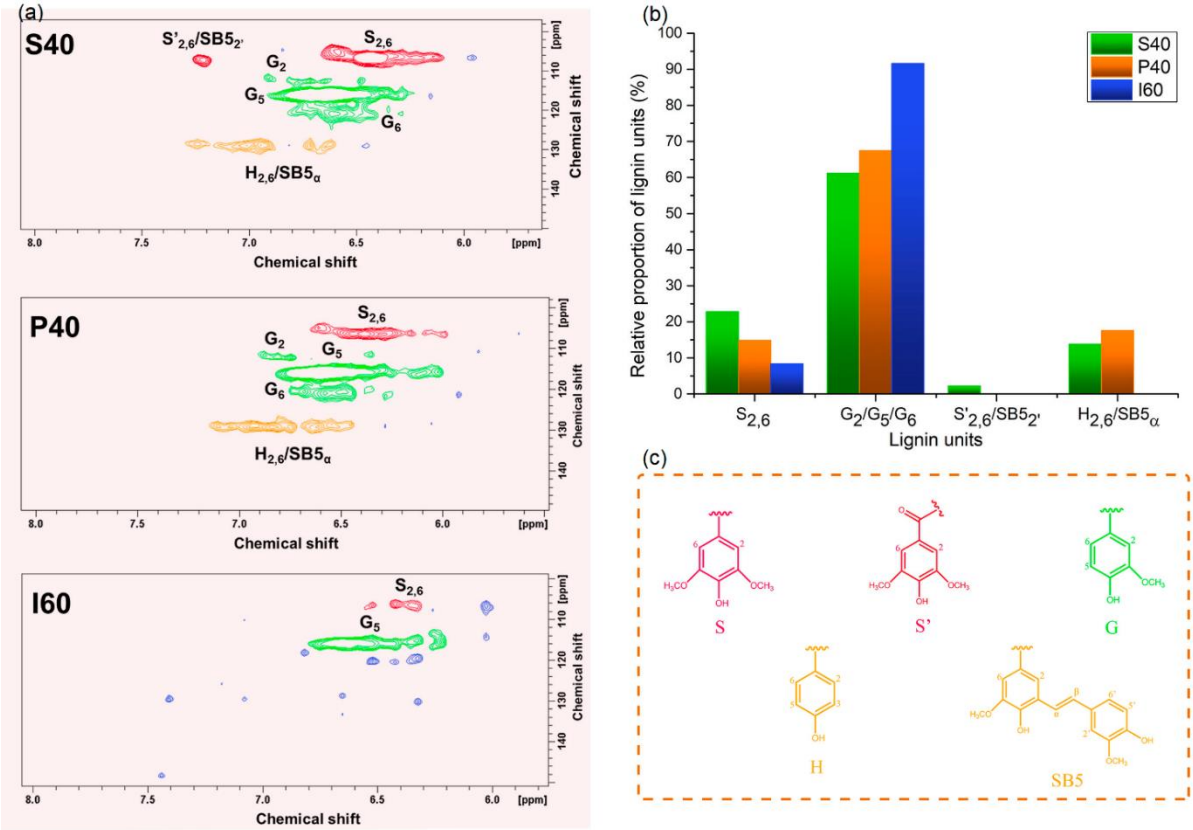

The TG curves of PL (

FIGURE III.S3) present a complex behavior, with the presence of several mass loss peaks (WANG et al., 2014a). However, it is possible to observe three stages of mass loss. The first, up to approximately 200 °C, is attributed to the loss of free water and the evaporation of lower molecular weight compounds. In the second stage, from 200 to 500 °C, there is the greatest loss of mass resulting in the cleavage of the main structure and, consequently, the release of volatiles. The last stage occurs at temperatures above 500 °C, where carbonization processes occur. The TG curves indicate that the S40 fraction is more sensitive to temperature, with its degradation onset temperature at 204 °C, exhibits a greater loss of mass in a low-temperature range, in addition to presenting the lowest char yield values (~32%). Meanwhile, P40 has a degradation onset temperature of 218 °C and residue content of ~37%. The formation of a greater amount of char, in P40, is due to the presence of PL with higher molecular weight (TABLE III.2), and a more condensed structure than the S40 fraction (FIGURE III.3c). However, it is important to note that although the I60 fraction has a more condensed structure than the P40, the char yield was lower (~35%), possibly due to the presence of lipids that are volatilized (at ~500 °C). Therefore, the char yield is virtually lower, since, discounting the lipids, the percentage of char would be higher.

TABLE III 3 - ASSIGNMENTS OF PL FRACTIONS $^{13}C/^{1}H$ CORRELATION SIGNALS IN THE 2D HSQC SPECTRA

Label	δ_C/δ_H (ppm)	Assignment
C_β	55/2.9, 3.15	C_β/H_β in β–β´ resinol substructures (**C**)
OMe	55.5/3.7	C/H in methoxyls (**OMe**)
A_γ	60/3.4, 3.7, 4.0	C_γ/H_γ in γ-hydroxylated β–O–4´ substructures (**A**)
LG_6	71.5/3.55	C_6/H_{6a} in levoglucosan (**LG**)
LG_2	72/3.2	C_2/H_2 in levoglucosan (**LG**)
LG_4	72/3.28	C_4/H_4 in levoglucosan (**LG**)
C_γ	72/3.7	C_γ/H_γ in β–β´ resinol substructures (**C**)
LG_3	73/3.35	C_3/H_3 in levoglucosan (**LG**)
$S'_{2,6}$	106/6.4	C_2/H_2 and C_6/H_6 in oxidized syringyl units (**S'**)
$SB5_{2'}$	108/7.2	C_2/H_2 in stilbene substructures (**SB5**)
G_2	112/6.85	C_2/H_2 in guaiacyl units (**G**)
G_5/G_6	115/6.7	C_5/H_5 and C_6/H_6 in guaiacyl units (**G**)

	120/6.6	
$SB5_{\alpha}$ /$H_{2,6}$	129/7.0	C_{α}/H_{α} in stilbene substructures (**SB5**) C_2/H_2 and C_6/H_6 in *p*-hydroxyphenyl units (**H**)

III.3.3 ANTIOXIDANT AND ANTIBACTERIAL PROPERTIES

The results of the ability of the PL fractions to reduce DPPH and ABTS radicals, and ferric ion reducing antioxidant power (FRAP) are shown in FIGURE III.6. It is already widely known that the reduction mechanism in FRAP and ABTS methods is based on electron transfer (ET) (FIGURE III.6d-e). In this mechanism, the reducing agent donates the electron necessary for the radical reduction and releases an H^+ ion. DPPH reduction is based on hydrogen atom transfer (HAT) (APAK et al., 2016). There is a clear tendency to increase the antioxidant capacity as the fraction is more soluble. Therefore, the antioxidant activity index (AAI) against to the radical DPPH were 6.2 mg DDPH mg^{-1} for S40 and 2.3 mg DPPH mg^{-1} for P40 and I60. Therefore, the three fractions have a very strong AAI, as they have an AAI greater than 2.0 (SCHERER; GODOY, 2009). The antioxidant power of S40 was also greater than that of the other fractions against the radical ABTS (2.1 mg TE mg^{-1}) and in the reduction of Fe^{3+} ions (1.4 mg FSE mg^{-1}). Since the antioxidant power of S40 was approximately twice the values found for P40 and I60.

The antioxidant capacity of PL may be due to the drastic depolymerization that occurs during pyrolysis, as well as the presence of new carbon-carbon bonds (DIZHBITE et al., 2004; PAN et al., 2006), as shown by the NMR data (FIGURE III.4a). The molecular weight of lignins can be considered as one of the main factors affecting the radical scavenging activity (DIZHBITE et al., 2004). Lignins with low molecular weights tend to have greater antioxidant activity (DOBELE et al., 2009). This is confirmed for the PL fractions, where S40 has lower molecular weight (TABLE III.2) and greater antioxidant activity (FIGURE III.6). In addition, Dizhbite et al. evaluated different types of wood lignin from Aspen, Spruce and Birch, came to the conclusion that high molecular weight, increased heterogeneity and polydispersity are among the factors that decrease radical scavenging activity (DIZHBITE et al., 2004).

The higher amount of free phenolic OH (TABLE III.1) and a high percentage of monomers and dimer detected by GC-MS are also justified by the fact that the S40 fraction is a more potent antioxidant (SADEGHIFAR et al., 2017) when compared to P40 and I60. Aromatic compounds derived from lignin, without the presence of OH groups do not have antioxidant activity. This means that OH groups are essential for antioxidant activity (ZHAO et al., 2018a). For example, Alkaline lignin depolymerized by hydrogenation using Pd/C as a catalyst and formic acid as a hydrogen donor, had an increase in the phenolic hydroxyl content, thus increasing antioxidant activity (ZHAO et al., 2018a). It is interesting to note that the I60 fraction has a higher content than aliphatic OH than the other fractions, and its antioxidant power is lower. This can occur because in polymeric lignins the positive influence of OH tends to be attenuated (DIZHBITE et al., 2004). In addition to the ability to form a phenoxyl radical, the elimination of radicals by phenolic compounds also depends on the stability of the phenoxyl radical. Phenolic structures with substituents that stabilize phenoxyl radicals tend to have greater antioxidant activity than those that do not (PAN et al., 2006; ZHAO et al., 2018a). For example, substituents such as methoxyl groups, stabilize phenoxyl radicals by resonance. Therefore, S units tend to be more antioxidant than G units, which in turn tend to be more antioxidant than H units. This is probably due to the greater number of resonant structures when there are substituents in the ring (FIGURE III.6g-i). It is worth mentioning that the presence of non-lignin compounds, such as lipids in P40 and I60, can reduce radical scavenging activity (THRING; GRIFFIN, 1995).

In addition, the ability to stabilize the formed radical, after eliminating free radicals, tends to be increased when there is some additional conjugation with substituents. However, if the extension of the conjugation occurs with the presence of carbonyl groups in the side chain, the antioxidant activity tends to decrease (DIZHBITE et al., 2004) due to the presence of this electron withdrawing group. This may be one of the reasons why the I60 fraction had lower antioxidant power than its analogues. The I60 fraction has a higher content of these electron withdrawing groups. The analysis of FTIR spectra also shows a greater number of these groups (FIGURE III.3b).

To compare the antimicrobial properties of the PL fractions, minimum inhibitory concentration (MIC) was determined against *S. aureus*, *E. coli* and *S. enterica* bacteria (FIGURE III.6j-k). *S. enterica* growth was not inhibited by the PL fractions tested in this work. The maximum concentration evaluated was 2.5 mg mL^{-1}. Fractions S40 and P40 showed the lowest MIC values, with 0.3 mg mL^{-1} for *E. coli* and *S. aureus*. Meanwhile, I60 had a lower MIC for *S. aureus* (0.6 mg mL^{-1}) than for *E. coli* (1.2 mg mL^{-1}). The results of GC-MS show the presence of simple phenols, it is known that these compounds have antimicrobial properties (ANDERSEN, 2006). However, they are not the only compounds, present in fractions, that inhibit the growth of bacteria. Fractions with the highest amount of phenolic OH (S40 and P40) showed lower MIC for *S. aureus* and *E. coli* (i.e. higher inhibitory potential). Previous studies have shown that the presence of phenolic OH is highly desirable for antibiotic activity (DONG et al., 2011; VATTEM et al., 2004). The phenolic compounds present in the PL fractions are weakly acidic. Therefore, they can dissociate in the plasma membrane at biological pH. This dissociation may be one of the mechanisms by which they exert their antibacterial effect. Since acidification of the plasma membrane of the microorganism, caused by the proton release, can lead to the rupture of the proton-translocating adenosine triphosphatase (H^+-ATPase), which is necessary for the production of ATP (adenosine triphosphate). The lack of ATP can affect the bacterial energy metabolism, leading to growth inhibition (VATTEM et al., 2004). The presence of OH from carboxylic groups (COOH) in PL fractions, mainly in S40 (TABLE III.1), can easily cause protonation, helping to disrupt the proton pump. It is important to remember that *S. aureus* is a gram-positive microorganism, therefore it has a unique cell membrane. This makes it more susceptible to interruption of H^+-ATPase. Another factor that can affect lignin activity is partial hydrophobicity. The most hydrophobic part of the macromolecule would tend to adhere to the plasma membrane. It can lead to weakening and rupture of the bacterial membrane (VATTEM et al., 2004). In addition to interfering with transport processes and intracellular Ca^{2+} metabolism (CHANDRAN et al., 2020). Therefore, this seems to be the preferable factor in the inhibition of *E. coli*, since the presence of the outer lipo-polysaccharide layer surrounding the plasma membrane hinders the acidification effect. Furthermore, enterohemorrhagic bacteria, such as *E.*

coli, have the ability to lengthen the cell membrane, controlling acid stress by diffusing the proton gradient created by acidification (LIN et al., 1996). However, differences in the internal membrane of gram-negative bacteria (*E. coli* and *S. enterica*) can be one of the reasons, for the non-inhibition of the growth of S. enterica and for the inhibition of *E. Coli* (YANG et al., 2017), in the tested concentrations. Carbonyl groups also collaborate for antimicrobial action on PL fractions (MILLY; TOLEDO; RAMAKRISHNAN, 2005). The MIC value of the I60 fraction is probably greater than the values of its analogues. Probably, due to the presence of nonpolar compounds, such as lipids, which tend not to have antibacterial properties (BEDMUTHA et al., 2011).

A recent study evaluated the action of fractions of lignin kraft from hardwood against the bacteria E. coli and S. aureus, in which the authors found MIC values higher than this study, greater than 3.125 mg mL^{-1} for *S. Aureus* and greater than 6.250 mg mL^{-1} for *E. Coli* (LOURENÇON et al., 2021). This difference is probably due to the higher molecular weight of the lignin kraft and the low concentration of monomeric phenolic compounds, this can lead to a decrease in the amount of H^+ released into the medium by dissociation. It is worth noting that these differences are mainly due to the process of obtaining lignin. Another study found a MIC value against *S. Aureus* of 1.25 mg mL^{-1} when using lignin extracted from corn straw residue. The authors also attributed the antibacterial activity to the presence of phenolic compounds (DONG et al., 2011).

FIGURE III.6 - ANTIOXIDANT ACTIVITY OF PYROLYTIC LIGNIN FRACTIONS AGAINST FREE RADICALS AND MINIMUM INHIBITORY CONCENTRATION (MIC) AGAINST BACTERIAS

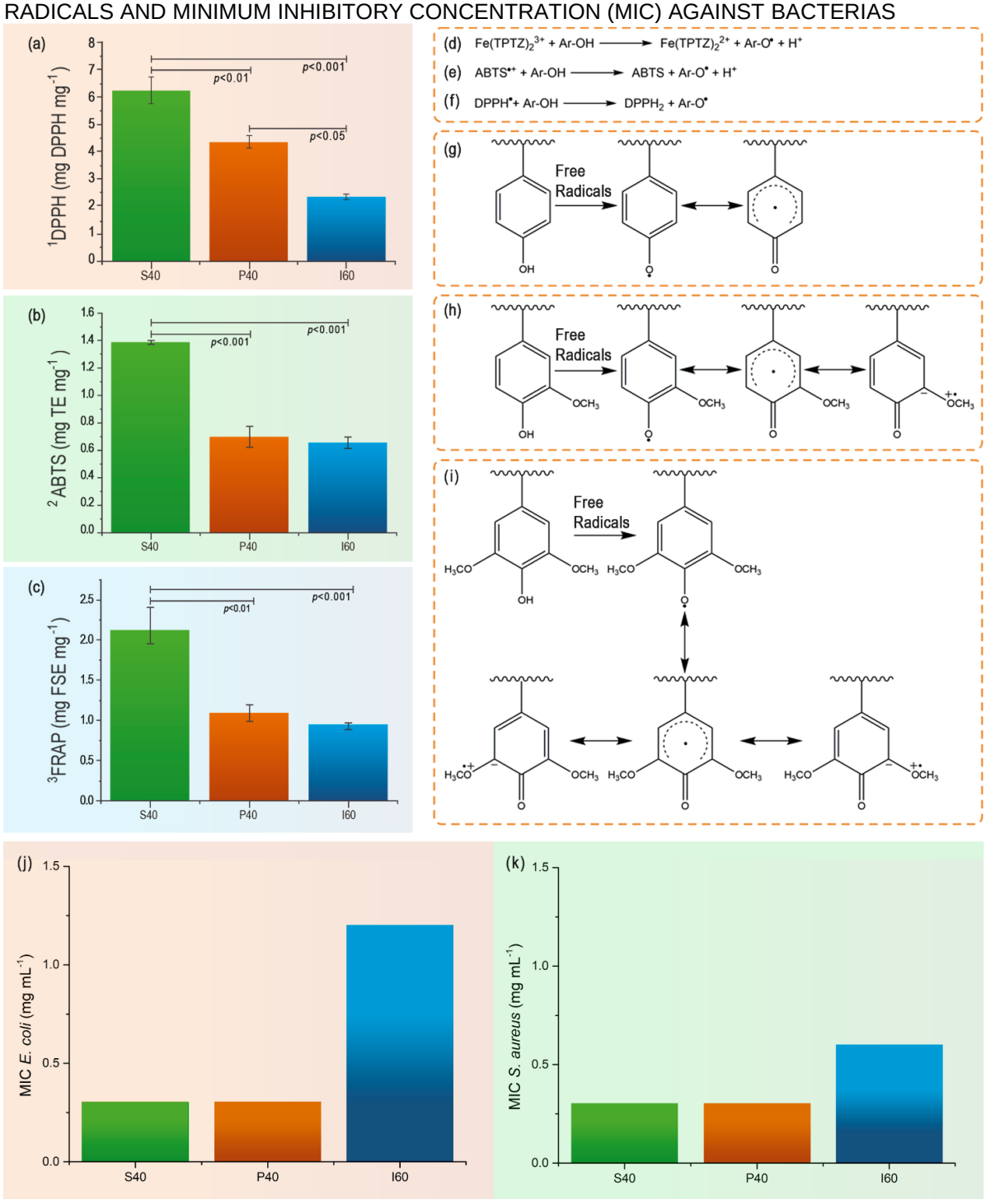

Antioxidant activity of pyrolytic lignin fractions against free radicals: **(a)** 2,2-Diphenyl-1-picrylhydrazyl, [1]result expressed in terms of antioxidant activity; **(b)** 2,2′-azinobis-(3-ethylbenzothiazoline-6-sulfonic acid), [2]result expressed in trolox equivalent (TE); **(c)** ferric ion reduction capacity, [3]expressed as equivalent to ferrous sulfate (FSE). **(d-f)** Free radical scavenging reaction equations. Trapping and stabilization mechanisms of radicals by lignin units, based on that proposed by Barclay et al. (1997): **(g)** *p*-Hydroxyphenyl units, **(h)** Guaiacyl units and **(i)** Syringyl units. Minimum Inhibitory Concentration (MIC)

of the pyrolytic lignin fractions: **(j)** Against *Escherichia coli*; **(k)** Against *Staphylococcus aureus*. *S. enterica* was not inhibited.

III.4 CONCLUSIONS

The fractionation of lignin in aqueous acetone solutions results in more homogeneous fractions, concentrating phenolic, carboxylic, and lower molecular weight compounds in the most soluble fraction. The antioxidant activity was mainly attributed to phenolic compounds with methoxyl substituents. The most soluble fraction of pyrolytic in acetone: water had a greater potential for antioxidant purposes, which can be used in several applications, such as smart packaging and additives for fuels. The fractionation process also furnished pyrolytic lignin fractions that possess good biological activity, which can be used to develop alternative antibacterial agents. Therefore, the reported fractionation procedure of pyrolytic lignin using acetone:water may be considered a potential alternative protocol for the valorization of this class of lignin as also for the development of novel technological bioproducts. Nevertheless, for its application in food or related products, it is still necessary to further study its cytotoxicity.

CHAPTER IV

ELUCIDATION OF THE BEHAVIOR OF MODEL COMPOUNDS OF BIO-OIL IN HYDROGENATION ON Ag/SiO_2 AND Pd/SiO_2 CATALYSTS

IV.1 INTRODUCTION

The pyrolysis of biomass is a complex process due to the varied structure of the raw material and several reactions that occur simultaneously in the reactor. One of the products, the liquid product obtained (bio-oil) has a large amount of oxygenated compounds, such as acids, phenols, ketones (HELLINGER et al., 2015; MCCORMICK et al., 2015). The presence of these oxygenated compounds leads to a deterioration of their calorific value (BHOI et al., 2020; MOHAN; PITTMAN; STEELE, 2006). Removing these oxygenated compounds will reduce the corrosivity of pyrolysis oil and make it more suitable for modern engines. In addition, phenolic compounds can be transformed into BTX (benzene, toluene and xylene) through hydrodeoxygenation (HDO) (RINALDI et al., 2016; WANG; RINALDI, 2013).

HDO of pyrolysis oil is a high-pressure heat treatment of bio-oil with hydrogen and catalysts. The optimal operating conditions for HDO are based on the type of pyrolysis oil produced. The main variables to be considered for upgrading bio-oil are temperature, pressure and type of catalyst (OUEDRAOGO; BHOI, 2020). Noble metal catalysts supported on ceramics are considered the most suitable catalysts for HDO in bio-oil due to their dual properties: metals and acidic sites (JAFARIAN; TAVASOLI; NIKKHAH, 2019). HDO performed under catalysts supported on Pd and Pt mainly promoted the hydrogenation reaction. C=C and C=O bonds and unsaturated hydrocarbons were hydrogenated to produce saturated hydrocarbons (FUNKENBUSCH et al., 2019; YANG et al., 2018). Due to the ability of Ruthenium to bind to oxygen, Ru-based catalysts show a greater deoxygenation capacity when compared to Pt and Pd-based catalysts (LIU et al., 2017).

In general, the main difficulty in the upgrading processes of bio-oil is the formation of carbonaceous deposits in the catalytic bed, originating from the heavy compounds derived from lignin (WANG; RINALDI, 2013). However, to clarify the contribution of each main components of bio-oil towards coking, more fundamental studies are required (HU; GHOLIZADEH, 2020). Moreover, for the difficulties in HDO bio-oil to be overcome, the first step must be the development of the catalyst. This

catalyst should reduce coking and accelerate the hydrodeoxygenation (HU; GHOLIZADEH, 2020; OUEDRAOGO; BHOI, 2020).

One strategy to understand the process of upgrading pyrolytic products is to study the behavior of different model compounds during the catalytic process. This tends to facilitate the understanding of the behavior of the different components of the bio-oil. By understanding the chemistry and reaction mechanisms of model compounds, you can control the selectivity of products to be obtained. This knowledge can then be exported to real pyrolysis bio-oils in order to obtain the desired fuels and chemicals (HE; WANG, 2013).

Considering the exposed scenario, this work evaluates the behavior of several model compounds of bio-oil (syringol, syringaldehyde, guaiacol, and vanillin), in the reaction with hydrogen catalyzed by Ag/SiO_2 and Pd/SiO_2 catalysts.

IV.2 MATERIAL AND METHODS

IV.2.1 CATALYSTS SYNTHESIS AND CHARACTERIZATIONS

The catalysts were prepared by the method of impregnating the support with a precursor solution of the metal. The silver catalysts ($5Ag/SiO_2$ and $10Ag/SiO_2$) were produced in concentrations of 5 and 10 mol% in reaction to the support. For this, aqueous solutions of $AgNO_3$ (3.5 mL) were impregnated in silica nanoparticles (SiO_2 - NPs, ~325 $m^2\ g^{-1}$) (2 g), followed by drying in an oven (60 °C) for 24 hours. Finally, the reduction of silver in a muffle at 500 °C was performed. The palladium catalysts ($1Pd/SiO_2$ and $2Pd/SiO_2$) were produced at concentrations of 1 and 2 mol% in reaction to the support. For this, 3.5 mL of $PdCl_3$ solutions, in 10% HCl, were impregnated in SiO_2-NPs (2 g), followed by drying in an oven (60 ° C) for 24 hours. The reduction from Pd^{3+} to Pd^0 was carried out at 700 °C.

The surface area of the catalysts and the pore size distribution were measured using N_2 adsorption. The adsorption of N_2 at 77 K was determined with a BET Surface Area Analyzer NOVA 1200 device and the adsorption data were analyzed using built-in calculation protocols. All samples were degassed at 200 °C for 3 h before analysis.

The surface areas of BET (Brunauer-Emmett-Teller) (S_{BET}) were calculated from the linear adjustment of the adsorption data (THOMMES et al., 2015). The morphological features and the elemental mapping of the obtained catalysts were investigated using a scanning electron microscope Tescan VEGA3 equipped with an energy-dispersive X-ray spectroscopy device.

IV.2.2 REACTION CONDITIONS

Reactions were carried out in an automated microactivity reactor (PID Eng&Tech, Spain). With the following reaction parameters: Feed temperature, 50 °C; Feed flow, 0.5 mL min^{-1}; Argon flow rate, 50 mL min^{-1}; Hydrogen flow rate, 50 mL min^{-1}; Pressure, 25 bar; Catalyst amount, 250 mg; Reactor temperature, 500 °C; Condenser temperature, 15 °C. The reactions occurred in a steady state for 90 min. Therefore, the total of model compound solutions fed was 45 mL. These solutions were prepared in ethanol at a model compound concentration of 5% (w/v).

IV.2.3 CHARACTERIZATION OF THE PRODUCTS OBTAINED

IV.2.3.1 Conversion

The percentage conversion of model compounds by the catalysts was calculated using the following equation:

$$Conversion(\%) = \frac{(m_f - m_p)}{m_f} \times 100$$

Where, m_p is the amount of model compound present in the collected product, and m_f represents the amount of model compound that was fed to the reactor. The amount of model compound in the product was calculated from the volume of solution collected and the concentration of model compound in solution. The concentration was determined based on a calibration curve constructed by GC-MS, using 5-α-Cholestane as an internal standard.

IV.2.3.2 Coke formation

The amount of coke formed and deposited on the catalyst was evaluated by thermogravimetry, where the coke formed is burned in an atmosphere of synthetic air. For this, about 5.0 mg of sample was added in alumina pans. The experiments were conducted under a synthetic air flow of 50 mL min^{-1}, in a Q600 SDT (TA Instruments, USA), heating samples up to 800 ºC at a rate of 20 °C min^{-1}. Three replicates were performed. The analysis of the thermograms was performed with the TA Instruments Universal Analysis 2000 software.

IV.2.3.3 Gas Chromatography-Mass Spectrometry (GC-MS)

For GC analysis 20 µL of each sample were transferred to a 2 mL micro-centrifuge tube, with 955 µL of acetone, and 25 µL of 5-α-Cholestane were added as internal standard (2 mg mL^{-1} in methanol). Soon after the solution was transferred to a vial with an insert (100 µL) suitable for gas chromatography - mass spectrometry analysis (GC- MS, Thermo, Focus-PolarisQ). One microliter of sample was injected in a split/splitless injector at 230 °C with a split ratio of 1:25. Compounds were separated on a DB-5ms capillary column (30 m × 0.25 mm, 0.25 µm film thickness). GC oven program: 70 °C to 320 °C (8 °C min^{-1}, held for 15 min). Helium served as the carrier gas (1.0 mL min^{-1}). The GC-MS interface and ion source temperatures were 250 °C and 200 °C, respectively. The ion-trap mass spectrometer was operated in the positive impact electronic mode at 70 eV, and the total scan time was 0.58 s for the m/z 50–650 range; emission current: 250 mA. Mass spectral deconvolution and automated calculation of RI were performed by the automated mass spectral deconvolution and identification system (AMDIS, National Institute of Standards and Technology, Gaithersburg, MD, USA). Standard solutions of linear alkanes (C7-C30, Sigma-Aldrich 49451-U) were used for retention index (RI) calibration. Compound mass spectra were identified using a target mass spectra library confectioned in the AMDIS software from previous biomass analysis (MELO et al., 2018) and by comparison with published MS data (MATTONAI et al., 2016; TAMBURINI et al., 2017).

IV.2.3.4 Volatile organic compounds (VOCs) semi-quantification

The FE/HS – GC (GC-2010 Shimadzu) was used for semi-quantification of VOCs in the liquid products obtained. VOCs were introduced via a split/splitless injector (0.5 mL, 200 °C, split 1:25). The compounds were separated using a DB624 UI column (30 m, 0.25 mm diameter 1.40 µm thick film). Headspace equilibration temperature and time were 105 °C and 3 min respectively. More details in LIMA et al. (2018). The sample preparation and measurement procedures were as follow: injection of 5 µL of sample (containing 62.5 mg mL^{-1} of dichloroethane, used as an internal standard) into a closed 20 mL vial using a microsyringe and immediate closure. The compounds were identified as described in item IV.2.3.3.

IV.2.3.5 Characterization of non-volatilized compounds at 320 °C

In order to assess the amount of material that was not volatilized in the GC-MS, a simulation was performed, by thermogravimetry, of the heating performed in gas chromatography. For this, about 50 uL of sample was added in platina pan. The experiments were conducted under a nitrogen flow of 50 mL min^{-1}, in a Q600 SDT (TA Instruments, USA), heating samples up to 300 ºC at a rate of 8 ° C min^{-1}, with 15 min isotherm. Three replicates were performed. The analysis of the thermograms was performed with the TA Instruments Universal Analysis 2000 software.

Size Exclusion Chromatography (SEC) was performed to assess whether the molecular weight range of the compounds present in the selected samples. The analysis was performed using an AKTA Pure chromatograph (GE, USA), using a Superdex Peptide 10/300 GL column, with isocratic elution with an aqueous solution containing 0.10 mol L^{-1} NaOH and 0.15 mol NaCl L^{-1} (pH 13), flow 0.5 mL min^{-1}. The detection of compounds was performed by UV absorption at 280 nm. Acetosyringone (Sigma-Aldrich, USA) was used as molecular weight standard (196.19 g mol^{-1}, boiling point: 335 °C).

IV.3 RESULTS AND DISCUSSION

IV.3.1 CATALYST CHARACTERIZATION

The surface areas of the catalysts are shown in FIGURE IV.1. After the addition of metals to silica there was a considerable reduction in the surface area of the material, up to 45% for silver catalysts and 53% for palladium catalysts. However, the surface area of 5Ag/SiO_2 and 10Ag/SiO_2 catalysts do not differ statistically by Tukey's test ($p < 0.05$). The same happens with the 1Pd/SiO_2 and 2Pd/SiO_2 catalysts. SEM images show that catalysts formed small clumps. However, chemical mapping by EDS shows that metals are evenly distributed in the silica matrix. The quantification of chemical elements present in the catalysts shows that each catalyst has the desired proportion of metals.

It is interesting to observe the color of the catalysts, silver catalysts have a dark shade of red (#2c1811), this color may indicate that the silver particles are on the order of 5 nm (GONZÁLEZ et al., 2014). Palladium catalysts have a medium dark shade of brown (#654321), which indicates the formation of nanoparticles (NGUYEN et al., 2010; ZHANG et al., 2012)

IV.3.2 CONVERSION OF MODEL COMPOUNDS

The conversion values of the model compounds are shown in TABLE IV.1. It is observed that there was a total conversion of syringol with all the catalysts used. For syringaldehyde the conversion was above 95% for all catalysts. As for guaiacyl derivatives, the conversion was a little lower, above 90% for guaiacol and more than 85% for vanillin. Therefore, it can be stated that the catalysts in this study have high conversion.

FIGURE IV.1 - IMAGES AND AREAS OF METALLIC CATALYSTS ANCHORED IN SILICA

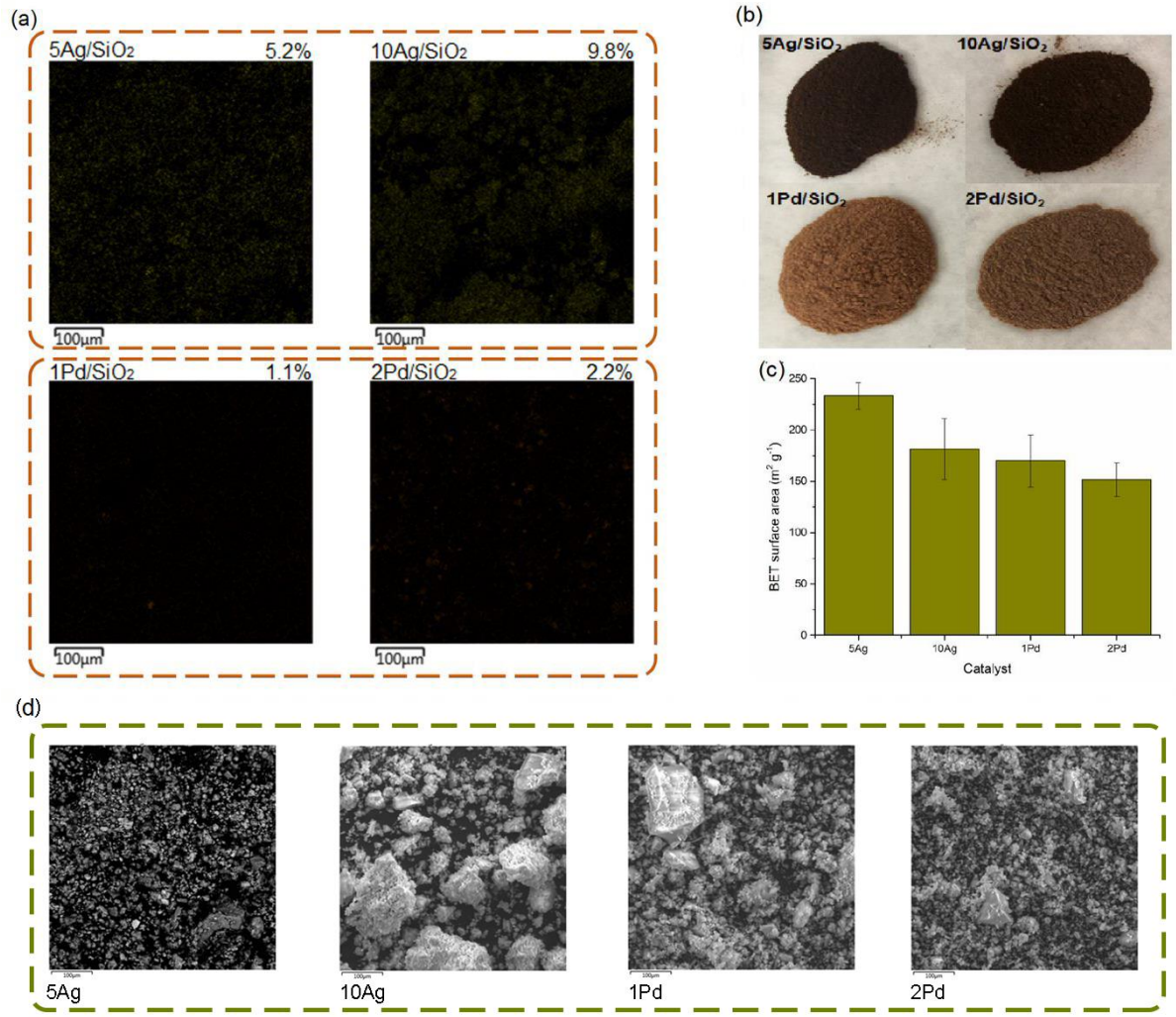

Chemical mapping of silver and palladium and molar concentration **(a)** in metallic catalysts anchored on silica **(b)**. Surface area of catalysts **(c)**. SEM imagens of catalysts **(d)**.

Other studies using Pd catalysts for the hydrogenation of guaiacol showed conversion ranging from 45 to 70% (LU et al., 2016, 2017), however such studies used temperatures in the order of 300 °C. Another work, when performing the hydrogenation of guaiacol, in a methanolic solution, catalyzed by Pd, found a conversion below 40% (ZHANG et al., 2018). When evaluating the hydrogenation of syringaldehyde, ZHANG et al. (2018) found 100% conversion. As for vanillin, they found conversion of at least 97%. LI et al. (2021) found more than 90% conversion for the hydrogenation of vanillin in an ethanolic solution, using palladium as a catalyst. The literature also shows that

the model compound syringol also has high conversion rates in hydrogenation reactions (SHU et al., 2017; VENKATESAN et al., 2021).

TABLE IV.1 – PERCENTAGE OF CONVERSION OF MODEL COMPOUNDS FOR EACH CATALYST

Catalyst	Guaiacol	Vanillin	Syringol	Syringaldehyde
1Pd	94.0 ± 0.3 a	86.1 ± 2.6 a	100 ± 0.0 a	95.0 ± 1.1 a
2Pd	95.0 ± 1.0 a	93.5 ± 1.8 b	100 ± 0.1 a	98.7 ± 0.1 b
5Ag	93.8 ± 0.2 a	96.5 ± 0.1 b	100 ± 0.0 a	96.2 ± 0.3 a
10Ag	93.9 ± 1.2 a	85.4 ± 2.6 a	100 ± 0.1 a	98.5 ± 0.1 b

Averages followed by the same letters in the same column do not differ statistically by Tukey's test ($p<0.05$).

A hydrogenation reaction of guaiacol using Ag/SiO_2 as catalyst showed just over 5% conversion. It is noteworthy that the study used n-heptane as a solvent. As for syringol and syringaldehyde, no studies were found in the literature that used silver as a catalyst in hydrogenation and hydrodeoxygenation reactions of this model compound. In the research, the keywords silver, hydrogen, and syringol or syringaldehyde were used. For vanillin, no relevant studies were found either.

IV.3.3 COKE FORMATION

For the model compounds, syringol and guaiacol, there was no relevant formation of coke (less than 1%) for all catalysts tested. As for the aldehydes, there was no relevant formation of coke for reactions with palladium. However, for the reactions with silver, the formation of carbon occurred which varied from 2 to 3% in relation to the total of model compound fed to the reaction.

CURTZE et al. (2017) demonstrated in a vanillin carbonization process, the formation of a polyaromatic network occurs, which is formed by aromatization reactions. This may have led to the formation of aliphatic bridges between the aromatic ring structures, thus generating coke formation. It is suspected that the same may have occurred in the present study, both for vanillin and for syringaldehyde, and that, in addition, the silver catalyst may have facilitated these aromatization reactions. Furthermore, hydrodeoxygenation in conjunction with decarbonylation of aldehydes can increase coke formation (ZHANG et al., 2016a).

FIGURE IV.2 - PERCENTAGE OF COKE DEPOSITED ON THE CATALYST IN RELATION TO THE TOTAL MASS OF THE MODEL COMPOUND FED TO THE PROCESS

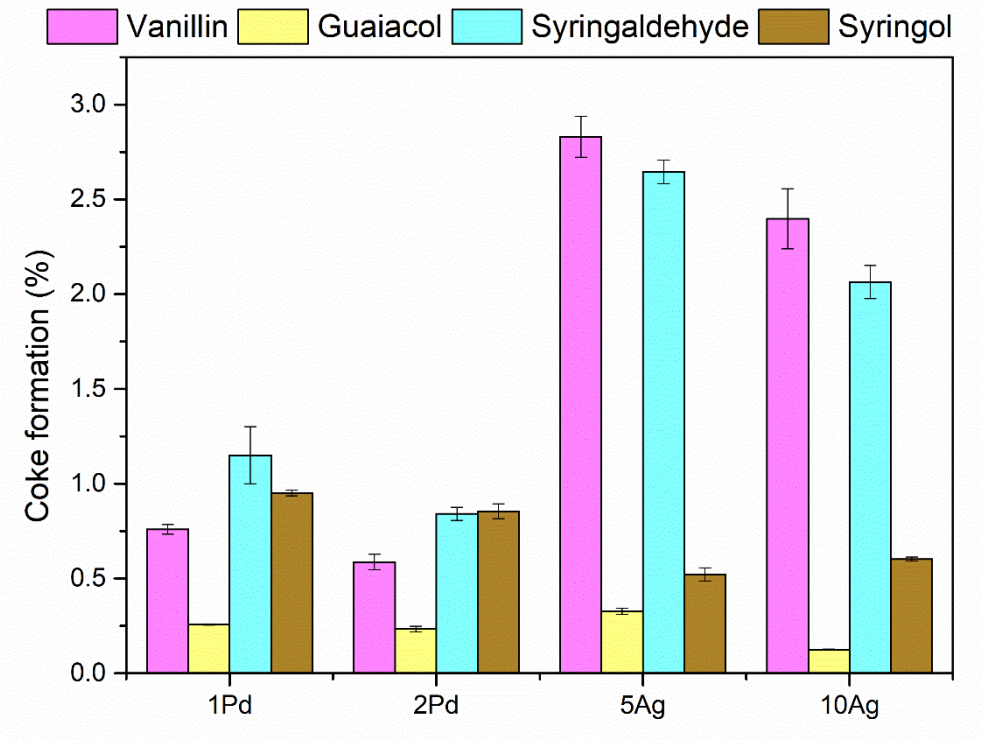

IV.3.4 VOLATILE ORGANIC COMPOUNDS (VOCS)

The main volatile compounds detected by HS-GC-MS are summarized in TABLE IV.2. The results are expressed as a concentration relative to the 1,2-dichloroethane internal standard. Of the identified compounds, it is observed that there is no statistical difference between some of the products formed in the reactions of model compounds in ethanolic solution compared to the control with pure ethanol. This specifically occurs with acetaldehyde and 1,1'-diethoxy-ethane. As for ethyl ether and ethyl acetate, there is an increase in their formation when the syringaldehyde model compound is reacted in the presence of silver catalyst. It is also observed that benzene was only detected in reactions with a silver catalyst. It is noteworthy that the 5Ag/SiO2 catalyst forms almost twice as much benzene as 10Ag/SiO2, when the model compounds are syringyl derivatives.

When ethanol is subjected to a reaction involving acid catalysts, such as silica, the formation of acetaldehyde by dehydrogenation can occur (FIGURE IV.3). This aldehyde can then react with ethanol, thus forming ethyl acetate (HONG THUY et al., 2011). Another reaction pathway, between acetaldehyde and ethanol, is possible, and leads to the formation of 1,1-diethoxy-ethane (CAPELETTI et al., 2000). Ethyl ether, on the other hand, can be formed by converting ethanol in the presence of acid catalysts (GALLO; BUENO; SCHUCHARDT, 2014).

TABLE IV.2 - CONCENTRATION RELATIVE TO THE INTERNAL STANDARD (1,2-DICHLOROETHANE) OF THE COMPOUNDS IDENTIFIED BY HS-GC

Catalyst	Model compound	Acetaldehyde	Diethyl ether	Ethyl acetate	1,1'-diethoxy-ethane	Benzene
$5Ag/SiO_2$	Ethanol	120 ± 17	1.8 ± 0.1	5.8 ± 0.5	12 ± 1	
	Syringaldehyde	124 ± 10	3.0 ± 0.2 *	14 ± 1 *	15 ± 2	0.38 ± 0.02
	Syringol	122 ± 25	1.6 ± 0.3	5.2 ± 0.4	14 ± 1	0.33 ± 0.14
	Guaiacol	122 ± 12	1.8 ± 0.3	5.7 ± 0.4	12 ± 2	0.17 ± 0.03
	Vanillin	127 ± 5	1.8 ± 0.1	6.0 ± 0.1	10 ± 1	0.17 ± 0.04
$10Ag/SiO_2$	Ethanol	246 ± 34	1.6 ± 0.4	5.8 ± 0.4	14 ± 1	
	Syringaldehyde	220 ± 19	2.1 ± 0.1 *	15 ± 1 *	14 ± 1	0.10 ± 0.02
	Syringol	207 ± 25	1.1 ± 0.1	5.8 ± 0.5	13 ± 1	0.09 ± 0.01
	Guaiacol	204 ± 27	1.4 ± 0.3	6.9 ± 0.1	16 ± 2	0.14 ± 0.01
	Vanillin	183 ± 5	1.9 ± 0.1	6.7 ± 0.1	15 ± 1	0.14 ± 0.02
$1Pd/SiO_2$	Ethanol	39 ± 3	1.5 ± 0.4	1.6 ± 0.1	5 ± 1	
	Syringaldehyde	45 ± 4	1.4 ± 0.3	1.5 ± 0.3	6 ± 1	
	Syringol	43 ± 3	1.4 ± 0.1	1.7 ± 0.1	5 ± 1	
	Guaiacol	42 ± 6	1.5 ± 0.1	1.6 ± 0.4	5 ± 1	
	Vanillin	36 ± 6	1.6 ± 0.5	1.5 ± 0.1	4 ± 1	
$2Pd/SiO_2$	Ethanol	40 ± 4	0.6 ± 0.1	1.4 ± 0.3	3 ± 1	
	Syringaldehyde	34 ± 11	0.5 ± 0.4	1.2 ± 0.2	4 ± 1	
	Syringol	38 ± 3	0.5 ± 0.3	1.8 ± 0.1	5 ± 1	
	Guaiacol	24 ± 4	1.9 ± 1.1	1.3 ± 0.2	5 ± 1	
	Vanillin	35 ± 4	1.2 ± 0.3	1.6 ± 0.1	4 ± 1	

*It differs statistically from ethanol, by the Tukey's test ($p<0.05$). Concentration in mg mL^{-1}

It is observed that the catalysts favored the ethanol conversion reactions, in some cases producing up to 6 times more acetaldehyde, 3 times more ethyl acetate and 1,1-diethoxy-ethane. This may have occurred because silver may have provided redox sites, and with that, under certain reaction conditions, the catalyst is active in

dehydrogenation (MATACHOWSKI et al., 2012), which can lead to greater formation of acetaldehyde, and consequently the formation of other by-products.

FIGURE IV.3 - SUGGESTED REACTION PATHWAYS FOR ETHANOL CONVERSION DURING REACTIONS

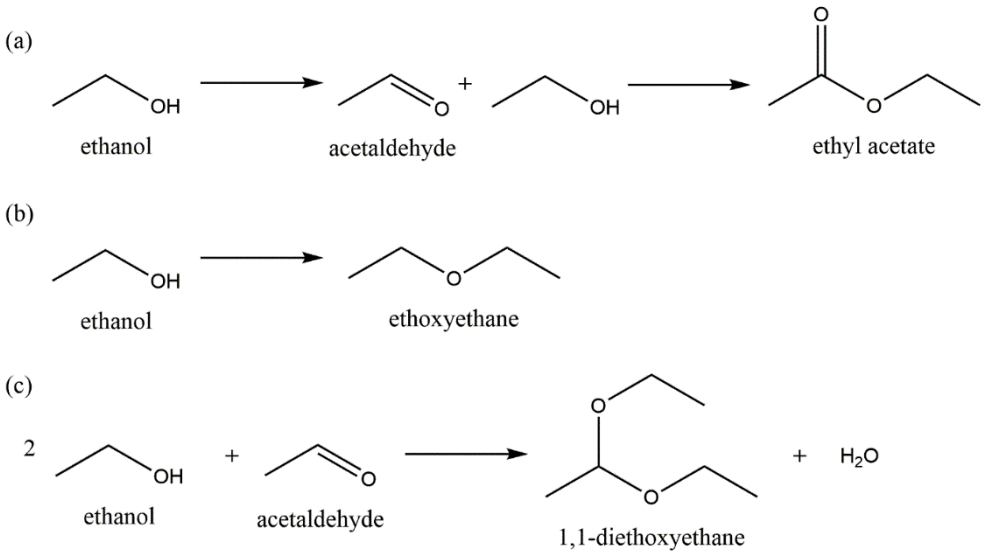

(a) formation of acetaldehyde. (b) formation of ethyl ether. (c) formation of 1,1-diethoxyethane.

IV.3.5 MAIN COMPOUNDS FORMED

The chemical composition of products formed from hydrodeoxygenation of model compounds of lignin derivatives are extremely dependent on reaction conditions, temperature, pressure, catalyst type and hydrogen source (OUEDRAOGO; BHOI, 2020) . Another important factor that can affect the composition of the product, both in chemical class and in major compounds, is the contact time with the catalyst (ZHAO et al., 2011).

Among the classes of compounds formed, the large presence of phenolic compounds stands out as a product of the conversion of all model compounds (FIGURE IV.4). Also noteworthy is the large presence of aldehydes in relation to the total of unidentified compounds. Throughout the text, it will be discussed which aldehydes are formed. A fact that stands out is that only the silver catalyst was able to produce hydrocarbons.

FIGURE IV.4 - RELATIVE DISTRIBUTION OF ORGANIC SPECIES PRODUCED IN THE REACTIONS OF MODEL COMPOUNDS WITH EACH CATALYST

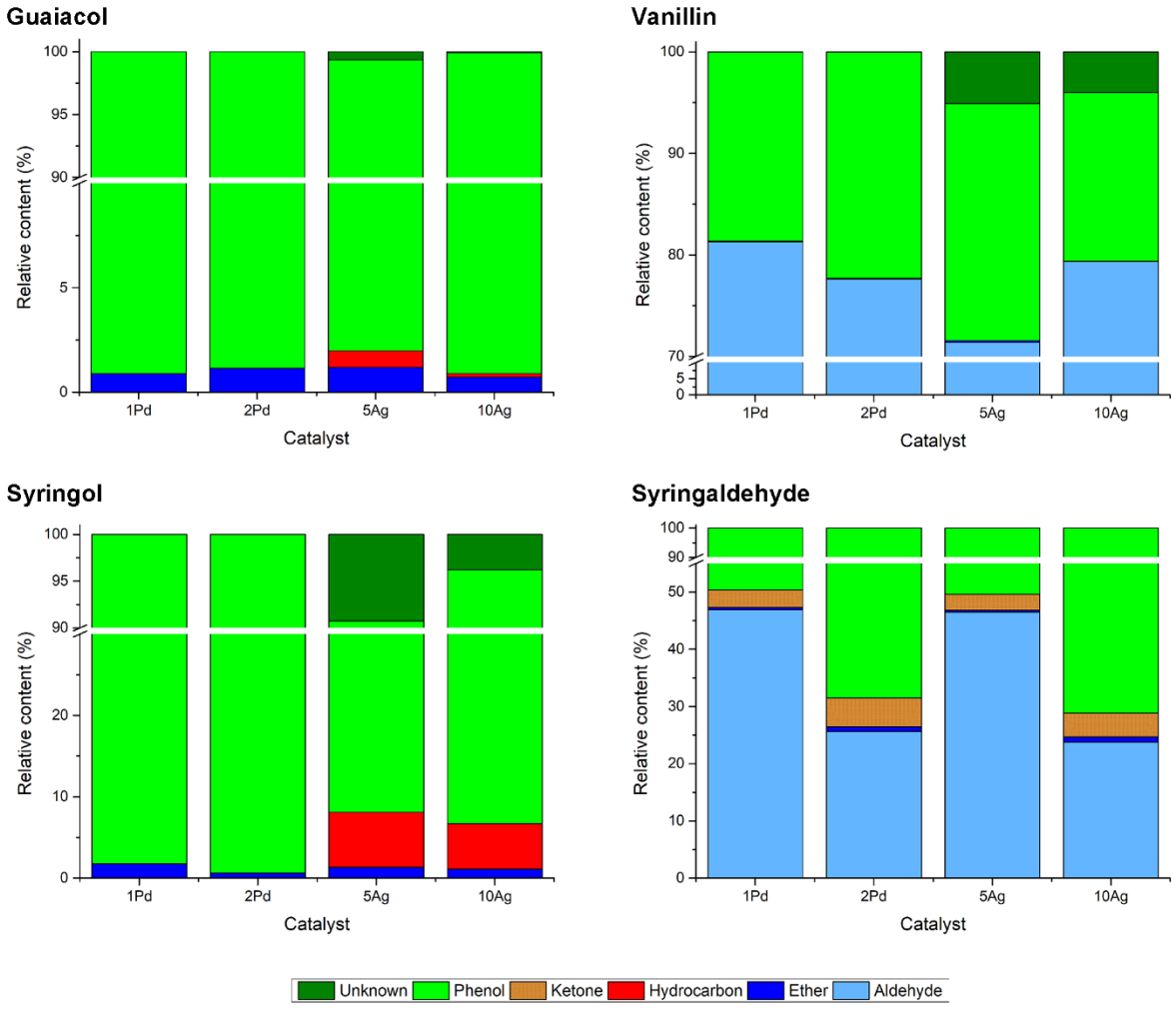

In figures FIGURE IV.6 and FIGURE IV.7 the main compounds formed in the conversion of the model compounds are summarized. These compounds represent at least 80% of the unidentified compounds in each sample.

Catechol, an important intermediate in the conversion of guaiacol and syringol (ZHAO et al., 2011), appears when the model compound is syringol, it represents approximately 5% of the sample, and as the second major compound (~30%) when the model compound is guaiacol. This large amount of catechol, in the conversion of guaiacol, indicates that the first bond to be broken is the bond between oxygen and the methyl carbon, and the replacement of the methyl by a hydrogen (FIGURE IV.1). Then there is the hydrodeoxygenation of the catechol, leading to the formation of

phenol (fourth major compound). It is observed that the relative concentrations of the formed products are higher for silver catalysts. Therefore, a greater amount of phenol formed may have facilitated the formation of benzene (TABLE IV.2), which only occurs with silver catalysts. The formation of benzene occurs through the deoxygenation of phenol. The presence of cresols (C1-phenol), as the third major compound for the conversion of guaiacol, suggests that there is a significant combined pathway through an ipso rearrangement (AFIFI et al., 1996).

FIGURE IV.5 - POSSIBLE REACTION PATHWAYS FOR THE CONVERSION OF SYRINGYL (BROWN) AND GUAIACYL (ORANGE)

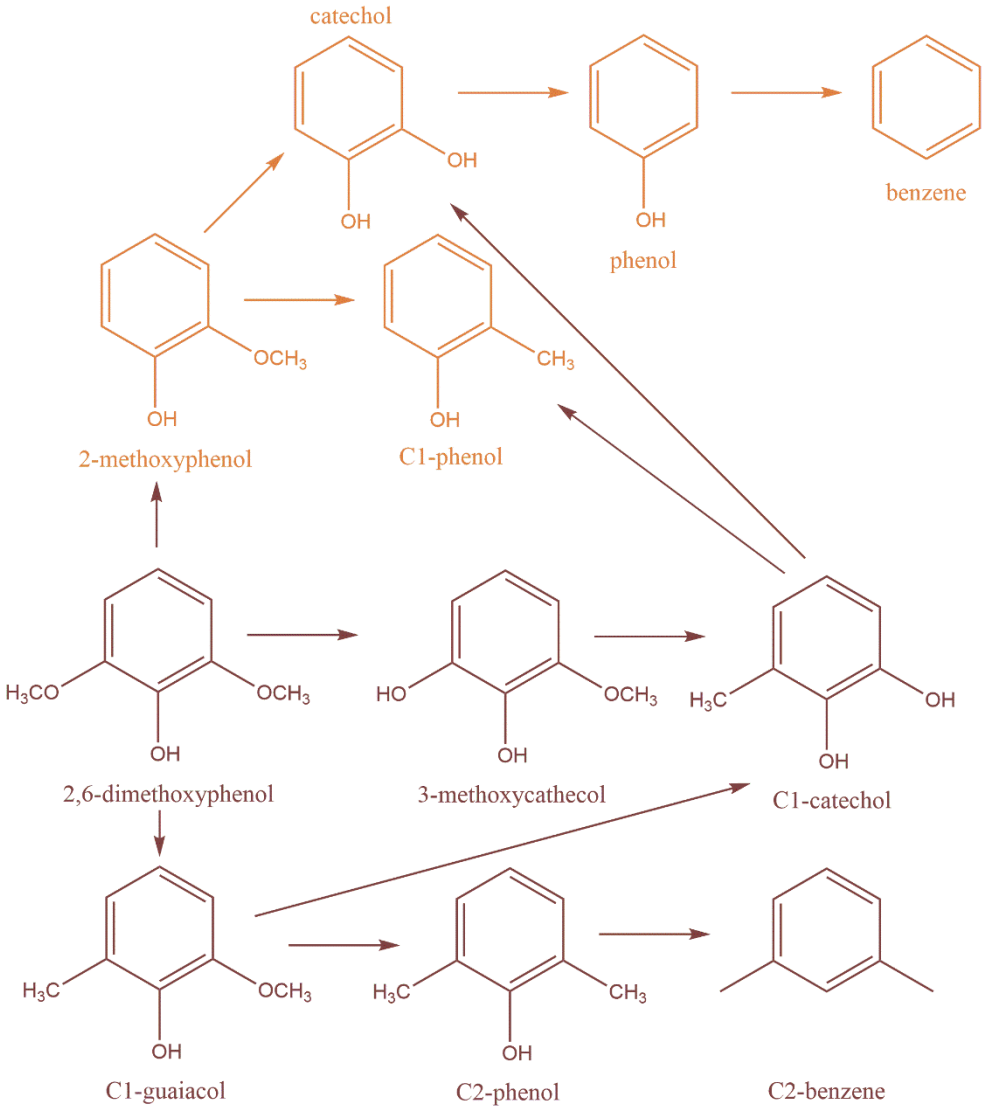

FIGURE IV.6 - DISTRIBUTION OF MAJOR COMPOUNDS PRODUCED IN THE REACTIONS OF GUAIACYL DERIVATIVES FOR EACH CATALYST

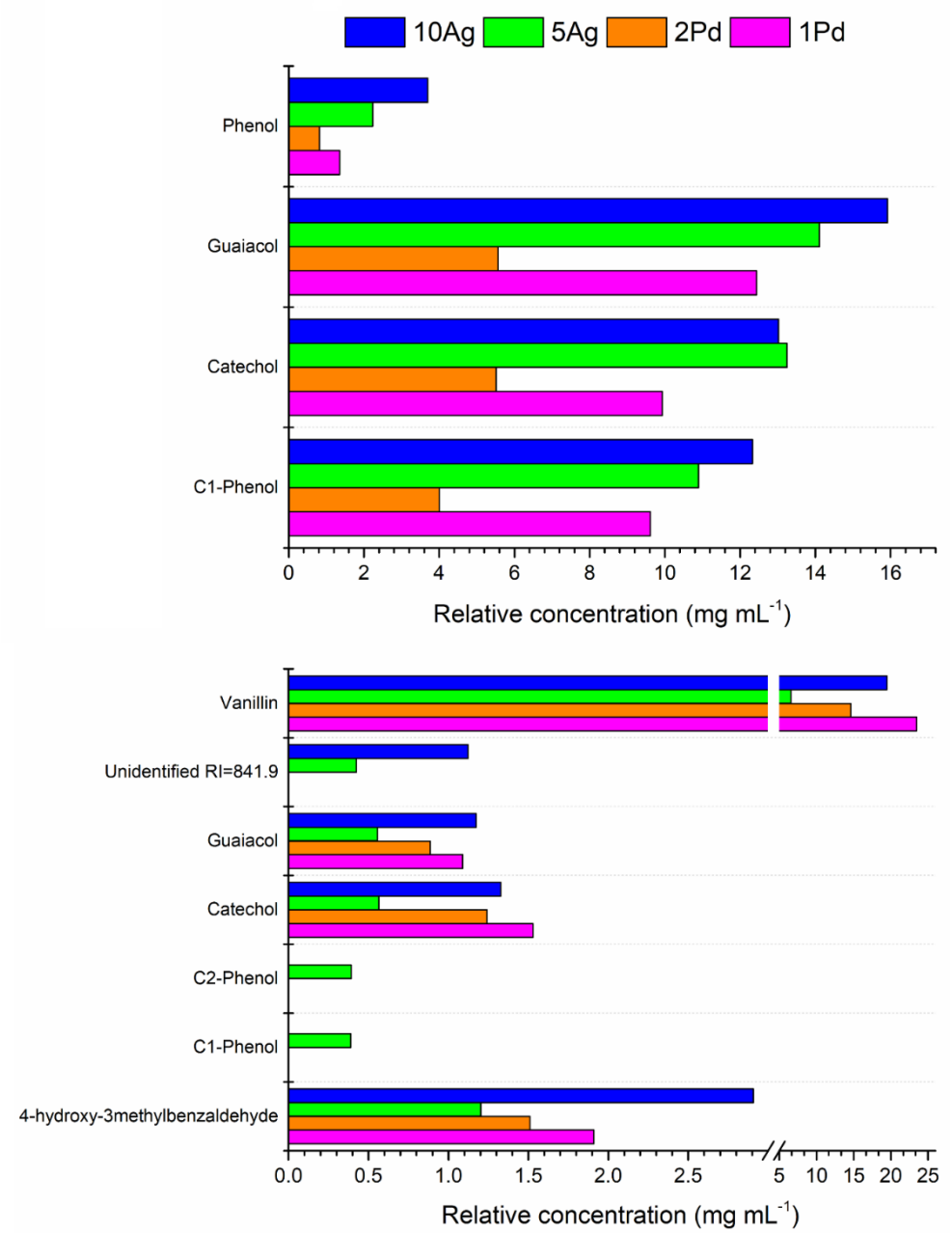

TOP: Major compounds formed from guaiacol. BOTTOM: Major compounds formed from vanillin.

It is worth noting that guaiacol hydrodeoxygenation forms a subset of the syringol hydrodeoxygenation mechanism (FIGURE IV.5). The methoxyl groups present in syringol and guaiacol can be easily cleaved. Therefore, syringol, with two methoxyl groups, is the least stable, followed by guaiacol (VENKATESAN et al., 2021). On the other hand, the removal of the hydroxyl group is relatively more difficult, resulting in low yields of hydrocarbons. It can be seen that silver catalysts seem to

overcome this difficulty in removing hydroxyls, forming more hydrocarbons than palladium catalysts for the conversion of syringol (FIGURE IV.4). For example, no hydrocarbon formation was detected in the conversion of syringol to palladium. With silver, there is a relevant formation of C2-benzene (FIGURE IV.7), which was possibly obtained from the hydrodeoxygenation of C2-phenol (FIGURE IV.5).

FIGURE IV.7 - DISTRIBUTION OF MAJOR COMPOUNDS PRODUCED IN THE REACTIONS OF SYRINGYL DERIVATIVES FOR EACH CATALYST

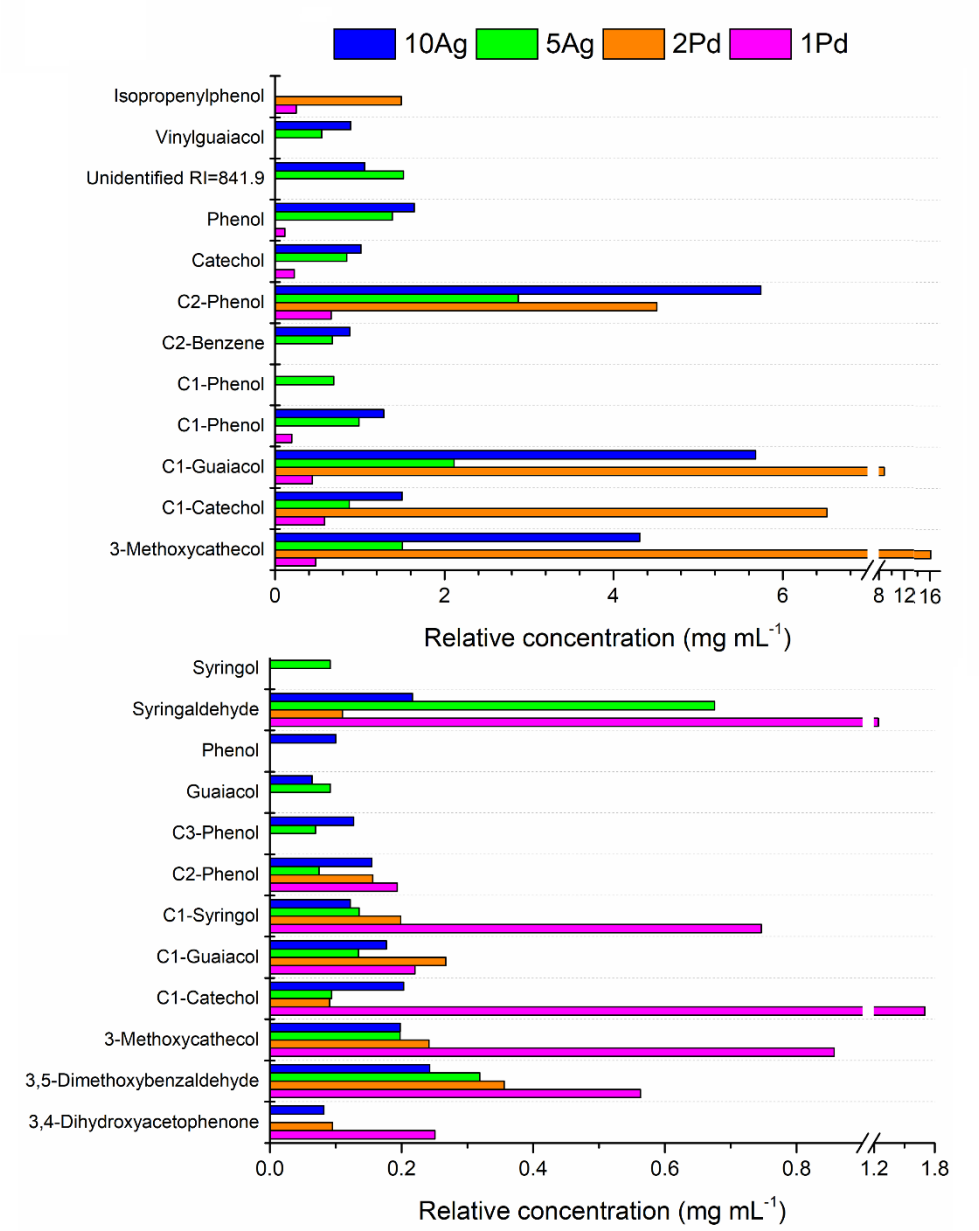

TOP: Major compounds formed from syringol. BOTTOM: Major compounds formed from syringaldehyde.

The difficulty of palladium catalysts in removing hydroxyls is evidenced by the major compounds formed. The four compounds in highest concentration are 3-methoxycatechol, C1-guaiacol, C1-cathecol, C2-phenol (FIGURE IV.7). It should be noted that the $2Pd/SiO_2$ catalyst is more selective for these compounds, corresponding to 90% of the identified compounds. When evaluating the reaction routes that lead to the formation of these compounds, it is observed that the deoxygenation of the molecule occurs mainly by ipso rearrangement, as in the conversion of syringol to C1-guaiacol and then the conversion to C2-phenol. This reaction pathway is also observed in the conversion of 3-methoxycatechol to C1-catechol. Meanwhile, the formation of 3-methoxycatechol from syringol and the conversion of C1-guaiacol into C2-phenol occurs by replacing the methyl group or methoxyl by a hydrogen, leading to the formation of another phenol group. This conversion can occur by two distinct mechanisms, namely, the homolytic splitting of the O-Me bond and the reaction of a concerted mechanism.

Aldehydes reactions as model compounds present a greater variety of formed products. This is precisely because they are larger molecules, thus allowing more cleavage options and, consequently, more product options. The conversion of syringaldehyde occurs mainly by removing the hydroxyl, thus forming 3,5-dimethoxybenzaldehyde, which is one of the compounds found in the greatest quantity. The presence of compounds that are formed in the conversion of syringyl and guaiacol is observed. Furthermore, the formation of vanillin as a product of syringaldehyde is observed. Therefore, the conversion mechanisms of vanillin, syringol, and guaiacol are a subset of syringaldehyde conversion.

In none of the reaction products the presence of hydrocarbons was detected (TABLES TABLE IV.S1 and TABLE IV.S2). Even though there are chemical species that could be converted into hydrocarbons, such as syringol derivatives. In addition to the difficulty of natural removal of hydroxyls, the contact time with the catalyst may have influenced the conversion.

FIGURE IV.8 - POSSIBLE REACTION PATHWAYS FOR THE CONVERSION OF SYRINGALDEHYDE (BLUE) AND VANILLIN (PINK)

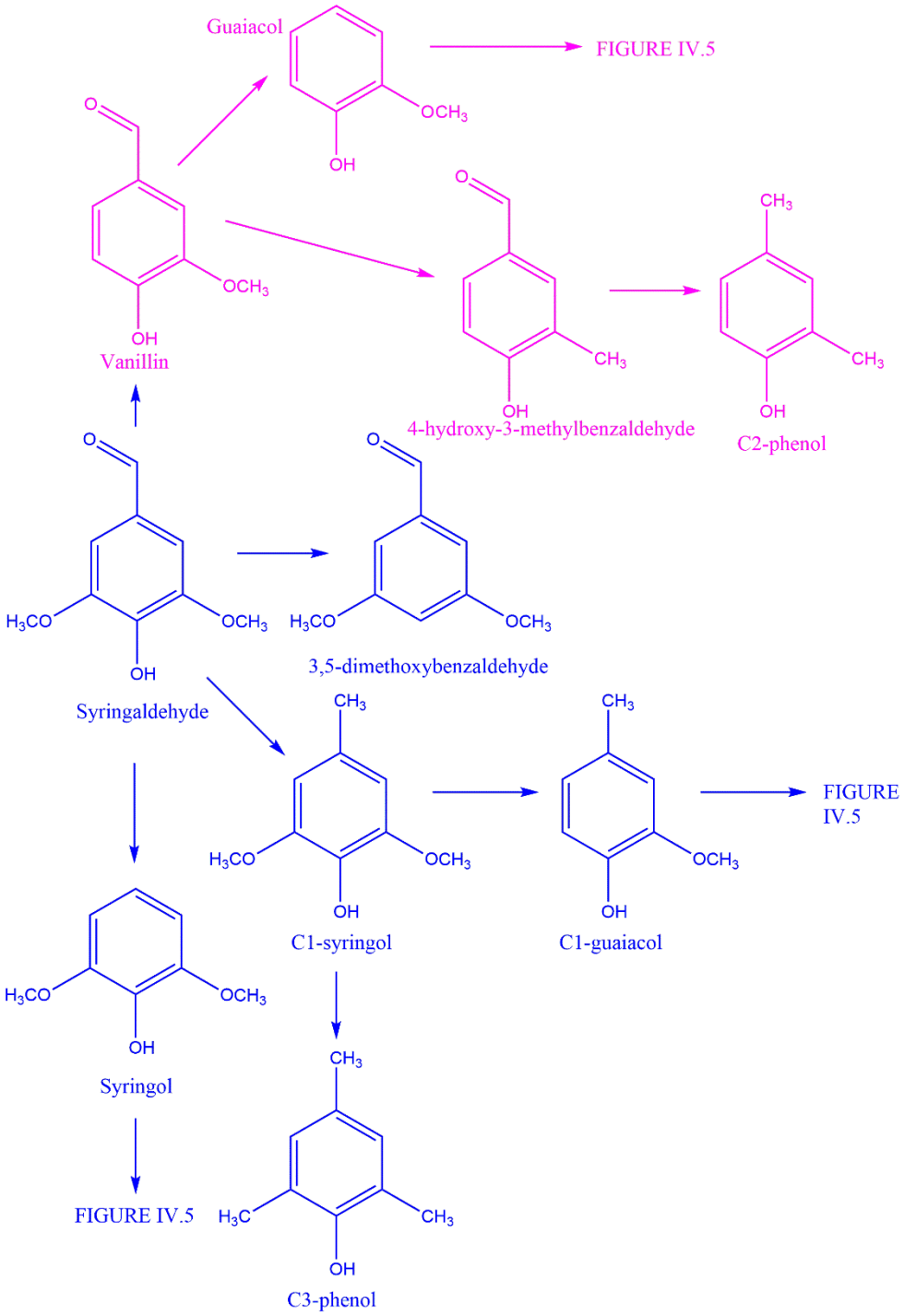

In order to assess whether complete volatilization of the compounds occurred during the GC analysis, evaporation was simulated by thermogravimetric analysis. The results obtained are shown in FIGURE IV.9. Interestingly, the samples that showed the

greatest amount (more than 5%) of residual material, specifically those derived from syringyl when reacted in the presence of silver catalyst. These are the same samples that the product formed was a dark purple colored solution. Coincidentally, for those samples with high residual material content, the material increase occurred linearly with the metal concentration in the catalyst. The products of the other reactions had volatile material content lower than 2%. Therefore, it was considered that there was no significant formation of material.

FIGURE IV.9 - AMOUNT OF MATERIAL REMAINING AFTER HEATING TO 320 °C

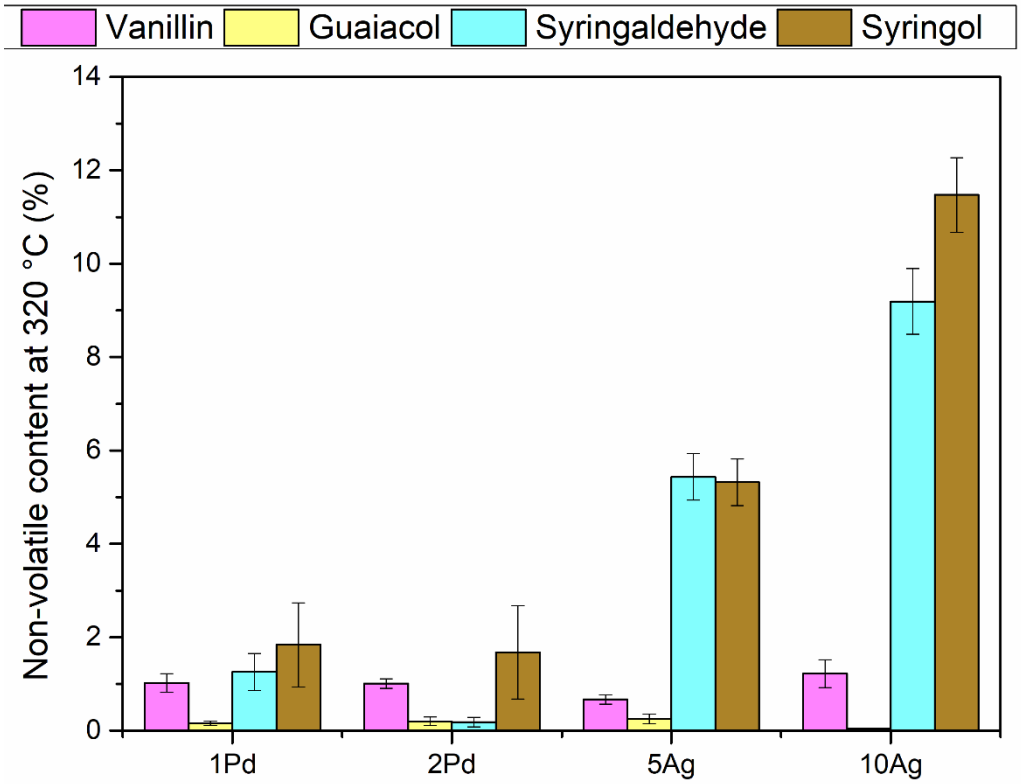

In an attempt to characterize this material, the present compounds were silylated with MSTFA (N-Methyl-N-(trimethylsilyl)trifluoroacetamide) followed by GC-MS analysis. However, compounds of higher molecular weight than compounds that had already been detected in the GC-MS analysis without derivatization, were not identified. For this reason, size exclusion chromatography was used to confirm whether polymerization of the syringyl derivatives occurred in the presence of silver. FIGURE IV.10 shows the SEC chromatograms obtained for the samples as well as for the internal standard of acetosyringone.

Acetosyringone has a molar mass of 196.19 g mol^{-1} and a retention time of 36.3 min. Therefore, the presence of peaks before the retention time of acetosyringone indicates the presence of compounds with higher molar masses in the sample, probably originating from the polymerization of the model compounds. The presence of the phenol function, which once deprotonated, can act as a nucleophilic species, thus leading to polymerization of the compounds (ROSTAGNO et al., 2016; VEITH et al., 2020). A study pointed out the polymerization of syringol, when reacted in the presence of catalysts containing silver (KOBAYASHI; HIGASHIMURA, 2003). It is suspected that the catalyzing action of silver may have led to the polymerization of syringyl derivatives.

FIGURE IV.10 - SEC CHROMATOGRAM OF REACTION PRODUCTS OF SYRINGYL DERIVATIVES WITH SILVER CATALYSTS AND ACETOSYRINGONE STANDARD

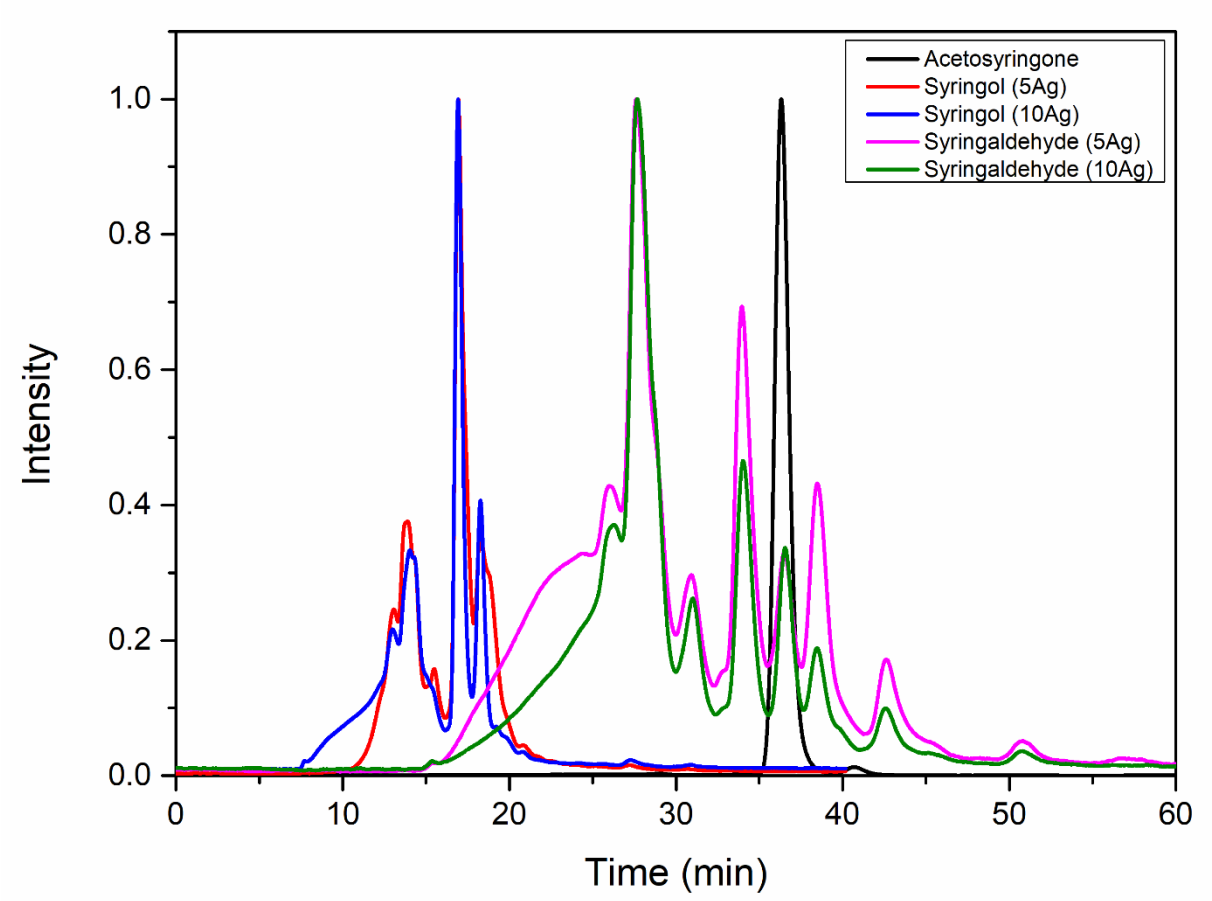

IV.4 CONCLUSIONS

In summary, the hydrodeoxygenation of the bio-oil model compounds mainly removed the methoxyl groups, thus generating a high conversion to phenolics. This is precisely because the hydrodeoxygenation of the phenol group is relatively difficult. These data obtained from the model compounds, suggest that such catalysts can have great importance in the improvement of bio-oil as well as lignin, can produce a low conversion to coal. Furthermore, the polymerization of syringyl derivatives opens the possibility of using these catalysts for the synthesis of polyphenols. As for the conversion of model compounds into hydrocarbons, silver catalysts have a greater ability to remove hydroxyls from phenols. The yield of this class of compounds could be increased if the time of counting with the catalysts.

REFERENCES

ADJAYE, J. D.; BAKHSHI, N. N. Production of hydrocarbons by catalytic upgrading of a fast pyrolysis bio-oil. Part II: Comparative catalyst performance and reaction pathways. **Fuel Processing Technology**, v. 45, n. 3, p. 185–202, 1995.

AFIFI, A. I. et al. The aryl ether bond reactions with H-donor solvents: guaiacol and tetralin in the presence of catalysts. **Fuel**, v. 75, n. 4, p. 509–516, mar. 1996.

AHO, A. et al. Catalytic pyrolysis of woody biomass in a fluidized bed reactor. **Fuel**, v. 87, p. 2493–2501, 2008.

ANDERSEN, A. Final Report on the Safety Assessment of Sodium p -Chloro- m -Cresol, p -Chloro- m -Cresol, Chlorothymol, Mixed Cresols, m -Cresol, o -Cresol, p -Cresol, Isopropyl Cresols, Thymol, o -Cymen-5-ol, and Carvacrol1. **International Journal of Toxicology**, v. 25, n. 1_suppl, p. 29–127, 25 jan. 2006.

APAK, R. et al. **Antioxidant activity/capacity measurement. 1. Classification, physicochemical principles, mechanisms, and electron transfer (ET)-based assaysJournal of Agricultural and Food Chemistry**American Chemical Society, , 10 fev. 2016.

ARISANDI, R. et al. Lipophilic extractives of the wood and bark from Eucalyptus pellita F. Muell grown in Merauke, Indonesia. **Journal of Wood Chemistry and Technology**, v. 40, n. 2, p. 146–154, 3 mar. 2020.

ASADULLAH, M. et al. Production and detailed characterization of bio-oil from fast pyrolysis of palm kernel shell. **Biomass and Bioenergy**, v. 59, p. 316–324, 2013.

BAJPAI, P. **Management of pulp and paper mill waste**. 1. ed. Switzerland: Springer, Cham, 2015.

BARCLAY, L. R. C.; XI, F.; NORRIS, J. Q. Antioxidant properties of phenolic lignin model compounds. **Journal of Wood Chemistry and Technology**, v. 17, n. 1–2, p. 73–90, 1997.

BARI, S. Performance, combustion and emission tests of a metro-bus running on biodiesel-ULSD blended (B20) fuel. **Applied Energy**, v. 124, p. 35–43, 1 jul. 2014.

BASU, P. **Biomass Gasification and Pyrolysis: Practical Design and Theory**. Oxford, UK: Elsevier, 2010.

BAYERBACH, R.; MEIER, D. Characterization of the water-insoluble fraction from fast pyrolysis liquids (pyrolytic lignin). Part IV: Structure elucidation of oligomeric molecules. **Journal of Analytical and Applied Pyrolysis**, v. 85, n. 1–2, p. 98–107, 2009.

BAZARGAN, A.; ROUGH, S. L.; MCKAY, G. Compaction of palm kernel shell

biochars for application as solid fuel. **Biomass and Bioenergy**, v. 70, n. Supplement C, p. 489–497, 2014.

BEDMUTHA, R. et al. Insecticidal and bactericidal characteristics of the bio-oil from the fast pyrolysis of coffee grounds. **Journal of Analytical and Applied Pyrolysis**, v. 90, n. 2, p. 224–231, 1 mar. 2011.

BEN, H.; RAGAUSKAS, A. J. Heteronuclear single-quantum correlation-nuclear magnetic resonance (HSQC-NMR) fingerprint analysis of pyrolysis oils. **Energy and Fuels**, v. 25, n. 12, p. 5791–5801, 15 dez. 2011.

BENNETT, N. M.; HELLE, S. S.; DUFF, S. J. B. Extraction and hydrolysis of levoglucosan from pyrolysis oil. **Bioresource Technology**, v. 100, n. 23, p. 6059–6063, 1 dez. 2009.

BENZIE, I. F. F.; STRAIN, J. J. The Ferric Reducing Ability of Plasma (FRAP) as a Measure of “Antioxidant Power”: The FRAP Assay. **Analytical Biochemistry**, v. 239, n. 1, p. 70–76, 15 jul. 1996.

BERTERO, M. et al. Characterization of the liquid products in the pyrolysis of residual chañar and palm fruit biomasses. **Fuel**, v. 116, p. 409–414, 15 jan. 2014.

BHOI, P. R. et al. **Recent advances on catalysts for improving hydrocarbon compounds in bio-oil of biomass catalytic pyrolysisRenewable and Sustainable Energy Reviews**Elsevier Ltd, , 1 abr. 2020.

BOATENG, A. A.; LANE, E. M.; PENNSYL, V. Characterization and Thermal Conversion of Charcoal Derived from Fluidized-Bed Fast Pyrolysis Oil Production of Switchgrass †. p. 8857–8862, 2007.

BRAMMER, J. G.; LAUER, M.; BRIDGWATER, A. V. Opportunities for biomass-derived “bio-oil” in European heat and power markets. **Energy Policy**, v. 34, n. 17, p. 2871–2880, 1 nov. 2006.

BRAND-WILLIAMS, W.; CUVELIER, M. E.; BERSET, C. Use of a free radical method to evaluate antioxidant activity. **LWT - Food Science and Technology**, v. 28, n. 1, p. 25–30, 1 jan. 1995.

BRIDGWATER, T. Biomass for energy. **Journal of the Science of Food and Agriculture**, v. 86, n. 12, p. 1755–1768, set. 2006.

BRIDGWATER, A. V. Renewable fuels and chemicals by thermal processing of biomass. **Chemical Engineering Journal**, v. 91, n. 2–3, p. 87–102, 15 mar. 2003.

BRIDGWATER, A. V. Review of fast pyrolysis of biomass and product upgrading. **Biomass and Bioenergy**, v. 38, p. 68–94, 2012.

BULUSHEV, D. A.; ROSS, J. R. H. Catalysis for conversion of biomass to fuels via

pyrolysis and gasification: A review. **Catalysis Today**, v. 171, n. 1, p. 1–13, 10 ago. 2011.

BYKOV, I. Characterization of Natural and Technical Lignins using FTIR Spectroscopy. 2008.

CAMPANELA, A.; HAROLD, M. P. Fast pyrolysis of microalgae in falling solids reactor. Effects of process variables and zeolite catalysts. **Biomass and Bioenergy**, v. 46, p. 218–232, 2012.

CAPELETTI, M. R. et al. Synthesis of acetal (1,1-diethoxyethane) from ethanol and acetaldehyde over acidic catalysts. **Applied Catalysis A: General**, v. 198, n. 1–2, p. L1–L4, maio 2000.

CHANDRAN, R. et al. Characteristics of bio-oil from continuous fast pyrolysis of Prosopis juliflora. **Energy**, v. 190, p. 116387, 1 jan. 2020.

CHATTANATHAN, S. A.; ADHIKARI, S.; ABDOULMOUMINE, N. A review on current status of hydrogen production from bio-oil. **Renewable and Sustainable Energy Reviews**, v. 16, n. 5, p. 2366–2372, jun. 2012.

CHEN, B.; CHEN, Z. Sorption of naphthalene and 1-naphthol by biochars of orange peels with different pyrolytic temperatures. **Chemosphere**, v. 76, n. 1, p. 127–133, jun. 2009.

CHEN, C. et al. Effect of structural characteristics on the depolymerization of lignin into phenolic monomers. **Fuel**, v. 223, p. 366–372, jul. 2018.

CHERUBINI, F.; STRØMMAN, A. H. Chapter 1 - Principles of Biorefining A2 - Pandey, Ashok. In: LARROCHE, C. et al. (Eds.). . Amsterdam: Academic Press, 2011. p. 3–24.

CHIARAMONTI, D. et al. Sustainable bio kerosene: Process routes and industrial demonstration activities in aviation biofuels. **Applied Energy**, v. 136, p. 767–774, 1 dez. 2014.

CURTZE, J. H. et al. Hydrothermal Carbonization of Lignin with Vanillin as a Model Component. **Chemical Engineering & Technology**, v. 40, n. 6, p. 1190–1195, jun. 2017.

CZERNIK, S.; BRIDGWATER, A. V. Overview of applications of biomass fast pyrolysis oil. **Energy Fuels**, v. 18, p. 590–598, 2004.

DEL RÍO, J. C. et al. **Determining the influence of eucalypt lignin composition in paper pulp yield using Py-GC/MS**. Journal of Analytical and Applied Pyrolysis. **Anais**...Elsevier, 1 ago. 2005

DENG, W. et al. Evolution of Aromatic Structures during the Low-Temperature

Electrochemical Upgrading of Bio-oil. **Energy and Fuels**, v. 33, n. 11, p. 11292–11301, 21 nov. 2019.

DIZHBITE, T. et al. Characterization of the radical scavenging activity of lignins - Natural antioxidants. **Bioresource Technology**, v. 95, n. 3, p. 309–317, 1 dez. 2004.

DOBELE, G. et al. Pyrolytic oil on the basis of wood and the antioxidant properties of its water-soluble and -insoluble fraction. **Journal of Analytical and Applied Pyrolysis**, v. 85, n. 1–2, p. 81–86, 1 maio 2009.

DODGE, L. A. et al. Sequential Extraction and Characterization of Lignin-Derived Compounds from Thermochemically Processed Biorefinery Lignins. **Energy and Fuels**, v. 33, n. 5, p. 4322–4330, 16 maio 2019.

DOMÍNGUEZ-ROBLES, J. et al. Aqueous acetone fractionation of kraft, organosolv and soda lignins. **International Journal of Biological Macromolecules**, v. 106, p. 979–987, 1 jan. 2018.

DONG, C. et al. Characteristics and mechanism study of analytical fast pyrolysis of poplar wood. **Energy Conversion and Management**, v. 57, p. 49–59, 1 maio 2012.

DONG, X. et al. Antimicrobial and antioxidant activities of lignin from residue of corn stover to ethanol production. **Industrial Crops and Products**, v. 34, n. 3, p. 1629–1634, 1 nov. 2011.

ELLIOTT, D. C.; BAKER, E. G. **Catalytic hydrotreating of biomass liquefaction products to produce hydrocarbon fuels: Interim report**. Richland, WA (United States): [s.n.]. Disponível em: <http://www.osti.gov/servlets/purl/6912635-hPAkiy/>. Acesso em: 12 ago. 2020.

EUFRADE JUNIOR, H. J. et al. Sustainable use of eucalypt biomass grown on short rotation coppice for bioenergy. **Biomass and Bioenergy**, v. 90, p. 15–21, 2016.

FAIX, O. Classification of Lignins from Different Botanical Origins by FT-IR Spectroscopy. **Holzforschung**, v. 45, n. s1, p. 21–28, 1991a.

FAIX, O. Condensation indices of lignins determined by FTIR-spectroscopy. **Holz als Roh- und Werkstoff**, v. 49, n. 9, p. 356, set. 1991b.

FAIX, O. et al. Determination of hydroxyl groups in lignins evaluation of 1H- 13C-, 31P-NMR, FTIR and wet chemical methods. **Holzforschung**, v. 48, n. 5, p. 387–394, 1994.

FAIX, O.; GRÜNWALD, C.; BEINHOFF, O. Determination of Phenolic Hydroxyl Group Content of Milled Wood Lignins (MWL's) from Different Botanical Origins Using Selective Aminolysis, FTIR, 1H-NMR, and UV Spectroscopy. **Holzforschung**, v. 46, n. 5, p. 425–432, 1992.

FAN, L. et al. **Bio-oil from fast pyrolysis of lignin: Effects of process and upgrading parametersBioresource Technology**Elsevier Ltd, , 1 out. 2017.

FENGEL, D.; WEGENER, G. **Wood: Chemistry, Ultrastructure and Reactions**. 1st. ed. Berlin: Walter de Gruyter, 1989.

FORTIN, M. et al. Structural Analysis of Pyrolytic Lignins Isolated from Switchgrass Fast-Pyrolysis Oil. **Energy and Fuels**, v. 29, n. 12, p. 8017–8026, 2015.

FRASSOLDATI, A.; RANZI, E. Modeling of Thermochemical Conversion of Biomasses. In: **Reference Module in Chemistry, Molecular Sciences and Chemical Engineering**. [s.l.] Elsevier, 2019.

FUNKENBUSCH, L. L. T. et al. Catalytic hydrotreatment of pyrolysis oil phenolic compounds over Pt/Al2O3 and Pd/C. **Fuel**, v. 243, p. 441–448, 1 maio 2019.

GALLO, J. M. R.; BUENO, J. M. C.; SCHUCHARDT, U. Catalytic Transformations of Ethanol for Biorefineries. **Journal of the Brazilian Chemical Society**, v. 25, n. 12, p. 2229, 2014.

GARCIA-PEREZ, M. et al. Characterization of bio-oils in chemical families. **Biomass and Bioenergy**, v. 31, n. 4, p. 222–242, 1 abr. 2007.

GE, J. et al. Effects of Pilot Injection Timing and EGR on Combustion, Performance and Exhaust Emissions in a Common Rail Diesel Engine Fueled with a Canola Oil Biodiesel-Diesel Blend. **Energies**, v. 8, n. 7, p. 7312–7325, 20 jul. 2015.

GELLERSTEDT, G. HENRIKSSON, G. Lignins: Major Sources, Structure and Properties. In: BELGACE, M. N.; GANDINI, A. (Eds.). . **Monomers, Polymers and Composites from Renewable Resources**. [s.l: s.n.]. p. 201–224.

GHOLIZADEH, M. et al. Effects of temperature on the hydrotreatment behaviour of pyrolysis bio-oil and coke formation in a continuous hydrotreatment reactor. **Fuel Processing Technology**, v. 148, p. 175–183, 1 jul. 2016.

GHORBANNEZHAD, P. et al. Sustainable production of value-added products from fast pyrolysis of palm shell residue in tandem micro-reactor and pilot plant. **Renewable Energy**, v. 145, p. 663–670, 1 jan. 2020.

GONZÁLEZ, A. L. et al. Size, Shape, Stability, and Color of Plasmonic Silver Nanoparticles. **The Journal of Physical Chemistry C**, v. 118, n. 17, p. 9128–9136, 15 abr. 2014.

GOODWIN, T. W.; MERCER, E. I. **Introduction to Plant Biochemistry: The Plant Cell Wall**. New york: . Pergamon Press, 1983.

GOSSELINK, R. J. A. et al. Characterisation and application of NovaFiber lignin. **Industrial Crops and Products**, v. 20, n. 2, p. 191–203, 1 set. 2004.

GRABBER, J. H. How Do Lignin Composition, Structure, and Cross-Linking Affect Degradability? A Review of Cell Wall Model Studies. **Crop Science**, v. 45, n. 3, p. 820–831, 1 maio 2005.

GREENHALF, C. E. et al. A comparative study of straw, perennial grasses and hardwoods in terms of fast pyrolysis products. **Fuel**, v. 108, p. 216–230, 2013.

HAN, Y. et al. **Hydrotreatment of pyrolysis bio-oil: A reviewFuel Processing Technology**Elsevier B.V., , 1 dez. 2019.

HATAKKA, A. **Biopolymers: biology, chemistry, biotechnology, applications, Lignin, humic substances and coal**. Weinheim: Wiley-VCH, 2001.

HAYASHI, T.; MARSDEN, M. P. F.; DELMER, D. P. Pea xyloglucan and cellulose. V. Xylogluan-cellulose interactions in vitro and vivo. **Plant Physiology**, v. 83, p. 384–389, 1987.

HE, Z.; WANG, X. Hydrodeoxygenation of model compounds and catalytic systems for pyrolysis bio-oils upgrading. **Catalysis for Sustainable Energy**, v. 1, n. 2013, p. 28–52, 13 fev. 2013.

HELLINGER, M. et al. Catalytic hydrodeoxygenation of guaiacol over platinum supported on metal oxides and zeolites. **Applied Catalysis A: General**, v. 490, p. 181–192, 25 jan. 2015.

HENRIKSSON, G. **The Ljungberg textbook Biofiber Chemistry**. Sweden: KTH, 2010.

HOENICH, N. A. Cellulose for Medical Applications: Past, Present, and Future. **BioResources**, v. 1, n. 2, p. 270–280, 2006.

HOFBAUER, H. Gasification: technology overview. In: BRIDGWATER, A. V; HOFBAUER, H.; VAN LOO, S. (Eds.). . **Thermal biomass conversion**. [s.l.] CPL Press, 2009.

HONG THUY, N. T. et al. Techno-economic and environmental assessment of bioethanol-based chemical process: A case study on ethyl acetate. **Environmental Progress & Sustainable Energy**, v. 30, n. 4, p. 675–684, dez. 2011.

HOU, S.-S. et al. Co-Firing of Fast Pyrolysis Bio-Oil and Heavy Fuel Oil in a 300-kWth Furnace. **Applied Sciences**, v. 6, n. 11, p. 326, 29 out. 2016.

HU, X. et al. Production of value-added chemicals from bio-oil via acid catalysis coupled with liquid-liquid extraction. **RSC Advances**, v. 2, n. 25, p. 9366–9370, 21 out. 2012.

HU, X. et al. Polymerization on heating up of bio-oil: A model compound study. **AIChE Journal**, v. 59, n. 3, p. 888–900, 1 mar. 2013.

HU, X. et al. One-pot conversion of biomass-derived xylose and furfural into levulinate esters via acid catalysis. **Chemical Communications**, v. 53, n. 20, p. 2938–2941, 7 mar. 2017.

HU, X. et al. Coke Formation during Thermal Treatment of Bio-oil. **Energy & Fuels**, 26 jun. 2020.

HU, X.; GHOLIZADEH, M. **Biomass pyrolysis: A review of the process development and challenges from initial researches up to the commercialisation stageJournal of Energy Chemistry**Elsevier B.V., , 1 dez. 2019.

HU, X.; GHOLIZADEH, M. **Progress of the applications of bio-oilRenewable and Sustainable Energy Reviews**Elsevier Ltd, , 1 dez. 2020.

ISIKGOR, F. H.; BECER, C. R. Lignocellulosic biomass: a sustainable platform for the production of bio-based chemicals and polymers. **Polym. Chem.**, v. 6, n. 25, p. 4497–4559, 2015.

IWAMOTO, S.; NAKAGAITO, A. N.; YANO, H. Nano-fibrillation of pulp fibers for the processing of transparent nanocomposites. **Applied Physics A: Materials Science and Processing**, v. 89, n. 2, p. 461–466, 2007.

JACOBSON, K.; MAHERIA, K. C.; DALAI, A. K. Bio-oil valorization: A review. **Renewable and Sustainable Energy Reviews**, v. 23, p. 91–106, jul. 2013.

JAFARIAN, S.; TAVASOLI, A.; NIKKHAH, H. Catalytic hydrotreating of pyro-oil derived from green microalgae spirulina the (Arthrospira) plantensis over NiMo catalysts impregnated over a novel hybrid support. **International Journal of Hydrogen Energy**, v. 44, n. 36, p. 19855–19867, 26 jul. 2019.

JAHIRUL, M. et al. Biofuels Production through Biomass Pyrolysis —A Technological Review. **Energies**, v. 5, n. 12, p. 4952–5001, 23 nov. 2012.

JIANG, X.; ELLIS, N.; ZHONG, Z. Characterization of pyrolytic lignin extracted from bio-oil. **Chinese Journal of Chemical Engineering**, v. 18, n. 6, p. 1018–1022, 2010.

JIE-WANG, Y.; GUI-ZHEN, F.; CHUN-DE, J. Hydrogenation of Alkali Lignin Catalyzed by Pd/C. **APCBEE Procedia**, v. 3, p. 53–59, 1 jan. 2012.

JOHANSSON, A. C. et al. Co-pyrolysis of woody biomass and plastic waste in both analytical and pilot scale. **Journal of Analytical and Applied Pyrolysis**, v. 134, p. 102–113, 1 set. 2018.

KAAL, J.; RUMPEL, C. Can pyrolysis-GC/MS be used to estimate the degree of thermal alteration of black carbon? **Organic Geochemistry**, v. 40, n. 12, p. 1179–1187, dez. 2009.

KABIR, G.; HAMEED, B. H. Recent progress on catalytic pyrolysis of lignocellulosic

biomass to high-grade bio-oil and bio-chemicals. **Renewable and Sustainable Energy Reviews**, v. 70, p. 945–967, 1 abr. 2017.

KAMM, B. et al. **Biorefineries - Industrial Processes and Products : Status Quo and Future Directions**. [s.l.] WILEY-VCH, 2005.

KAN, T.; STREZOV, V.; EVANS, T. J. **Lignocellulosic biomass pyrolysis: A review of product properties and effects of pyrolysis parametersRenewable and Sustainable Energy Reviews**Elsevier Ltd, , 1 maio 2016.

KARNJANAKOM, S. et al. Selectively catalytic upgrading of bio-oil to aromatic hydrocarbons over Zn, Ce or Ni-doped mesoporous rod-like alumina catalysts. **Journal of Molecular Catalysis A: Chemical**, 2016.

KOBAYASHI, S.; HIGASHIMURA, H. Oxidative polymerization of phenols revisited. **Progress in Polymer Science**, v. 28, n. 6, p. 1015–1048, jun. 2003.

KOKOSA, J. M. **Selecting an extraction solvent for a greener liquid phase microextraction (LPME) mode-based analytical methodTrAC - Trends in Analytical Chemistry**Elsevier B.V., , 1 set. 2019.

LANCEFIELD, C. S. et al. Identification of a diagnostic structural motif reveals a new reaction intermediate and condensation pathway in kraft lignin formation. **Chemical Science**, v. 9, n. 30, p. 6348–6360, 1 ago. 2018.

LEHTO, J. et al. **Review of fuel oil quality and combustion of fast pyrolysis bio-oils from lignocellulosic biomassApplied Energy**Elsevier Ltd, , 1 mar. 2014.

LENG, F. et al. Characterization of pyrolytic lignins with different activities obtained from bio-oil. **Chinese Journal of Chemical Engineering**, v. 25, n. 3, p. 324–329, 2017.

LI, H. et al. Preparation and characterization of bio-polyol and bio-based flexible polyurethane foams from fast pyrolysis of wheat straw. **Industrial Crops and Products**, v. 103, p. 64–72, 1 set. 2017.

LI, S. et al. Characterization of pyrolytic lignin and insight into its formation mechanisms using novel techniques and DFT method. **Fuel**, v. 262, p. 116516, 15 fev. 2020.

LI, Z. et al. One-step synthesis of single palladium atoms in WO2.72 with high efficiency in chemoselective hydrodeoxygenation of vanillin. **Applied Catalysis B: Environmental**, v. 298, p. 120535, 2021.

LIAN, J.; GARCIA-PEREZ, M.; CHEN, S. Fermentation of levoglucosan with oleaginous yeasts for lipid production. **Bioresource Technology**, v. 133, p. 183–189, 2013.

LIMA, N. K. et al. Determination of volatile organic compounds in eucalyptus fast pyrolysis bio-oil by full evaporation headspace gas chromatography. **Talanta**, v. 176, p. 47–51, 1 jan. 2018.

LIN, J. et al. Mechanisms of acid resistance in enterohemorrhagic Escherichia coli. **Applied and Environmental Microbiology**, v. 62, n. 9, p. 3094–3100, set. 1996.

LIU, P. et al. Modification of bio-char derived from fast pyrolysis of biomass and its application in removal of tetracycline from aqueous solution. **Bioresource Technology**, v. 121, p. 235–240, 2012.

LIU, S. et al. Hydrodeoxygenation of 2-Methoxyphenol over Ru, Pd, and Mo2C Catalysts Supported on Carbon. **Energy and Fuels**, v. 31, n. 6, p. 6378–6388, 15 jun. 2017.

LOURENÇON, T. V. et al. Bio-oil from a fast pyrolysis pilot plant as antifungal and hydrophobic agent for wood preservation. **Journal of Analytical and Applied Pyrolysis**, v. 122, p. 1–6, 2016.

LOURENÇON, T. V. et al. Antioxidant, antibacterial and antitumoural activities of kraft lignin from hardwood fractionated by acid precipitation. **International Journal of Biological Macromolecules**, v. 166, p. 1535–1542, 1 jan. 2021.

LU, M. et al. TiO2-Modified Pd/SiO2 for Catalytic Hydrodeoxygenation of Guaiacol. **Energy & Fuels**, v. 30, n. 8, p. 6671–6676, 29 jul. 2016.

LU, M. et al. Catalytic Hydrodeoxygenation of Guaiacol over Palladium Catalyst on Different Titania Supports. **Energy & Fuels**, v. 31, n. 10, p. 10858–10865, 19 out. 2017.

LU, Q. et al. Selective fast pyrolysis of biomass impregnated with ZnCl2 to produce furfural: Analytical Py-GC/MS study. **Journal of Analytical and Applied Pyrolysis**, v. 90, n. 2, p. 204–212, 1 mar. 2011.

LU, Q.; LI, W.-Z.; ZHU, X.-F. Overview of fuel properties of biomass fast pyrolysis oils. **Energy Conversion and Management**, v. 50, n. 5, p. 1376–1383, maio 2009.

ŁUCEJKO, J. J. et al. Analytical pyrolysis vs. classical wet chemical analysis to assess the decay of archaeological waterlogged wood. **Analytica Chimica Acta**, v. 745, p. 70–77, 1 out. 2012.

LV, G.-J.; WU, S.-B.; LOU, R. CHARACTERISTICS OF CORN STALK HEMICELLULOSE PYROLYSIS IN A TUBULAR REACTOR. **BioResources**, v. 5, n. 4, p. 2051–2062, 4 ago. 2010.

LV, P. M. et al. Bio-syngas production from biomass catalytic gasification. **Energy Convers**, v. 48, p. 1132–1139, 2007.

LYU, G.; WU, S.; ZHANG, H. Estimation and Comparison of Bio-Oil Components from Different Pyrolysis Conditions. **Frontiers in Energy Research**, v. 3, 15 jun. 2015.

MALINS, K. Production of bio-oil via hydrothermal liquefaction of birch sawdust. **Energy Conversion and Management**, v. 144, n. Supplement C, p. 243–251, 2017.

MANTE, O. D. et al. Catalytic conversion of biomass pyrolysis vapors into hydrocarbon fuel precursors. **Green Chemistry**, v. 17, n. 4, p. 2362–2368, 1 abr. 2015.

MATACHOWSKI, L. et al. Ecofriendly production of ethylene by dehydration of ethanol over Ag3PW12O40 salt in nitrogen and air atmospheres. **Applied Catalysis B: Environmental**, v. 123–124, p. 448–456, jul. 2012.

MATOS, M. et al. Pilot-Scaled Fast-Pyrolysis Conversion of Eucalyptus Wood Fines into Products: Discussion Toward Possible Applications in Biofuels, Materials, and Precursors. **BioEnergy Research**, p. 1–12, 4 fev. 2020.

MATTONAI, M. et al. Timing in Analytical Pyrolysis: Py(HMDS)-GC/MS of Glucose and Cellulose Using Online Micro Reaction Sampler. **Analytical Chemistry**, v. 88, n. 18, p. 9318–9325, 20 set. 2016.

MCCORMICK, R. L. et al. Properties of oxygenates found in upgraded biomass pyrolysis oil as components of spark and compression ignition engine fuels. **Energy and Fuels**, v. 29, n. 4, p. 2453–2461, 16 abr. 2015.

MELO, T. O. et al. Simultaneous pyrolysis and trimethylsilylation with N-methyl-(trimethylsilyl) trifluoroacetamide for the characterisation of lignocellulosic materials from kraft pulping. **Holzforschung**, v. 72, n. 10, p. 851–862, 25 out. 2018.

MILHÉ, M. et al. **Autothermal and allothermal pyrolysis in a continuous fixed bed reactor**. Journal of Analytical and Applied Pyrolysis. **Anais**...Elsevier B.V., 2013

MILLY, P. J.; TOLEDO, R. T.; RAMAKRISHNAN, S. Determination of Minimum Inhibitory Concentrations of Liquid Smoke Fractions. **Journal of Food Science**, v. 70, n. 1, p. M12–M17, 1 jan. 2005.

MIRKOUEI, A. et al. A review and future directions in techno-economic modeling and optimization of upstream forest biomass to bio-oil supply chains. **Renewable and Sustainable Energy Reviews**, v. 67, p. 15–35, 2017.

MOHAN, D. et al. Fungicidal values of bio-oils and their lignin-rich fractions obtained from wood/bark fast pyrolysis. **Chemosphere**, v. 71, n. 3, p. 456–465, 2008.

MOHAN, D.; PITTMAN, C. U.; STEELE, P. H. **Pyrolysis of wood/biomass for bio-oil: A critical reviewEnergy and Fuels** American Chemical Society , , maio 2006. Disponível em: <https://pubs.acs.org/doi/abs/10.1021/ef0502397>. Acesso em: 11

ago. 2020

MOHARAM, M. A.; ABBAS, L. M. A study on the effect of microwave heating on the properties of edible oils using FTIR spectroscopy. **African Journal of Microbiology Research**, v. 4, n. 19, p. 1921–1927, 2010.

MONIZ, P. et al. Membrane separation and characterisation of lignin and its derived products obtained by a mild ethanol organosolv treatment of rice straw. **Process Biochemistry**, v. 65, p. 136–145, 1 fev. 2018.

MULLEN, C. A.; BOATENG, A. A. Characterization of water insoluble solids isolated from various biomass fast pyrolysis oils. **Journal of Analytical and Applied Pyrolysis**, v. 90, n. 2, p. 197–203, 1 mar. 2011.

NASSAR, M.; MACKAY, G. Mechanism of thermal decomposition of lignin. **Wood Fiber Science**, v. 16, p. 441–453, 1984.

NEGAHDAR, L. et al. Characterization and Comparison of Fast Pyrolysis Bio-oils from Pinewood, Rapeseed Cake, and Wheat Straw Using 13C NMR and Comprehensive GC ?? GC. **ACS Sustainable Chemistry and Engineering**, v. 4, n. 9, p. 4974–4985, 2016.

NEIVA, D. et al. Chemical composition and kraft pulping potential of 12 eucalypt species. **Industrial Crops and Products**, v. 66, p. 89–95, 2015.

NGUYEN, V. L. et al. Chemical synthesis and characterization of palladium nanoparticles. **Advances in Natural Sciences: Nanoscience and Nanotechnology**, v. 1, n. 3, p. 035012, 4 nov. 2010.

OASMAA, A.; MEIER, D. Norms and standards for fast pyrolysis liquids. 1. Round robin test. **J. Anal Appl Pyrolysis**, v. 73, n. 2, p. 323–334, 2005.

OUEDRAOGO, A. S.; BHOI, P. R. Recent progress of metals supported catalysts for hydrodeoxygenation of biomass derived pyrolysis oil. **Journal of Cleaner Production**, p. 119957, jan. 2020.

PAN, X. et al. Organosolv ethanol lignin from hybrid poplar as a radical scavenger: Relationship between lignin structure, extraction conditions, and antioxidant activity. **Journal of Agricultural and Food Chemistry**, v. 54, n. 16, p. 5806–5813, 9 ago. 2006.

PAPARI, S.; HAWBOLDT, K. **A review on the pyrolysis of woody biomass to bio-oil: Focus on kinetic modelsRenewable and Sustainable Energy Reviews**Elsevier Ltd, , 1 dez. 2015.

PARK, J. et al. Activated carbon from biochar: Influence of its physicochemical properties on the sorption characteristics of phenanthrene. **Bioresource Technology**, v. 149, p. 383–389, 2013.

PARK, J. Y. et al. Production of bio-oil from fast pyrolysis of biomass using a pilot-scale circulating fluidized bed reactor and its characterization. **Journal of Environmental Management**, v. 234, p. 138–144, 15 mar. 2019.

PEREIRA, A. et al. Lignin Films from Spruce, Eucalyptus, and Wheat Straw Studied with Electroacoustic and Optical Sensors: Effect of Composition and Electrostatic Screening on Enzyme Binding. **Biomacromolecules**, v. 18, n. 4, p. 1322–1332, 10 abr. 2017.

PETERSON, A. A. et al. **Thermochemical biofuel production in hydrothermal media: A review of sub- and supercritical water technologiesEnergy and Environmental Science**Royal Society of Chemistry, , 23 jul. 2008. Disponível em: <https://pubs.rsc.org/en/content/articlehtml/2008/ee/b810100k>. Acesso em: 9 ago. 2020

PIDTASANG, B.; SUKKASI, S.; PATTIYA, A. Effect of in-situ addition of alcohol on yields and properties of bio-oil derived from fast pyrolysis of eucalyptus bark. **Journal of Analytical and Applied Pyrolysis**, v. 120, p. 82–93, 2016.

POLETTO, M. et al. Thermal decomposition of wood: Influence of wood components and cellulose crystallite size. **Bioresource Technology**, v. 109, p. 148–153, 2012.

POUTEAU, C. et al. Structural modification of Kraft lignin after acid treatment: characterisation of the apolar extracts and influence on the antioxidant properties in polypropylene. **Industrial Crops and Products**, v. 21, n. 1, p. 101–108, 1 jan. 2005.

RE, R. et al. Antioxidant activity applying an improved ABTS radical cation decolorization assay. **Free Radical Biology and Medicine**, v. 26, n. 9–10, p. 1231–1237, 1 maio 1999.

REMÓN, J. et al. Bio-oil upgrading in supercritical water using Ni-Co catalysts supported on carbon nanofibres. **Fuel Processing Technology**, v. 154, p. 178–187, 2016.

RINALDI, R. et al. Paving the Way for Lignin Valorisation: Recent Advances in Bioengineering, Biorefining and Catalysis. **Angewandte Chemie International Edition**, v. 55, n. 29, p. 8164–8215, 11 jul. 2016.

ROGERS, J. G.; BRAMMER, J. G. Estimation of the production cost of fast pyrolysis bio-oil. **Biomass and Bioenergy**, v. 36, p. 208–217, 2012.

ROPPONEN, J. et al. **Solvent extraction as a means of preparing homogeneous lignin fractions**. Holzforschung. **Anais**...De Gruyter, 1 jun. 2011

ROSTAGNO, M. et al. Sustainable polyacetals from erythritol and bioaromatics. **Journal of Applied Polymer Science**, v. 133, n. 45, p. app.44089, 5 dez. 2016.

ROUX, É. LE et al. Impact of a pressurized hot water treatment on the quality of bio-

oil produced from aspen. **Biomass and Bioenergy**, v. 81, p. 202–209, 2015.

ROWELL, R. M. (ED.). **Handbook of Wood Chemistry and Wood Composites**. 2nd. ed. Boca Raton: CRC Press, 2012.

SADEGHIFAR, H. et al. Fractionation of Organosolv Lignin Using Acetone:Water and Properties of the Obtained Fractions. **ACS Sustainable Chemistry & Engineering**, v. 5, n. 1, p. 580–587, 3 jan. 2017.

SALEM, M. Z. M.; ABDEL-MEGEED, A.; ALI, H. M. Stem wood and bark extracts of delonix regia (boj. ex. hook): Chemical analysis and antibacterial, antifungal, and antioxidant properties. **BioResources**, v. 9, n. 2, p. 2382–2395, 2014.

SANDSTRÖM, L. et al. Pyrolysis of Nordic biomass types in a cyclone pilot plant — Mass balances and yields. **Fuel Processing Technology**, v. 152, p. 274–284, 1 nov. 2016.

SCHERER, R.; GODOY, H. T. Antioxidant activity index (AAI) by the 2,2-diphenyl-1-picrylhydrazyl method. **Food Chemistry**, v. 112, n. 3, p. 654–658, 1 fev. 2009.

SCHOLZE, B.; HANSER, C.; MEIER, D. Characterization of the water-insoluble fraction from fast pyrolysis liquids (pyrolytic lignin). **Journal of Analytical and Applied Pyrolysis**, v. 58–59, p. 387–400, abr. 2001.

SCHOLZE, B.; MEIER, D. Characterization of the water-insoluble fraction from pyrolysis oil (pyrolytic lignin). Part I. PY–GC/MS, FTIR, and functional groups. **Journal of Analytical and Applied Pyrolysis**, v. 60, n. 1, p. 41–54, jun. 2001.

SCHROEDER, B. G. et al. Evaluation of biotechnological processes to obtain ethanol from recycled paper sludge. **Journal of Material Cycles and Waste Management**, v. 19, n. 1, p. 463–472, 1 jan. 2017.

SCHUTYSER, W. et al. **Chemicals from lignin: An interplay of lignocellulose fractionation, depolymerisation, and upgradingChemical Society Reviews**Royal Society of Chemistry, , 7 fev. 2018. Disponível em: <https://pubs.rsc.org/en/content/articlehtml/2018/cs/c7cs00566k>. Acesso em: 4 ago. 2020

SEVERIAN, G. N. **Polysaccharides: Structural Diversity and Functional Versatility**. New york: Marcel Dekker, 2008.

SHAFIZADEH, F. **Introduction to pyrolysis of biomassJournal of Analytical and Applied Pyrolysis**Elsevier, , 1 abr. 1982.

SHAH, Z. et al. Separation of Phenol from Bio-oil Produced from Pyrolysis of Agricultural Wastes. **Mod Chem Appl**, v. 5, n. 1, p. 199, 2017.

SHARMA, A.; PAREEK, V.; ZHANG, D. **Biomass pyrolysis - A review of**

modelling, process parameters and catalytic studiesRenewable and Sustainable Energy Reviews Elsevier Ltd, , 13 jun. 2015.

SHEN, D. K.; GU, S. The mechanism for thermal decomposition of cellulose and its main products. **Bioresource Technology**, v. 100, n. 24, p. 6496–6504, 1 dez. 2009.

SHU, R. et al. Efficient and product-controlled depolymerization of lignin oriented by metal chloride cooperated with Pd/C. **Bioresource Technology**, v. 179, p. 84–90, 1 mar. 2015.

SHU, R. et al. Synergistic effects of highly active Ni and acid site on the hydrodeoxygenation of syringol. **Catalysis Communications**, v. 91, p. 1–5, 2017.

SHU, R. et al. Controllable production of guaiacols and phenols from lignin depolymerization using Pd/C catalyst cooperated with metal chloride. **Chemical Engineering Journal**, v. 338, p. 457–464, 15 abr. 2018.

SILVANI, L. et al. Characterizing Biochar as Alternative Sorbent for Oil Spill Remediation. **Scientific Reports**, v. 7, p. 43912, 8 mar. 2017.

SINGH, R. et al. Strategies for selection of thermo-chemical processes for the valorisation of biomass. **Renewable Energy**, v. 98, p. 226–237, 2016.

SJÖSTRÖM, E. **Wood Chemistry**. 2nd. ed. [s.l.] Elsevier, 1993.

SLUITER, A. et al. Determination of Extractives in Biomass. **Biomass Analysis Technology Team Laboratory Analytical Procedure**, n. January, p. 1–8, 2004.

SLUITER, A. et al. Determination of Ash in Biomass. **NREL/TP-510-42622**, p. 5, 2005.

SLUITER, A. et al. **Determination of structural carbohydrates and lignin in biomass determination of structural carbohydrates and lignin in biomassNational Renewable Energy Laboratory (NREL)**. [s.l: s.n.].

STEFANIDIS, S. D. et al. A study of lignocellulosic biomass pyrolysis via the pyrolysis of cellulose, hemicellulose and lignin. **Journal of Analytical and Applied Pyrolysis**, v. 105, p. 143–150, 1 jan. 2014.

SUKHBAATAR, B. et al. Inhibitors removal from bio-oil aqueous fraction for increased ethanol production. **Bioresource Technology**, v. 161, p. 379–384, 1 jun. 2014.

SUNDQVIST, T.; OASMAA, A.; KOSKINEN, A. Upgrading Fast Pyrolysis Bio-Oil Quality by Esterification and Azeotropic Water Removal. **Energy & Fuels**, v. 29, n. 4, p. 2527–2534, 2015.

TAMBURINI, D. et al. The short-term degradation of cellulosic pulp in lake water and peat soil: A multi-analytical study from the micro to the molecular level. **International**

Biodeterioration and Biodegradation, v. 116, p. 243–259, 1 jan. 2017.

THOMMES, M. et al. Physisorption of gases, with special reference to the evaluation of surface area and pore size distribution (IUPAC Technical Report). **Pure and Applied Chemistry**, v. 87, n. 9–10, p. 1051–1069, 2015.

THRING, R. W.; GRIFFIN, S. L. The heterogeneity of two Canadian kraft lignins. **Canadian Journal of Chemistry**, v. 73, n. 5, p. 629–634, 1 maio 1995.

TOBISZEWSKI, M.; NAMIEŚNIK, J.; PENA-PEREIRA, F. Environmental risk-based ranking of solvents using the combination of a multimedia model and multi-criteria decision analysis. **Green Chemistry**, v. 19, n. 4, p. 1034–1042, 21 fev. 2017.

TRANE, R. et al. Catalytic steam reforming of bio-oil. **International Journal of Hydrogen Energy**, v. 37, n. 8, p. 6447–6472, abr. 2012.

TUCK, C. O. et al. **Valorization of biomass: Deriving more value from wasteScience**American Association for the Advancement of Science, , 10 ago. 2012. Disponível em: <https://science.sciencemag.org/content/337/6095/695>. Acesso em: 11 ago. 2020

VAN DE BELD, B.; HOLLE, E.; FLORIJN, J. The use of pyrolysis oil and pyrolysis oil derived fuels in diesel engines for CHP applications. **Applied Energy**, v. 102, p. 190–197, 1 fev. 2013.

VATTEM, D. A. et al. Phenolic antioxidant mobilization in cranberry pomace by solid-state bioprocessing using food grade fungus Lentinus edodes and effect on antimicrobial activity against select food borne pathogens. **Innovative Food Science and Emerging Technologies**, v. 5, n. 1, p. 81–91, 1 mar. 2004.

VEITH, C. et al. Synthesis and polymerization of bio-based acrylates: a review. **Polymer Chemistry**, v. 11, n. 47, p. 7452–7470, 2020.

VENDERBOSCH, R. H. et al. Stabilization of biomass-derived pyrolisis oils. **Journal of Chemical Technology and Biofuels technology**, v. 85, n. 5, p. 674–686, 2010.

VENDERBOSCH, R. H.; PRINS, W. **Fast pyrolysis technology developmentBiofuels, Bioproducts and Biorefining**John Wiley & Sons, Ltd, , 1 mar. 2010. Disponível em: <https://onlinelibrary.wiley.com/doi/full/10.1002/bbb.205>. Acesso em: 11 ago. 2020

VENDERBOSCH, R. H.; PRINS, W. Fast pyrolysis. In: BROWN, R. C.; STEVENS, C. (Eds.). . **Wiley Series in Renewable Resource, Thermochemical Processing of Biomass: Conversion into Fuels, Chemicals and Power**. Hoboken, UK: Wiley, 2011. p. 124–156.

VENKATESAN, K. et al. Hydrodeoxygenation kinetics of syringol, guaiacol and phenol over H-ZSM-5. **Catalysis Communications**, v. 148, p. 106164, 2021.

WANG, J. et al. Separation of Biomass Pyrolysis Oil by Supercritical CO2 Extraction. **Smart Grid and Renewable Energy**, v. 01, n. 02, p. 98–107, 31 ago. 2010.

WANG, L. et al. Aromatics and phenols from catalytic pyrolysis of Douglas fir pellets microwave with ZSM-5 as a cayalyst. **Journal of Analytical and Applied Pyrolysis**, v. 98, p. 194–200, 2012.

WANG, S. et al. Comparison of the pyrolysis behavior of pyrolytic lignin and milled wood lignin by using TG-FTIR analysis. **Journal of Analytical and Applied Pyrolysis**, v. 108, p. 78–85, 2014a.

WANG, S. et al. Multi-step separation of monophenols and pyrolytic lignins from the water-insoluble phase of bio-oil. **Separation and Purification Technology**, v. 122, p. 248–255, fev. 2014b.

WANG, S. et al. Stepwise Enrichment of Sugars from the Heavy Fraction of Bio-oil. **Energy and Fuels**, v. 30, n. 3, p. 2233–2239, 17 mar. 2016.

WANG, X.; RINALDI, R. A Route for Lignin and Bio-Oil Conversion: Dehydroxylation of Phenols into Arenes by Catalytic Tandem Reactions. **Angewandte Chemie International Edition**, v. 52, n. 44, p. 11499–11503, 25 out. 2013.

WANG, X.; RINALDI, R. Bifunctional Ni catalysts for the one-pot conversion of Organosolv lignin into cycloalkanes. **Catalysis Today**, v. 269, p. 48–55, 2016.

WANG, Y. et al. Formation of coke during the pyrolysis of bio-oil. **Fuel**, v. 108, p. 439–444, 2013.

WANG, Y. et al. Separation and characterization of pyrolytic lignins from the heavy fraction of bio-oil by molecular distillation. **Separation and Purification Technology**, v. 152, p. 123–132, set. 2015.

WEN, J. L. et al. Unveiling the Structural Heterogeneity of Bamboo Lignin by In Situ HSQC NMR Technique. **Bioenergy Research**, v. 5, n. 4, p. 886–903, dez. 2012.

WEXLER, A. S. Characterization of Lignosulfonates by Ultraviolet Spectrometry. Direct and Difference Spectrograms. **Analytical Chemistry**, v. 36, n. 1, p. 213–221, jan. 1964.

WIEGAND, I.; HILPERT, K.; HANCOCK, R. E. W. Agar and broth dilution methods to determine the minimal inhibitory concentration (MIC) of antimicrobial substances. **Nature Publishing Group**, v. 3, n. 2, p. 163–175, 2008.

WIGLEY, T.; YIP, A. C. K.; PANG, S. A detailed product analysis of bio-oil from fast pyrolysis of demineralised and torrefied biomass. **Journal of Analytical and Applied Pyrolysis**, v. 123, p. 194–203, 2017.

WISE, L. E.; MAXINE, M.; D'ADDIECO, A. A. Chlorite holocellulose, its fractionation

and bearing on summative wood analysis and on studies on the hemicelluloses. **Technical association of pulp and paper industry**, v. 29, p. 210–218, 1946.

XIAO, X.; CHEN, Z.; CHEN, B. H/C atomic ratio as a smart linkage between pyrolytic temperatures, aromatic clusters and sorption properties of biochars derived from diverse precursory materials. **Scientific Reports**, v. 6, p. 22644, mar. 2016.

XIONG, Z. et al. Assessing the chemical composition of heavy components in bio-oils from the pyrolysis of cellulose, hemicellulose and lignin at slow and fast heating rates. **Fuel Processing Technology**, v. 199, p. 106299, 1 mar. 2020.

YANG, H. et al. Characteristics of hemicellulose, cellulose and lignin pyrolysis. **Fuel**, v. 86, n. 12–13, p. 1781–1788, 1 ago. 2007.

YANG, J.-F. et al. Chemical Composition, Antioxidant, and Antibacterial Activity of Wood Vinegar from Litchi chinensis. **Molecules**, v. 21, n. 9, p. 1150, 30 ago. 2016.

YANG, N. et al. Antibacterial and detoxifying activity of NZ17074 analogues with multi-layers of selective antimicrobial actions against Escherichia coli and Salmonella enteritidis. **Scientific Reports**, v. 7, n. 1, p. 1–19, 1 dez. 2017.

YANG, X. et al. Upgrading Biocrude of *Grindelia Squarrosa* to Jet Fuel Precursors by Aqueous Phase Hydrodeoxygenation. **Energy Technology**, v. 6, n. 9, p. 1832–1843, 1 set. 2018.

ZACHER, A. H. et al. **A review and perspective of recent bio-oil hydrotreating researchGreen Chemistry**Royal Society of Chemistry, , 28 jan. 2014. Disponível em: <https://pubs.rsc.org/en/content/articlehtml/2014/gc/c3gc41382a>. Acesso em: 12 ago. 2020

ZAKIS, G. F. **Functional Analysis of Lignins and Their Derivatives**. Atlanta: TAPPI Press, 1994.

ZAKZESKI, J. et al. The Catalytic Valorization of Ligning for the Production of Renewable Chemicals. **Chem. Rev.**, v. 110, p. 3552–3599, 2010.

ZHANG, H. et al. An aqueous-phase catalytic process for the selective hydrogenation of acetylene with monodisperse water soluble palladium nanoparticles as catalyst. **Catalysis Science & Technology**, v. 2, n. 7, p. 1319–1323, 2012.

ZHANG, H. et al. Catalytic conversion of lignin pyrolysis model compound- guaiacol and its kinetic model including coke formation. **Scientific Reports**, v. 6, n. 1, p. 37513, 21 dez. 2016a.

ZHANG, L. et al. Hydrogenation of fourteen biomass-derived phenolics in water and in methanol: their distinct reaction behaviours. **Sustainable Energy & Fuels**, v. 2, n. 4, p. 751–758, 2018.

ZHANG, S. et al. Production of aromatic hydrocarbons by hydrogenation-cocracking of bio-oil and methanol. **Fuel Processing Technology**, 2016b.

ZHANG, X.-S. et al. Mass production of chemicals from biomass-derived oil by directly atmospheric distillation coupled with co-pyrolysis. **Scientific Reports**, v. 3, p. 1120, jan. 2013.

ZHANG, X. et al. Sequential Fractionation of Lignin-derived Pyrolysis Oil via Extraction with a Combination of Water and Organic Solvents. **BioResources**, v. 14, n. 1, p. 2144–2158, 2019a.

ZHANG, X. et al. Oligomers obtained from sequential fractionation of lignin pyrolysis oil. **Energy Conversion and Management**, v. 201, p. 112181, 1 dez. 2019b.

ZHAO, H. Y. et al. Hydrodeoxygenation of guaiacol as model compound for pyrolysis oil on transition metal phosphide hydroprocessing catalysts. **Applied Catalysis A: General**, v. 391, n. 1–2, p. 305–310, jan. 2011.

ZHAO, L. et al. Improving antioxidant activity of lignin by hydrogenolysis. **Industrial Crops and Products**, v. 125, p. 228–235, 1 dez. 2018a.

ZHAO, Y. et al. Separation of aromatic monomers from oxidatively depolymerized products of lignin by combining Sephadex and silica gel column chromatography. **Separation and Purification Technology**, v. 191, p. 250–256, 31 jan. 2018b.

ZHOU, S. et al. Lignin Valorization through Thermochemical Conversion: Comparison of Hardwood, Softwood and Herbaceous Lignin. **ACS Sustainable Chemistry and Engineering**, v. 4, n. 12, p. 6608–6617, 5 dez. 2016.

LIST OF PUBLICATIONS

MATOS, MAILSON; CLARO, FRANCINE C.; LIMA, TIELIDY A.M.; AVELINO, FRANCISCO ; HANSEL, FABRICIO A. ; MACIEL, GISELLE M. ; LOMONACO, DIEGO ; MAGALHÃES, WASHINGTON L.E. . Acetone:Water fractionation of pyrolytic lignin improves its antioxidant and antibacterial activity. JOURNAL OF ANALYTICAL AND APPLIED PYROLYSIS, v. 156, p. 105175, 2021.

SUOTA, MARIA JULIANE; KOCHEPKA, DÉBORA MEREDIANE; GANTER MOURA, MARLON GUALBERTO; PIRICH, CLEVERTON LUIZ; **MATOS, MAILSON**; MAGALHÃES, WASHINGTON LUIZ ESTEVES; RAMOS, LUIZ PEREIRA. Lignin functionalization strategies and the potential applications of its derivatives - A Review. BioResources. Fator de Impacto(2019 JCR): 1,4090, v.16, p.6471 - 6511, 2021.

PRESTES, A.; VERRUCK, S.; VARGAS, M. O.; CANELLA, M. H. M.; SILVA, C. C.; BARROS, E. L S; DANTAS, A; OLIVEIRA, LUAN V A; MARAN, B M; **MATOS, M.**; HELM, C V; PRUDENCIO, E S. Influence of guabiroba pulp (campomanesia xanthocarpa o. berg) added to fermented milk on probiotic survival under in vitro simulated gastrointestinal conditions. FOOD RESEARCH INTERNATIONAL, v. x, p. 110135, 2021.

THÁ, EMANOELA LUNDGREN ; **MATOS, MAILSON** ; AVELINO, FRANCISCO ; LOMONACO, DIEGO ; RODRIGUES-SOUZA, ISISDORIS ; GAGOSIAN, VIVIANA STEPHANIE COSTA ; CESTARI, MARTA MARGARETE ; MAGALHÃES, WASHINGTON LUIZ ESTEVES ; LEME, DANIELA MORAIS . Safety aspects of kraft lignin fractions: Discussions on the in chemico antioxidant activity and the induction of oxidative stress on a cell-based in vitro model. INTERNATIONAL JOURNAL OF BIOLOGICAL MACROMOLECULES, v. 182, p. 977-986, 2021.

DE LIMA, GABRIEL GOETTEN ; ALIABADI, MEYSAM ; **MATOS, M.** ; CHEE, BOR SHIN ; ANGELINA MORAES DE LIMA, TIELIDY ; MAGALHÃES, WASHINGTON L. E. . Microfibrillated cellulose films containing chitosan and tannic acid for wound healing applications. JOURNAL OF MATERIALS SCIENCE-MATERIALS IN MEDICINE, v. 32, p. x, 2021.

MATOS, M.; MATTOS, B. D.; CADEMARTORI, P. H. G.; LOURENCON, T. V.; HANSEL, F. A.; ZANONI, P.; YAMAMOTO, C.; Magalhães, W. L. E. Pilot-Scaled Fast-Pyrolysis Conversion of Eucalyptus Wood Fines into Products: Discussion Toward Possible Applications in Biofuels, Materials, and Precursors. BioEnergy Research. Impact Factor(2018 JCR): 2,5000, p.1 - 12, 2020.

DE LIMA, GABRIEL GOETTEN ; DE MIRANDA, NELI BRANCO ; TIMM, THAYNÃ GONÇALVES ; **MATOS, MAILSON** ; ANGELINA MORAES DE LIMA, TIELIDY ; LUIZ ESTEVES MAGALHÃES, WASHINGTON ; BENATHAR BALLOD TAVARES, LORENA ; HANSEL, FABRÍCIO AUGUSTO ; HELM, CRISTIANE VIEIRA . Characterisation and in vivo evaluation of Araucaria angustifolia pinhão seed coat

nanosuspension as a functional food source. Food & Function, v. 11, p. 9820-9832, 2020.

ALIABADI, MEYSAM; CHEE, BOR SHIN; **MATOS, MAILSON**; CORTESE, YVONNE J.; NUGENT, MICHAEL J. D.; DE LIMA, TIELIDY A. M.; MAGALHÃES, WASHINGTON L. E.; DE LIMA, GABRIEL GOETTEN. Yerba Mate Extract in Microfibrillated Cellulose and Corn Starch Films as a Potential Wound Healing Bandage. Polymers. Impact Factor (2017 JCR): 2.9350, v.12, p.2807, 2020.

DE LIMA, G. G.; FERREIRA, B. DIAS; **MATOS, M.**; PEREIRA, B. L.; NUGENT, M. J. D.; HANSEL, F. A.; MAGALHÃES, W. L.. Effect of cellulose size-concentration on the structure of polyvinyl alcohol hydrogels. CARBOHYDRATE POLYMERS. Impact Factor(2018 JCR): 6.0440, v.245, p.116612 - , 2020.

TIMM, T. G.; DE LIMA, G. G.; **MATOS, M.**; MAGALHÃES, W. L.; TAVARES, L. B. B.; HELM, C. V.. Nanosuspension of pinhão seed coat development for a new high-functional cereal bar. JOURNAL OF FOOD PROCESSING AND PRESERVATION. Impact Factor(2018 JCR): 1,2880, v.44, p.e14464 - , 2020.

CLARO, F. C.; **MATOS, M.**; JORDÃO, C.; AVELINO, F.; LOMONACO, D.; M., W. L. E. Enhanced microfibrillated cellulose-based film by controlling the hemicellulose content and MFC Rheology. CARBOHYDRATE POLYMERS. Impact Factor(2018 JCR): 6,0440, p.307 - 314, 2019.

DE LIMA, G. G.; RUIZ, H. Z.; **MATOS, M.**; HELM, C. V.; DE LIZ, M. V.; MAGALHÃES, W. L. E. Prediction of yerba mate caffeine content using near infrared spectroscopy. SPECTROSCOPY LETTERS. Impact Factor(2018 JCR): 1,0810, v.52, p.282 - 287, 2019.

MAGALHÃES, WASHINGTON L. E.; **MATOS, M.**; LOURENCON, T. V. Metodologia científica: determinação da capacidade antioxidante de lignina pela captura do radical livre DPPH. EMBRAPA FLORESTAS. COMUNICADO TÉCNICO. , v.1, p.1 - 8, 2018.

MALUCELLI, L. C.; **MATOS, M**.; JORDÃO, C.; LACERDA, L. G.; CARVALHO FILHO, M. A. S.; Magalhães, W. L. E. Grinding severity influences the viscosity of cellulose nanofiber (CNF) suspensions and mechanical properties of nanopaper. Cellulose. Impact Factor(2018 JCR): 3,9170, v.25, p.6581 - 6589, 2018.

MALUCELLI, L. C.; **MATOS, M.**; JORDÃO, C.; LOMONACO, D.; LACERDA, L. G.; CARVALHO FILHO, M. A. S.; Magalhães, W. L. E. Influence of cellulose chemical pretreatment on energy consumption and viscosity of produced cellulose nanofibers (CNF) and mechanical properties of nanopaper. Cellulose. Impact Factor(2018 JCR): 3,9170, p.1667 - 1681, 2018.

MATTOS, B. D.; GOMES, G. R.; **DE MATOS, M.**; RAMOS, L. P.; MAGALHÃES, W. L. E. Consecutive Production of Hydroalcoholic Extracts, Carbohydrates Derivatives and Silica Nanoparticles from Equisetum arvense. Waste and Biomass Valorization. Impact Factor(2018 JCR): 2,3580, v.xx, p.1 - 10, 2017.

MAGALHAES, W. L. E.; CLARO, F. C.; **MATOS, M.**; LENGOWSKI, E. C. Produção de nanofibrilas de celulose por desfibrilação mecânica em moinho coloidal. EMBRAPA FLORESTAS. COMUNICADO TÉCNICO. , v.404, p.01 - 05, 2017.

MATOS, M. ; MATTOS, BRUNO DUFAU; TARDY, BLAISE L.; ROJAS, ORLANDO J.; MAGALHAES, WASHINGTON LUIZ ESTEVES Use of biogenic silica in porous alginate matrices for sustainable fertilization with tailored nutrient delivery. ACS Sustainable Chemistry & Engineering. Impact Factor(2018 JCR): 6,9700, v.6, p.2716 - 2723, 2017.

SUPPLEMENTARY MATERIAL

FIGURE III.S1 - CONTOUR PLOT OF UNDISSOLVED MATERIAL VS. AMOUNT OF BIO-OIL IN WATER AND STIRRING SPEED.

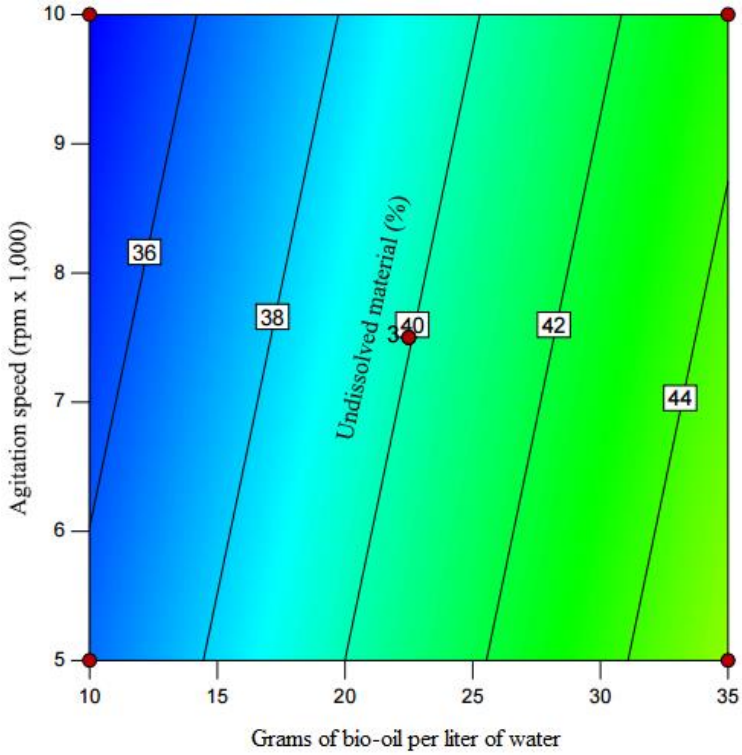

FIGURE III.S2 - SIDE-CHAIN REGION IN THE 2D HSQC NMR SPECTRA OF THE EXP1 AND EXP10

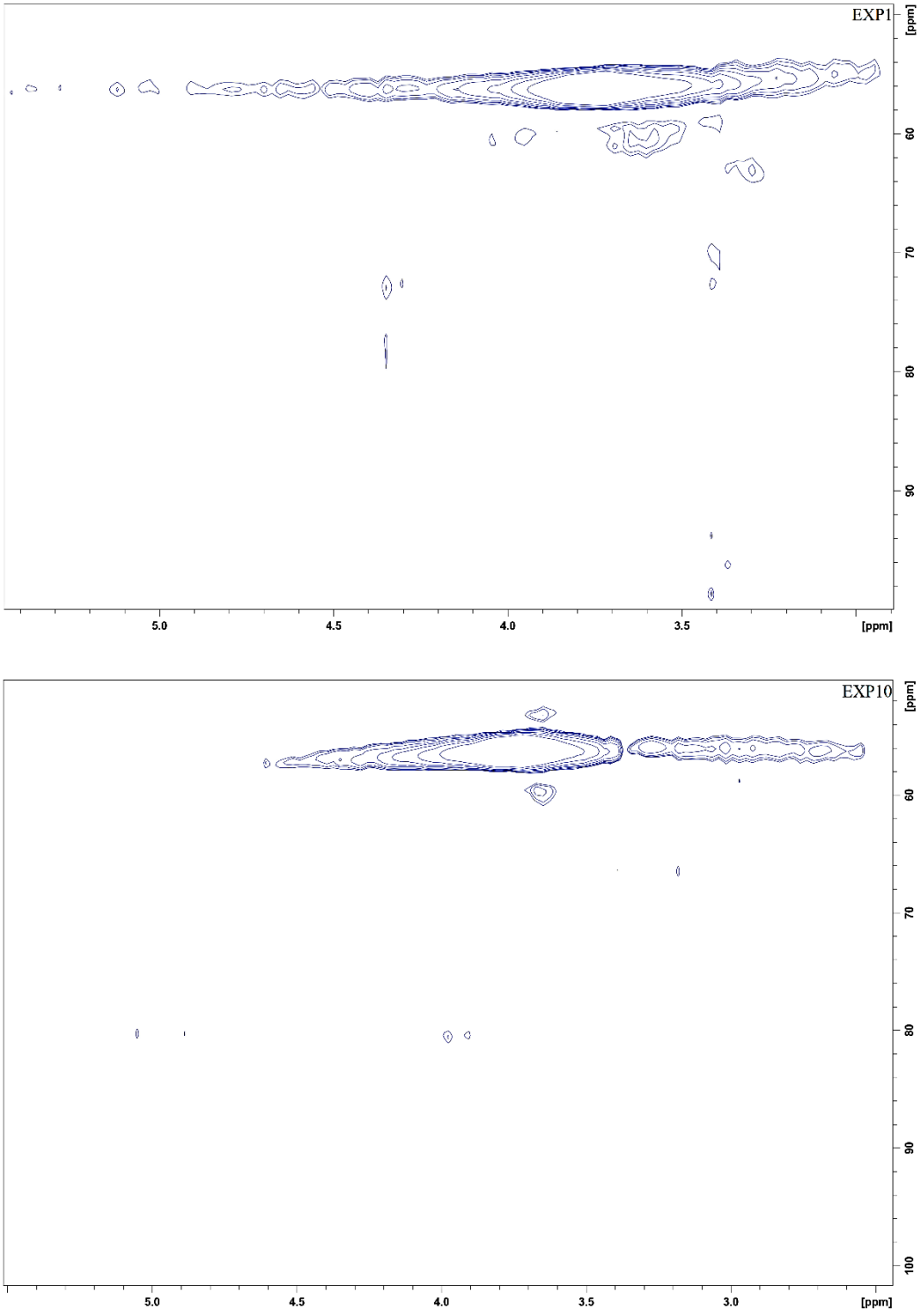

FIGURE III.S3 - THERMOGRAVIMETRY AND DERIVATIVE THERMOGRAVIMETRY CURVES OF PL FRACTIONS

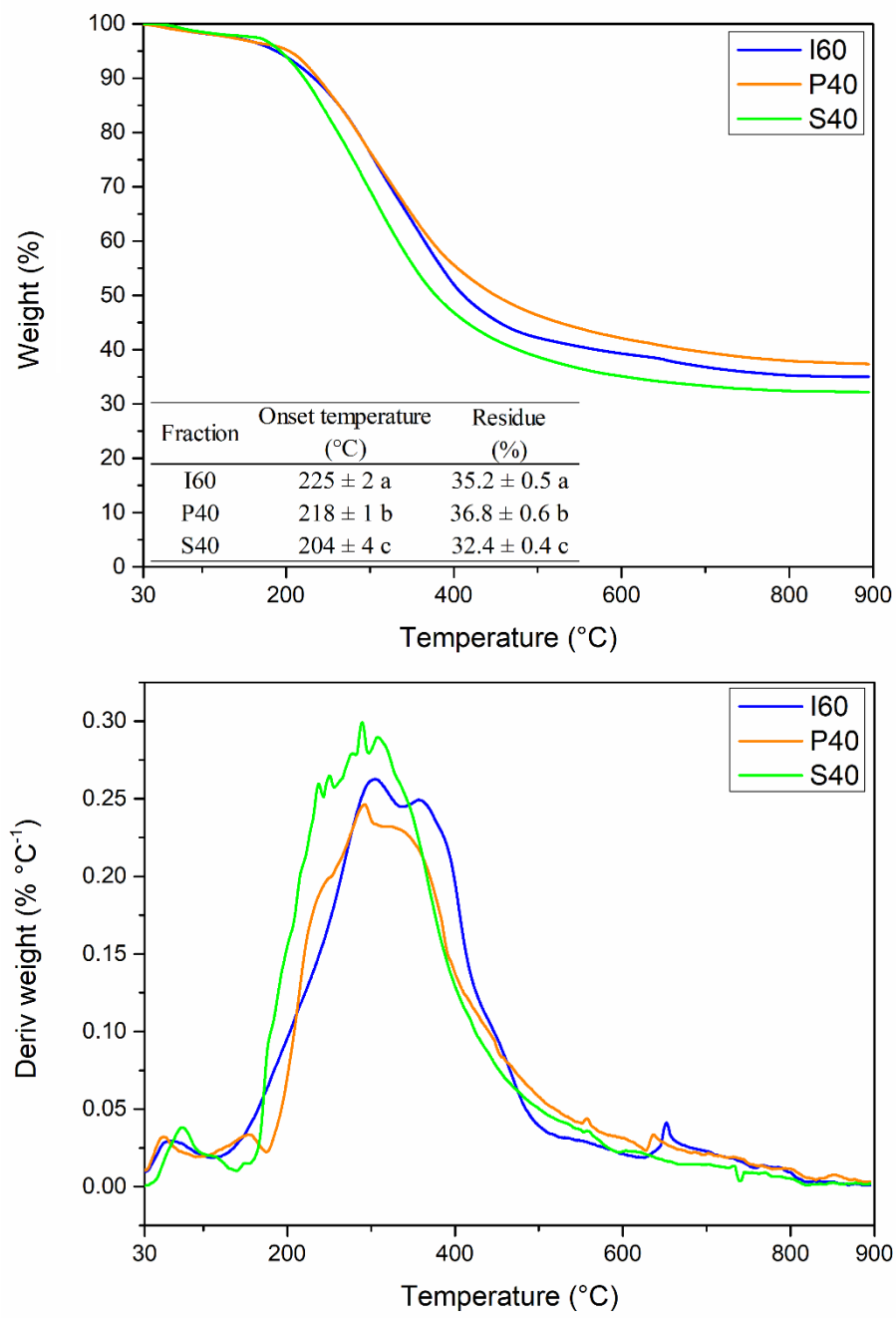

Fraction	Onset temperature (°C)	Residue (%)
I60	225 ± 2 a	35.2 ± 0.5 a
P40	218 ± 1 b	36.8 ± 0.6 b
S40	204 ± 4 c	32.4 ± 0.4 c

TABLE III.S1 - YIELD IN NON-SOLUBILIZED MATERIAL IN EXPERIMENTS PERFORMED UNDER CONDITIONS OTHER THAN EXPERIMENTAL DESIGN.

Fractionation Conditions	Undissolved material (%)
All bio-oil added in one go (10 g L^{-1} and 10k rpm)	65 ± 2
Mild agitation speed (10 g L^{-1} and 2.0k rpm)	53 ± 1
Non-shear agitation - magnetic stirrer (10 g L^{-1} 2.0k rpm)	88 ± 2
Dropwise in water at 20 °C (10 g L^{-1} and 10k rpm)	45 ± 3
Dropwise in water at 50 °C (10 g L^{-1} and 10k rpm)	46 ± 2
Dropwise in water at 90 °C (10 g L^{-1} and 10k rpm)	32 ± 4

TABLE III.S2 - PHYSICOCHEMICAL CHARACTERIZATION AS A FUNCTION OF SEPARATION CONDITIONS.

Experiment	Agitation speed (rpm x 1,000)	Bio-oil (g/ L of water)	Undissolved material (%)	Insoluble lignin (%)	Soluble lignin (%)	Carbohydrates (%)	Ashes (%)
EXP1	7.5	40	51.5	66 ± 2 a	27 ± 2 a	4.70 ± 0.04 a	2.22 ± 0.06 a
EXP2	5	35	44.0	68 ± 1 a	28 ± 1 a	1.56 ± 0.02 bcf	2.31 ± 0.04 a
EXP3	10	35	40.5	80 ± 1 bc	15 ± 1 bc	1.60 ± 0.02 cf	2.89 ± 0.02 b
EXP4	4	22.5	40.9	69 ± 0 ab	25 ± 0 ab	2.11 ± 0.03 d	2.79 ± 0.01 b
EXP5	7.5	22.5	41.2	72 ± 1 ab	24 ± 2 ab	1.59 ± 0.02 cf	2.77 ± 0.01 b
EXP6	7.5	22.5	40.2	75 ± 2 b	20 ± 3 b	1.59 ± 0.02 cf	2.84 ± 0.06 b
EXP7	7.5	22.5	40.4	74 ± 1 b	22 ± 2 b	1.60 ± 0.02 cf	2.82 ± 0.04 b
EXP8	11	22.5	40.2	78 ± 1 bc	17 ± 1 b	1.65 ± 0.02 c	2.81 ± 0.03 b
EXP9	5	10	36.5	84 ± 2 cd	12 ± 4 cd	1.22 ± 0.02 fh	2.81 ± 0.08 b
EXP10	10	10	34.5	90 ± 0 d	6.0 ± 0.1 d	0.90 ± 0.02 g	2.74 ± 0.01 b
EXP11	7.5	5	34.8	87 ± 3 d	8.6 ± 1.7 d	0.97 ± 0.02 g	2.89 ± 0.06 b

Averages followed by the same letters in the same column do not differ statistically by Tukey's test ($p<0.05$).

TABLE III.S3 - WEIGHT-AVERAGE (M_w) AND NUMBER-AVERAGE (M_n) MOLECULAR WEIGHTS DATA AND POLYDISPERSITY INDEX (PDI) OF THE OBTAINED SAMPLES.

Experiment	M_w (g mol^{-1})	M_n (g mol^{-1})	M_w/M_n
EXP1	773	431	1.80
EXP2	651	401	1.62
EXP3	630	413	1.53
EXP4	639	410	1.56
EXP5	626	406	1.54
EXP6	627	406	1.54
EXP7	645	419	1.54
EXP8	649	416	1.56
EXP9	657	433	1,52
EXP10	623	412	1.51
EXP11	659	426	1.55

TABLE III.S4 - CONCENTRATION, BIOLOGICAL ASSIGNMENT AND RETENTION INDEX OF COMPOUNDS, PRESENT IN THE LIGNIN FRACTIONS, DETECTED BY GC-MS AS TMS DERIVATIVES.

	Compound[a]	RI	Mass fragments (m/z)	Biological Assignment (BA)	Chemical class	Content (mg g^{-1})		
						S40	P40	I60
C1	Hydroxyacetic acid (Glycolic acid)	1080	205/177/147	Carbohydrates	Organic acids	6.80	1.94	14.01
C2	2-Hydroxypropenoic acid (Pyruvic acid)	1086	217/189/147	Carbohydrates	Organic acids	0.41	1.09	4.12
C3	α-Hydroxyisobutyric acid (Acetonic acid)	1124	233/205/147	Carbohydrates	Organic acids	0.64	0.31	0.62
C4	C1-Phenol[1]	1128	180/165/135	Lignin/CHO	Phenols	0.72	0.84	2.37
C5	Furan-2-carboxylic acid (2-Furoic acid)	1134	184/169/125	Carbohydrates	Organic acids	0.40	0.18	0.60
C6	3-Hydroxypropanoic acid (Hydracrylic acid)	1143	219/177/147	Carbohydrates	Organic acids	4.22	1.58	4.77

C7	C1-Phenol[1]	1150	180/165/135	Lignin/CHO	Phenols	2.30	1.83	5.64
C8	U#01	1164	159/131/115	Unidentified	Unidentified	1.98	0.66	0.87
C9	3-Hydroxy-4H-pyran-4-one (Pyromeconic acid)	1199	169/95/75	Carbohydrates	Ketones	5.58	1.10	3.45
C10	C2-Phenol[2]	1208	194/179/163	Lignin/CHO	Phenols	0.34	0.44	0.89
C11	2-Methoxyphenol (Guaiacol)	1224	196/181/166	Lignin (G)	Phenols	1.67	2.02	6.60
C12	C2-Phenol[2]	1236	194/179/163	Lignin/CHO	Phenols	9.92	8.24	16.18
C13	4-Ethenylphenol (4-Vinylphenol)	1277	192/177/161	Lignin (H)	Phenols	2.58	3.09	14.21
C14	U#02	1304	208/193/163	Unidentified	Unidentified	1.28	1.38	2.43
C15	1,2-Dihydroxybenzene (Catechol)	1313	254/239/73	Carbohydrates	Phenols	14.26	1.57	6.23
C16	C1-Guaiacol	1313	210/195/180	Lignin (G)	Phenols	7.78	7.28	15.16
C17	4-Hydroxybenzaldehyde (p-Formylphenol)	1375	151/179/194	Lignin (H)	Aldehydes	4.82	2.49	4.65
C18	C1-Dihydroxybenzene[3]	1383	268/253/73	Lignin/CHO	Phenols	6.43	0.83	2.42
C19	C2-Guaiacol	1390	224/209/194	Lignin (G)	Phenols	6.51	5.76	9.53
C20	C1-Dihydroxybenzene[3]	1393	268/253/73	Lignin/CHO	Phenols	4.36	0.55	2.03
C21	2,6-Dimethoxyphenol (Syringol)	1397	226/211/196	Lignin (S)	Phenols	67.91	9.38	30.45
C22	1,4-Dihydroxybenzene (Hydroquinone)	1397	254/239/223	Lignin/CHO	Phenols	14.01	6.97	4.73
C23	2-Methoxy-4-vinylphenol (p-Vinylguaiacol)	1434	222/207/192	Lignin (G)	Phenols	1.18	1.28	4.82
C24	4-Allyl-2-methoxyphenol (Eugenol)	1468	236/221/206	Lignin (G)	Phenols	7.41	3.05	6.31
C25	4-Propylguaiacol (Dihydroeugenol)	1472	238/223/179	Lignin (G)	Phenols	2.11	2.24	2.19
C26	3-Hydroxy-4-methoxyphenol (4-Methoxyresorcinol)	1475	284/269/254	Lignin (G)	Phenols	2.83	0.43	1.20
C27	C1-Syringol	1478	240/225/210	Lignin (S)	Phenols	60.34	9.65	21.91
C28	cis-2-Methoxy-4-propenylphenol ((Z)-Isoeugenol)	1517	236/221/206	Lignin (G)	Phenols	2.05	0.50	1.82
C29	4-Hydroxy-3-methoxybenzaldehyde (Vanillin)	1534	224/209/194	Lignin (G)	Aldehydes	14.28	7.30	13.53
C30	U#03	1536	284/269/254	Unidentified	Unidentified	0.69	0.27	0.32
C31	C2-syringol	1545	254/224/209	Lignin (S)	Phenols	19.54	3.88	6.42
C32	trans-2-Methoxy-4-propenylphenol ((E)-Isoeugenol)	1567	236/221/206	Lignin (G)	Phenols	3.79	2.12	2.63
C33	4-Vinylsyringol (Canolol)	1592	252/237/222	Lignin (S)	Phenols	0.45	0.40	1.19
C34	4-Allyl-2,6-dimethoxyphenol (Methoxyeugenol)	1618	266/251/236	Lignin (S)	Phenols	23.57	3.25	7.61
C35	1-(4-Hydroxy-3-methoxyphenyl)ethanone (Acetovanillone)	1617	238/223/208	Lignin (G)	Ketones	14.36	2.57	5.05

C36	2,6-Dimethoxy-4-propylphenol (4 -Propylsyringol)	1621	268/253/209	Lignin (S)	Phenols	6.50	2.20	3.14
C37	(Z)-2,6-Dimethoxy-4-propenylphenol (cis-4-Propenylsyringol)	1666	266/251/236	Lignin (S)	Phenols	1.00	0.24	0.23
C38	U#04	1670	314/299/284	Unidentified	Unidentified	0.80	0.14	-
C39	1,6-Anhydro-beta-D-glucopyranose (Levoglucosan)	1696	333/217/204	Carbohydrates	Carbohydrates	51.37	-	-
C40	4-Hydroxy-3,5-dimethoxybenzaldehyde (Syringaldehyde)	1693	254/239/224	Lignin (S)	Aldehydes	48.05	10.71	19.55
C41	U#05	1703	217/204/191	Unidentified	Unidentified	1.13	-	-
C42	(E)-2,6-Dimethoxy-4-propenylphenol (trans-4-Propenylsyringol)	1724	266/251/236	Lignin (S)	Phenols	4.91	2.56	2.14
C43	4-hydroxy-3-methoxybenzoic acid (Vanillic acid)	1759	312/297/267	Lignin (G)	Organic acids	2.23	0.52	0.75
C44	1-(4-hydroxy-3,5-dimethoxyphenyl)ethanone (Acetosyringone)	1764	268/238/223	Lignin (S)	Ketones	40.71	3.82	7.51
C45	1-(4-hydroxy-3,5-dimethoxyphenyl)-2-propanone (Syringyl Acetone)[b]	1780	282/239/209	Lignin (S)	Ketones	15.21	1.44	1.13
C46	U#06	1819	326/311/269	Unidentified	Unidentified	2.67	0.25	0.53
C47	(E)-4-Hydroxy-3-methoxycinnamaldehyde ((E)-Coniferylaldehyde)	1842	250/235/220	Lignin (G)	Aldehydes	3.02	0.83	1.60
C48	1-(4-hydroxy-3,5-dimethoxyphenyl)-2-propanone (Propiosyringone) [b]	1851	282/253/223	Lignin (S)	Ketones	12.15	1.89	3.47
C49	4-Hydroxy-3,5-dimethoxybenzoic acid (Syringic acid)	1891	342/327/297	Lignin (S)	Organic acids	2.82	-	-
C50	4-Hydroxycinnamic acid (p-Coumaric acid)	1936	308/293/249	Lignin (H)	Organic acids	2.65	0.21	0.36
C51	(E)-3,5-Dimethoxy-4-hydroxycinnamaldehyde ((E)-Sinapalaldehyde)	2001	280/250/222	Lignin (S)	Aldehydes	7.63	2.63	6.10
C52	(+)-Dehydroabietic acid	2387	372/357/239	Extractive	Organic acids	-	1.00	-
C53	U#07	2393	476/461/374	Unidentified	Unidentified	2.82	0.80	1.20
C54	U#08	2428	394/379/349	Unidentified	Unidentified	2.61	0.37	0.47
C55	Icosanoic acid (Arachidic acid)	2439	369/129/117	Extractive	Fatty acids	-	-	3.49
C56	1-Guaiacyl-1'-syringyl-methane	2526	491/434/404	Lignin (GS)	Phenols	0.75	0.16	0.23
C57	Docosanoic acid (Behenic acid)	2642	397/129/117	Extractive	Fatty acids	-	-	10.47

C58	1,1'-Disyringyl-methane	2647	464/434/404	Lignin (S)	Phenols	16.57	1.95	4.30
C59	U#09	2711	518/292/262	Unidentified	Unidentified	1.26	0.47	0.48
C60	U#10	2718	479/239/209	Unidentified	Unidentified	0.97	0.25	0.25
C61	Tricosanoic acid	2738	411/129/117	Extractive	Fatty acids	-	-	5.38
C62	4,4'-dihydroxy-3',5'-dimethoxy--trans-stilbene (1-Hydroxyphenyl-1'-syringyl-ethene)	2829	416/386/356	Lignin (HS)	Stilbenoids	50.97	25.83	21.95
C63	Tetracosanoic acid (Lignoceric acid)	2834	425/129/117	Extractive	Fatty acids	-	-	36.27
C64	3,3',5'-Trimethoxy-4,4'-dihydroxy-trans-stilbene (1-Guaiacyl-1'syringyl-ethene)	2987	446/416/386	Lignin (GS)	Stilbenoids	18.30	7.91	7.52
C65	Hexacosanoic acid (Cerotic acid)	3031	453/129/117	Extractive	Fatty acids	-	-	7.40
C66	β-Sitosterol acetate	3095	396/288/255	Extractive	Steroids	-	0.13	9.64
C67	2,2',6,6'-Tetramethoxy-4,4'-dihydroxy-trans-stilbene (1,1'-Disyringyl-ethene)	3137	476/446/416	Lignin (S)	Stilbenoids	10.09	3.94	3.58
C68	Octacosanoic acid (Montanic acid)	3218	481/129/117	Extractive	Fatty acids	-	-	15.93
C69	Campesterol	3233	472/382/343	Extractive	Steroids	-	0.09	1.69
C70	Stigmasterol	3257	484/394/255	Extractive	Steroids	-	0.07	1.80
C71	β-Sitosterol	3320	486/396/357	Extractive	Steroids	-	0.15	5,62
Biological Assignment (BA)			**Carbohydrates[c] (%)**			**8.4**	**0.8**	**3.4**
			Lignin[c] (%)			**48.7**	**13.4**	**23.9**
			Lignin/carbohydrates[c] (%)			**3.8**	**2.0**	**3.4**
			Extractive[c] (%)			**0.0**	**0.1**	**9.8**
			Unidentified[c] (%)			**1.6**	**0.5**	**0.7**
Total GC-MS detectables (%)						**62.5**	**16.7**	**41.1**

[a] Compounds followed by the same number are isomers. Isomer abbreviations: C1 – methyl, C2 - dimethyl or ethyl; RI: Retention Index; [b] Compounds identified by interpretation of mass spectra; [c] Percentage of compounds detected by GC-MS in relation to the entire sample.

TABLE IV.S1 - CONCENTRATION RELATIVE (IN µg mL^{-1}) TO THE INTERNAL STANDARD (5-α-CHOLESTANE) AND CHEMICAL CLASS OF COMPOUNDS FORMED IN THE CATALYSIS REACTIONS OF GUAIACYL MODEL COMPOUNDS, IDENTIFIED BY GC-MS

RI	Compound	Chemical class	Mass fragments			Vanilin				Guaiacol			
			m/z (1)	m/z (2)	m/z (3)	1Pd	2Pd	5Ag	10Ag	1Pd	2Pd	5Ag	10Ag
842	RI=841.9 in MDM1245	Unknown	43	59				555	1122			276	37
861	C2-Benzene	Hydrocarbon	91	106	65							172	38
870	C2-Benzene	Hydrocarbon	91	106								77	23
891	C2-Benzene	Hydrocarbon	91	106								90	19
987	Phenol	Phenol	94	66	65	83	107	204	98	1351	819	2233	3699
994	Benzofuran	Ether	118	89	63	6	4	7		146	56	91	93
1031	C3-Phenol	Phenol	121	136	122			33				152	
1051	C1-Phenol	Phenol	108	107	79	692	485	564	473	9612	4008	10891	12334
1073	C1-Phenol	Phenol	108	107	77	41	34	175	84	109	99	99	112
1085	Guaicol	Phenol	124	109	81	1529	1241	389	1174	12444	5564	14107	15920
1105	C2-Phenol	Phenol	122	107	77	6				42	42	39	49
1110	Isopropenylphenol	Phenol								95	98	75	78
1111	C1-Benzofuran	Ether	131	132		10	6	12	8	161	139	106	247
1121	Vinylguaiacol	Phenol	135	150	77						17		15
1133	C2-Phenol	Phenol	122	107	77	12	11	19		191	141	116	217
1145	C2-Phenol	Phenol	107	122	121	292	186	425	315	14	16	6	29
1150	Dihydrobenzofuran	Ether	110	91	120							239	
1164	C2-Phenol	Phenol	107	122				16	1	35	63	26	83
1176	C1-Guaiacol	Phenol	138	123	77					7		8	6
1183	C3-Phenol	Phenol	121	136	91					43	32	33	39
1186	Catechol	Phenol	110	63	81	1909	1511	391	1327	9929	5512	13243	13025
1189	C1-Guaiacol	Phenol	138	110		676	561	195	647	22	19	22	35
1198	Dihydrobenzofuran	Ether	91	120	119							64	
1204	C3-Phenol	Phenol	121	136	91			15			10	6	10
1208	C2-Benzofuran	Ether	145	146	131							7	
1252	C1-Catechol	Phenol	78	124	123	38	48		57	103	78	99	130
1275	3,4-Dihydroxyacetophenone	Ketone	152	137	109	8	6		6				
1280	C1-Catechol	Phenol	124	66	65	310	238	115	479	42	28	43	52

1332	C2-Catechol	Phenol	123	138	77	21	22		18	112	134	132	177
1346	Syringol	Phenol	236	154	139								
1374	C2-Catechol	Phenol	123	138		28	18		20	110	123	102	213
1383	C2-Guaiacol	Phenol	137	152							8	4	10
1396	Vanillin	Aldehyde	151	152	123	23480	14635	6566	19476				
1424	4-hydroxy-3methylbenzaldehyde	Aldehyde	135	136	77	1089	886	1203	2906				

TABLE IV.S2 - CONCENTRATION RELATIVE (IN µg mL^{-1}) TO THE INTERNAL STANDARD (5-α-CHOLESTANE) AND CHEMICAL CLASS OF COMPOUNDS FORMED IN THE CATALYSIS REACTIONS OF SYRINGYL MODEL COMPOUNDS, IDENTIFIED BY GC-MS

RI	Compound	Chemical class	Mass fragments			Syringaldehyde				Syringol			
			m/z (1)	m/z (2)	m/z (3)	1Pd	2Pd	5Ag	10Ag	1Pd	2Pd	5Ag	10Ag
842	RI=841.9 in MDM1245	Unknown	43	59								1515	1056
861	C2-Benzene	Hydrocarbon	91	106	65							676	781
870	C2-Benzene	Hydrocarbon	91	106								286	384
891	C2-Benzene	Hydrocarbon	91	106								146	296
987	Phenol	Phenol	94	66	65		42	43	100	113	100	1384	1643
994	Benzofuran	Ether	118	89	63	2					10		
1031	C3-Phenol	Phenol	121	136	122							342	190
1051	C1-Phenol	Phenol	108	107	79	46	48	15	46	196	292	693	1282
1073	C1-Phenol	Phenol	108	107	77		33	35	54	51	45	989	463
1085	Guaicol	Phenol	124	109	81	27	20	92		45	220	203	519
1096	C1-Benzofuran	Ether	131	132	78	14	8	3	6	28	93	77	152
1105	C2-Phenol	Phenol	122	107	77	221	156	75	155	661	4513	2875	5739
1110	Isopropenylphenol	Phenol				100	51	25	64	247	1489		
1111	C1-Benzofuran	Ether	131	132						5	16	25	
1121	Vinylguaiacol	Phenol	135	150	77	7		6	25	27	66	551	890
1133	C2-Phenol	Phenol	122	107	77						21	101	77
1145	C2-Phenol	Phenol	107	122	121	23	22	15	27			34	
1164	C2-Phenol	Phenol	107	122				5	12	14	16	234	137
1176	C1-Guaiacol	Phenol	138	123	77	563	267	135	177	439	8852	2111	5678
1183	C3-Phenol	Phenol	121	136	91	14	11	6	14	50	226	221	398
1186	Catechol	Phenol	110	63	81	71	24	20	43	225	483	845	1014
1189	C1-Guaiacol	Phenol	138	110		10	11	4			19		
1204	C3-Phenol	Phenol	121	136	91	117	70	69	127				
1208	C2-Benzofuran	Ether	145	146	131	11	8	4	11	26	129	114	159
1252	C1-Catechol	Phenol	78	124	123	251	91	94	203	582	6522	877	1500
1254	3-Methoxycathecol	Phenol	140	97	25	857	241	197	198	478	16129	1502	4310
1274	Hydroquinone	Phenol	110	82	121					49	17	50	
1275	3,4-Dihydroxyacetophenone	Ketone	152	137	109	194	95	60	82				

1280	C1-Catechol	Phenol	124	66	65	29		15	26		24	17	
1332	C2-Catechol	Phenol	123	138	77	14				45	140	61	97
1346	Syringol	Phenol	236	154	139			91					38
1358	Benzetriol	Phenol									119		
1374	C2-Catechol	Phenol	123	138		9				13	37	72	131
1383	C2-Guaiacol	Phenol	137	152		23		5		35	53	95	330
1396	Vanillin	Aldehyde	151	152	123	44	17	12	10				
1424	4-hydroxy-3methylbenzaldehyde	Aldehyde	135	136	77							94	90
1437	C2-Guaiacol	Phenol	137	152		30	6	7	10	23	88	155	577
1440	C1-Syringol	Phenol	168	153	125	746	199	136	122		6		47
1495	3,5-Dimethoxybenzaldehyde	Aldehyde	166	165	123	1241	356	319	243				
1653	Syringaldehyde	Aldehyde	182	181		1699	110	676	217				